UNIVERSIDAD COMPLUTENSE DE MADRID

FACULTAD DE CIENCIAS QUÍMICAS

Departamento de Bioquímica y Biología Molecular I

TESIS DOCTORAL

Análisis biofísico y reconstitución en microesferas funcionalizadas de FtsZ, proteína esencial en la división

Biophysical analysis and reconstitution of functionalized microbeads of FtsZ, and essential protein in bacterial cell division

MEMORIA PARA OPTAR AL GRADO DE DOCTOR

PRESENTADA POR

Rubén Ahijado Guzmán

Directores

Germán Rivas Caballero
Carlos Alfonso Botello
Begoña Monterroso Marco

Madrid, 2013

Análisis Biofísico y Reconstitución en Microesferas Funcionalizadas de FtsZ, Proteína Esencial en la División

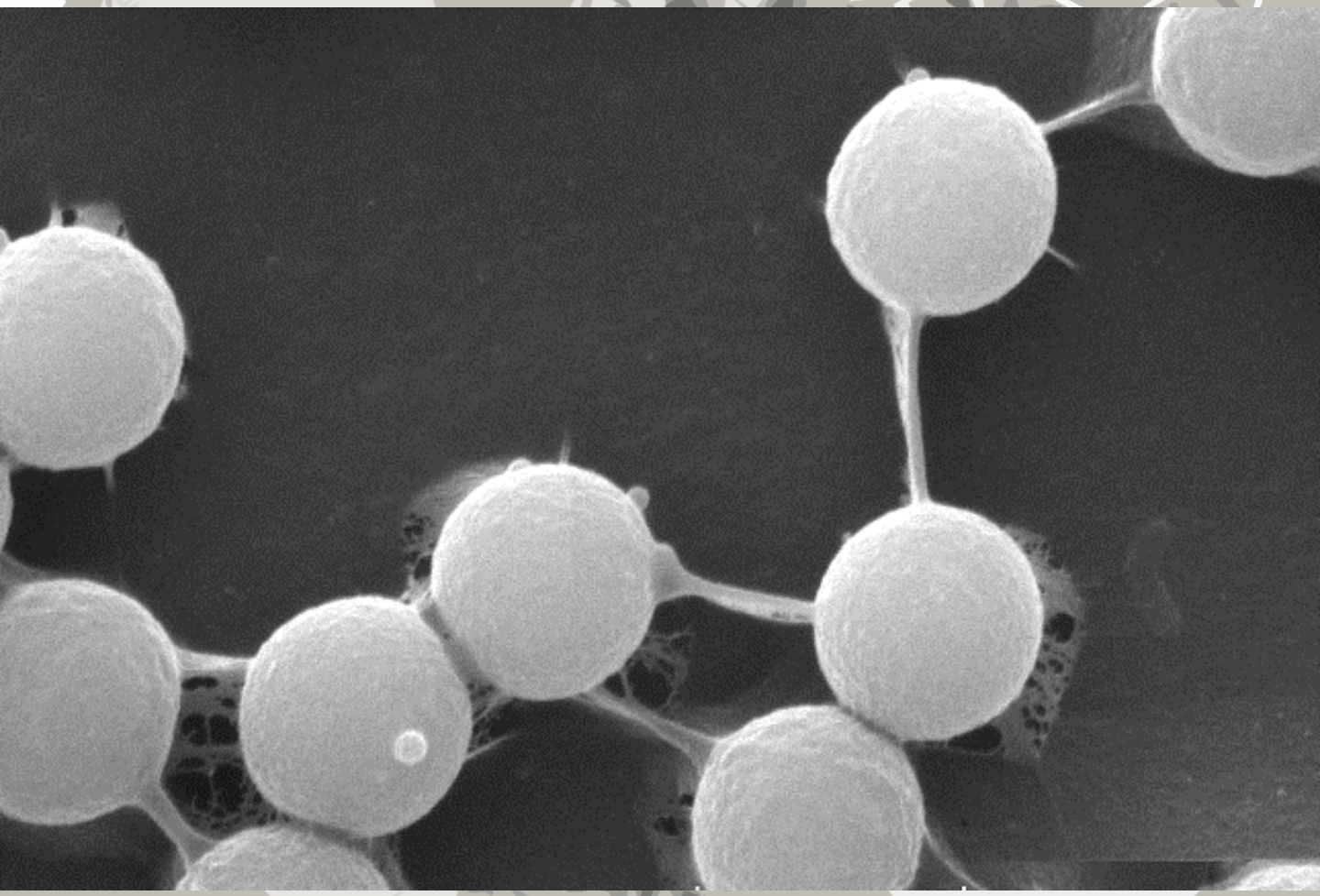

Rubén Ahijado Guzmán

Universidad Complutense de Madrid

Facultad de Ciencias Químicas

Departamento de Bioquímica y Biología Molecular I

Análisis Biofísico y Reconstitución en Microesferas Funcionalizadas de FtsZ, Proteína Esencial en la División

Biophysical Analysis and Reconstitution on Functionalized Microbeads of FtsZ, an Essential protein in Bacterial Cell Division

Trabajo presentado para optar al grado de Doctor

Rubén Ahijado Guzmán

Directores

Germán Rivas Caballero, Carlos Alfonso Botello y Begoña Monterroso Marco

Centro de Investigaciones Biológicas-Consejo Superior de Investigaciones Científicas

Madrid 2012

A mis Padres

INDICE GENERAL

1.-INTRODUCCIÓN

1.1.-La maquinaria de división bacteriana en *Escherichia coli*

Escherichia coli es una bacteria gram negativa ampliamente distribuida en los ecosistemas naturales. Esta característica, refleja su elevada capacidad para adaptar sus funciones esenciales al medio en el que vive. Así, la bacteria, es capaz de adaptar el proceso esencial de su división celular al entorno, con el fin de asegurar su supervivencia. Durante el proceso de división, la bacteria crece hasta alcanzar un tamaño determinado. Llegado a este punto, se produce la replicación del único cromosoma de *Escherichia coli*. A continuación, durante el proceso de división, aparece una invaginación en el punto medio de la bacteria generado por la maquinaria de división, la cual ejerce una fuerza constrictora sobre la membrana. Este proceso, finaliza con la división de la bacteria, dando lugar a dos células hijas.

El motor de la maquinaria de división bacteriana, es un complejo macromolecular dinámico que forma un anillo situado en el punto medio de la bacteria. Este anillo de división o divisoma, está formado por al menos 15 proteínas citoplasmáticas, de membrana o periplasmáticas. En *Escherichia coli,* los componentes del divisoma son reclutados de acuerdo a un orden lineal y estricto, lo que determina un proceso de ensamblaje paso a paso en el siguiente orden: FtsZ > ZipA, FtsA > ZapA > FtsE, FtsX > FtsK > FtsQ > FtsB, FtsL > FtsW > FtsI > FtsN > AmiC > EnvC. Como vemos en esta secuencia de interacciones, FtsZ juega un papel esencial para la posterior localización del resto de proteínas que intervienen en la división celular.

Durante el ensamblaje del anillo de división, podemos distinguir varias etapas como se describe esquemáticamente en la Figura 1A. El autoensamblaje de la proteína citoplasmática FtsZ para formar proto-filamentos. La formación del primer complejo multiproteico o proto-anillo, formado por las proteínas FtsZ, ZipA y FtsA. Donde FtsA es una proteína citoplasmática anfitrópica, ZipA es una proteína de membrana que ancla los complejos de FtsZ a la membrana y FtsZ es una proteína citoplasmática. Por último, y

siguiendo un orden secuencial, se unen al proto-anillo el resto de proteínas citadas anteriormente [1, 2].

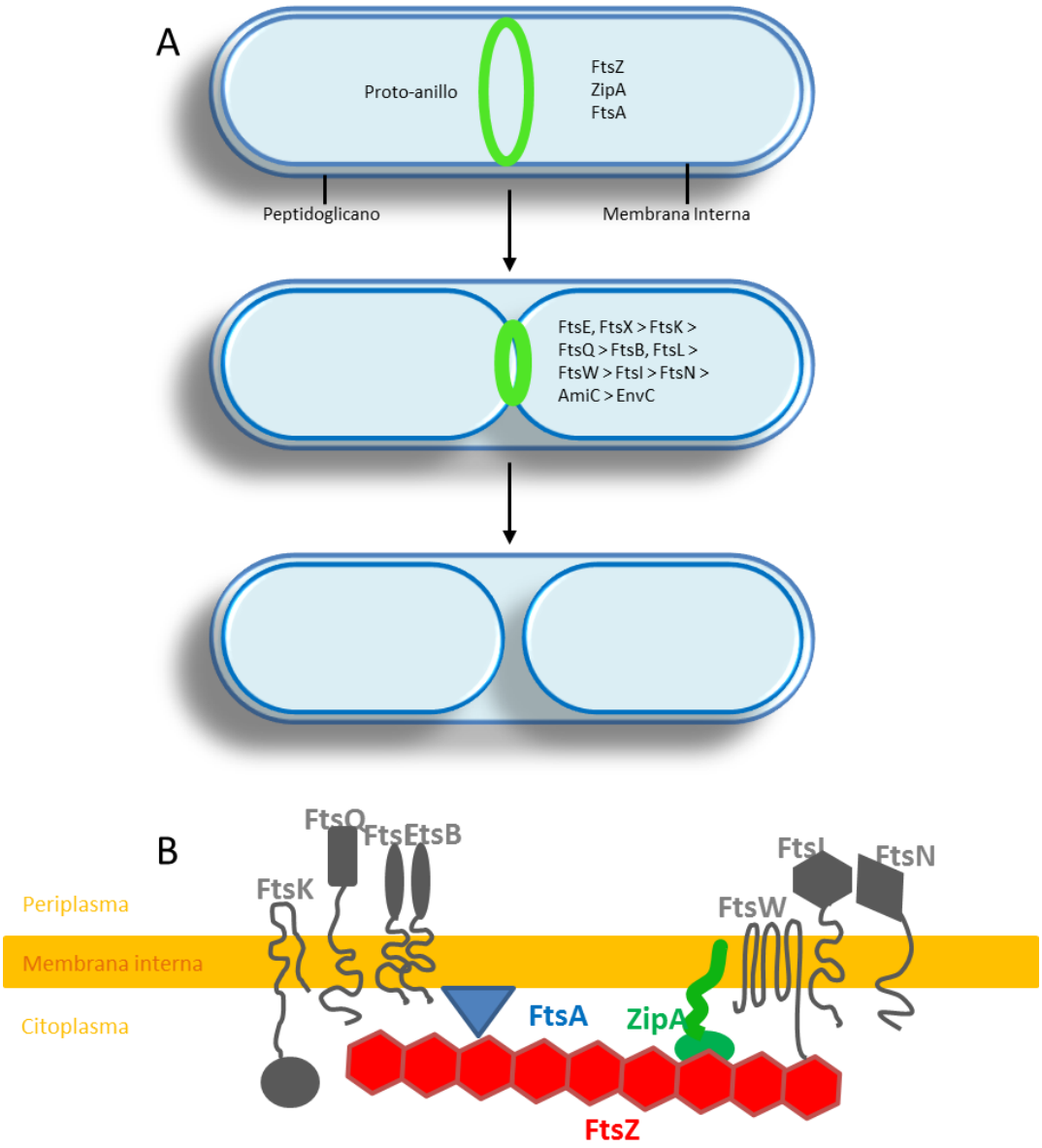

Figura 1. El ensamblaje del proto-anillo se produce en la parte interior de la membrana citoplasmática. (A) Al proto-anillo se van sumando de forma secuencial el resto de proteínas de la maquinaria de división para dar lugar al divisoma o anillo de división. El anillo de división produce una fuerza constrictora, que finaliza con la división total de la bacteria para dar lugar a dos bacterias hijas. (B) En la etapa temprana, el proto-anillo (FtsZ (rojo), ZipA (verde) y FtsA (azul)) se ensambla en el punto medio de la bacteria. Una vez formado el proto-anillo, se reclutan al sitio de división el resto de proteínas esenciales que forman el divisoma.

1.1.1.-El proto-anillo de *Escherichia coli*

Durante la formación del proto-anillo, se produce la localización de FtsZ en el sitio de división. La localización de FtsZ, depende de dos mecanismos de inhibición, el sistema MinCDE y el sistema de oclusión del nucleoide (Noc) [3]. El modelo de oclusión del nucleoide se refiere a un mecanismo inhibitorio, mediante el cual, se previene que la división ocurra en las inmediaciones del nucleoide [4]. En *E. coli* el sistema MinCDE está formado por tres proteínas, MinC, MinD y MinE. MinC es realmente el inhibidor de la polimerización de FtsZ. MinD es una proteína de membrana con actividad GTPasa que interacciona con MinC. Finalmente, MinE, se requiere para la oscilación polo a polo del complejo MinCD, de manera que resulta una menor concentración de MinC en la región central de la bacteria, permitiendo así, la polimerización de FtsZ en este lugar [5, 6].

Una vez que FtsZ se encuentra en el sitio de división, se produce el ensamblaje con ZipA y FtsA, para formar el proto-anillo. El proto-anillo, es el primer complejo multi-proteico formado durante el proceso de división, y su correcto ensamblaje es de esencial importancia para la posterior formación del anillo maduro de división o divisoma. ZipA, se encuentra anclada a la membrana y FtsA se encuentra asociada a ella ya que es una proteína anfitrópica. El ensamblaje de ZipA y FtsA en el proto-anillo, es dependiente únicamente de FtsZ [3]. Ambas proteínas, (ZipA y FtsA) estabilizan el proto-anillo mediante su interacción con la región C-terminal de FtsZ, esto sugiere que ZipA y FtsA sirven como anclaje dinámico de FtsZ a la membrana [7, 8, 9].

Como se ha descrito, y puede verse esquemáticamente en la Figura 1B, las interacciones macromoleculares implicadas en la formación del proto-anillo suceden en el entorno citoplasmático y de la membrana interna. Por este motivo, es esencial el estudio biofísico de las interacciones macromoleculares involucradas tanto en disolución como en sistemas modelo de membrana.

1.1.1.1.-FtsZ de *E. coli*

FtsZ es la proteína mayoritaria en el anillo de división, se encuentra soluble en el citoplasma de procariotas y en algunos orgánulos celulares como cloroplastos o mitocondrias. FtsZ, tiene gran homología estructural con la tubulina eucariota [10, 11]. Tiene actividad GTPasa y su masa molecular es de 40.3 kDa [12, 13]. Está formada por dos dominios alrededor de una hélice central. El dominio N-terminal, que interacciona con otra subunidad de FtsZ, para formar un dominio de actividad GTPasa, y el dominio C-terminal, de unión con ZipA y FtsA para formar el proto-anillo.

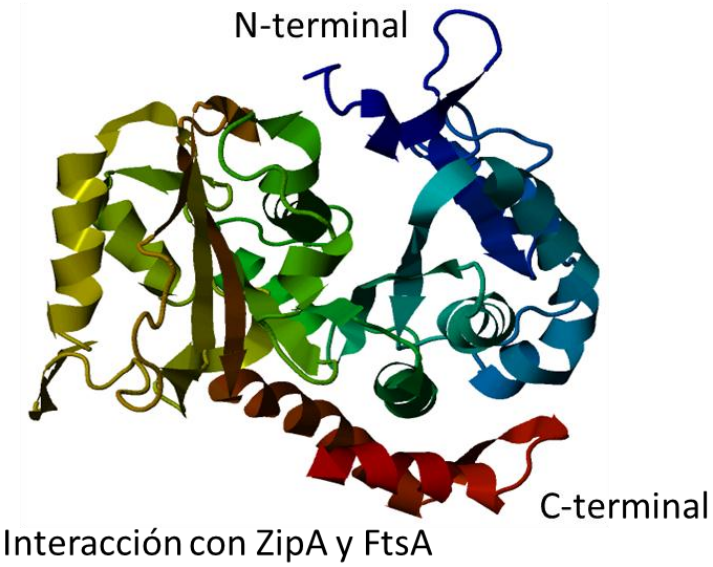

Figura 2. Modelo teórico de la estructura de la proteína FtsZ de E. coli cedido por el grupo de modelado molecular del CBM-CSIC (Prof. Paulino Gómez Puertas). En la imagen se indican las principales regiones. En azul oscuro, el dominio N-terminal, y en rojo, el dominio C-terminal de interacción con ZipA y FtsA.

FtsZ es la proteína encargada del inicio en el proceso de división, y es capaz de formar proto-filamentos. El proto-filamento es una estructura dinámica que esta en continua actividad mediante procesos de polimerización y despolimerización. FtsZ forma una red

filamentosa en el citoplasma bacteriano actuando de soporte estructural o citoesqueleto [14]. Actúa como estructura de andamiaje sobre la cual se van anclando el resto de componentes de la maquinaria de división. Cuando el proto-filamento de FtsZ interacciona con ZipA y FtsA se forma el proto-anillo y por tanto se inicia la formación del divisoma [15, 16].

FtsZ y agentes antibióticos. FtsZ, es una de las dianas terapéuticas más estudiadas en el desarrollo de nuevos agentes antibacterianos activos contra bacterias resistentes a antibióticos [17]. Existen inhibidores de la actividad de FtsZ que se han obtenido centrándose en el conocimiento de las características de esta proteína, su función e interacciones. Las zantrinas son inhibidores análogos de GTP [18]. El compuesto PC190723 actúa como inhibidor de FtsZ al interaccionar con una región de la proteína análoga al sitio de unión del taxol en tubulina. La viriditoxina, un derivado natural dimérico del ácido naftalénico, es un inhibidor de la polimerización y de la actividad GTPasa de FtsZ [19]. Algunos análogos bromados de nucleótido, Br-GTP, inhiben la actividad GTPasa de FtsZ incluso en su forma polimérica [20]. La sanguinarina, un alcaloide antimicrobiano, además de despolimerizar los filamentos tiene un efecto desestabilizador sobre el proto-anillo [21]. Sin embargo, a pesar de su demostrado efecto inhibidor, estos compuestos presentan una actividad antibiótica muy débil o resultan potencialmente tóxicos para las células eucariotas.

Aunque FtsZ es la proteína más estudiada de la maquinaria de división, existen gran cantidad de cuestiones sin resolver, algunas de ellas son: ¿Es el anillo de división una estructura continua? ¿Son los proto-filamentos de FtsZ, los encargados de ejercer la fuerza de constricción? o ¿es solamente una estructura de andamiaje para el resto de la maquinaria de división? ¿Tiene algún papel el gran polimorfismo de FtsZ en la dinámica de los polímeros? ¿Cuál es la naturaleza de las interacciones laterales observadas? Además de la gran cantidad de cuestiones abiertas, los resultados obtenidos a lo largo de la literatura de sus propiedades a partir de medidas bioquímicas y biofísicas generan gran cantidad de controversias, probablemente, al menos en parte, debidas, como estudiamos y presentamos en esta tesis, a diferencias en las condiciones experimentales empleadas.

1.1.1.2.-ZipA de *E. coli*

ZipA de *Escherichia coli* es una proteína esencial en la división. La masa molecular de ZipA es de 36.4 KDa, y su función es la de mantener anclado los filamentos de FtsZ a la membrana. Además, ésta proteína no está conservada fuera de la familia de las γ-proteobacterias [22]. Tiene una hélice N-terminal transmembrana asociada a la cara interna de la membrana bacteriana. Un dominio P/Q desestructurado que es rico en prolina y glutamina, que sirve de conexión entre el fragmento transmembrana y el dominio globular C-terminal. El dominio globular C-terminal, se localiza en el citoplasma, y cuando ZipA es reclutada al proto-anillo, lo hace mediante una interacción directa entre este dominio y el dominio C-terminal de FtsZ siguiendo un mecanismo que no se conoce aún de manera detallada [23, 24]. Además, como se describe en Martos *et al.* (2010) [25], la heteroasociación de ZipA con FtsZ en disolución y en presencia de GDP es dependiente de la concentración de Mg^{2+} (ver Apendice 2).

Figura 3. Modelo de la estructura de la proteína ZipA de E. coli tomado de la referencia 9, PDB 1fsx. En la imagen se indican las principales regiones, el dominio N-terminal o fragmento transmembrana y dominio C-terminal de interacción con FtsZ.

Para su estudio, tanto en disolución como en sistemas reconstituidos, la utilización de mutantes solubles es de gran ayuda. Se han utilizado dos mutantes solubles de ZipA, s1 y s2-ZipA [25]. En el caso de s1-ZipA la proteína carece del fragmento transmembrana N-

terminal desde el aminoácido 1 hasta el 25. En el caso del mutante s2-ZipA, además del dominio transmembrana, se eliminó el dominio P/Q, desde el aminoácido 1 hasta el 188. En ambos mutantes, los fragmentos eliminados, han sido sustituidos por un fragmento de seis histidinas. Estos mutantes, nos permiten además, estudiar interacciones en sistemas reconstituidos de membrana dopados con grupos Ni-NTA o en superficies de oro y/o plata, a los que la cola de histidinas se une fuertemente.

1.2.- Oligomerización y ensamblaje de FtsZ

En presencia de GDP, FtsZ de *E. coli* experimenta una oligomerización reversible y no cooperativa modulada por factores como el pH, la fuerza iónica, la concentración de cationes monovalentes, divalentes y la aglomeración macromolecular [25, 26, 27]. En presencia de Mg^{2+} y moderada fuerza iónica, la proteína asocia para dar lugar a la formación de oligómeros lineales con longitud variable de FtsZ (Ver Figura 4). Dicha asociación se ha descrito como una asociación cuasi-isodésmica y ligeramente anti-cooperativa a partir del monómero de proteína [26].

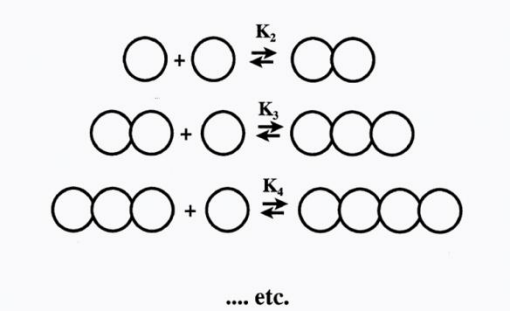

Figura 4. En presencia de GDP, FtsZ experimenta una asociación reversible para formar oligómeros lineales. Representación esquemática del modelo de asociación cuasi-isodésmico propuesto por Rivas *et al* 2000 (13).

El análisis de la dependencia en la oligomerización de la proteína con la concentración de Mg^{2+} fue en parte descrito por Rivas *et al.* (2000) [26]. Deduciendo que se produce la unión de un ión Mg^{2+} por cada subunidad de FtsZ en el oligómero. Además, esta oligomerización, se ve atenuada por el aumento de la fuerza iónica del medio, [25, 26] y

moderadamente acentuada por la aglomeración macromolecular debida a altas concentraciones de macromoléculas que simulan el aglomerado citoplasma bacteriano [28].

El estudio de la oligomerización dependiente de Mg^{2+} llevado a cabo anteriormente [26], no cubrió en detalle el estudio a concentraciones submilimolares de Mg^{2+} y alta fuerza iónica, donde predomina el equilibrio entre las formas monoméricas y diméricas. Además de esto, en el estudio presentado en el Apendice 1 de esta tesis doctoral, se comparan resultados obtenidos mediante ultracentrifugación analítica (velocidad de sedimentación) con los obtenidos por dispersión de luz estática, estando ambos en buen acuerdo.

El ensamblaje de FtsZ en presencia de GTP, en principio, fue descrito como cooperativo, y se determinó la concentración crítica de ensamblaje en distintas condiciones experimentales [29-33]. El ensamblaje cooperativo, se produce en dos etapas, en la primera se forma el núcleo de polimerización y en la segunda el polímero crece mediante adición de nuevas subunidades. La formación del núcleo es energéticamente costosa, pero una vez formado, la adición de nuevas subunidades es más favorable. Por último, el ensamblaje exhibe una concentración crítica de polimerización, por encima de la cual las subunidades de proteína se distribuyen en dos poblaciones distintas, especies pequeñas y polímeros largos [34].

Otros autores, describieron el mecanismo de ensamblaje de FtsZ como no cooperativo o isodésmico,[35] basándose en que FtsZ ensamblaba mayoritariamente en filamentos de una sola cadena a pH 6.5 y a concentraciones muy bajas de FtsZ (por debajo de 2 µM) y en que no existía una concentración crítica de ensamblaje. Los polímeros formados de manera isodésmica, son polímeros de una sola cadena y ensamblan a través de la formación de un enlace que es idéntico a cada paso del ensamblaje, por tanto, no hay una fase de nucleación. Más recientemente, los mismos autores, describían el ensamblaje de FtsZ como aparentemente cooperativo [29].

Posteriormente, fue propuesto un modelo de ensamblaje que implicaba un crecimiento isodésmico del polímero seguido de una ciclación preferencial [36]. La ciclación, se produce cuando la cadena polimérica tiene suficiente longitud (Ver Figura 5). Este último modelo,

tiene en cuenta la formación de especies de tamaño definido observadas por medidas de velocidad de sedimentación y tiene en cuenta la formación de especies de geometría circular observadas por microscopía electrónica y microscopía de fuerzas atómicas [36].

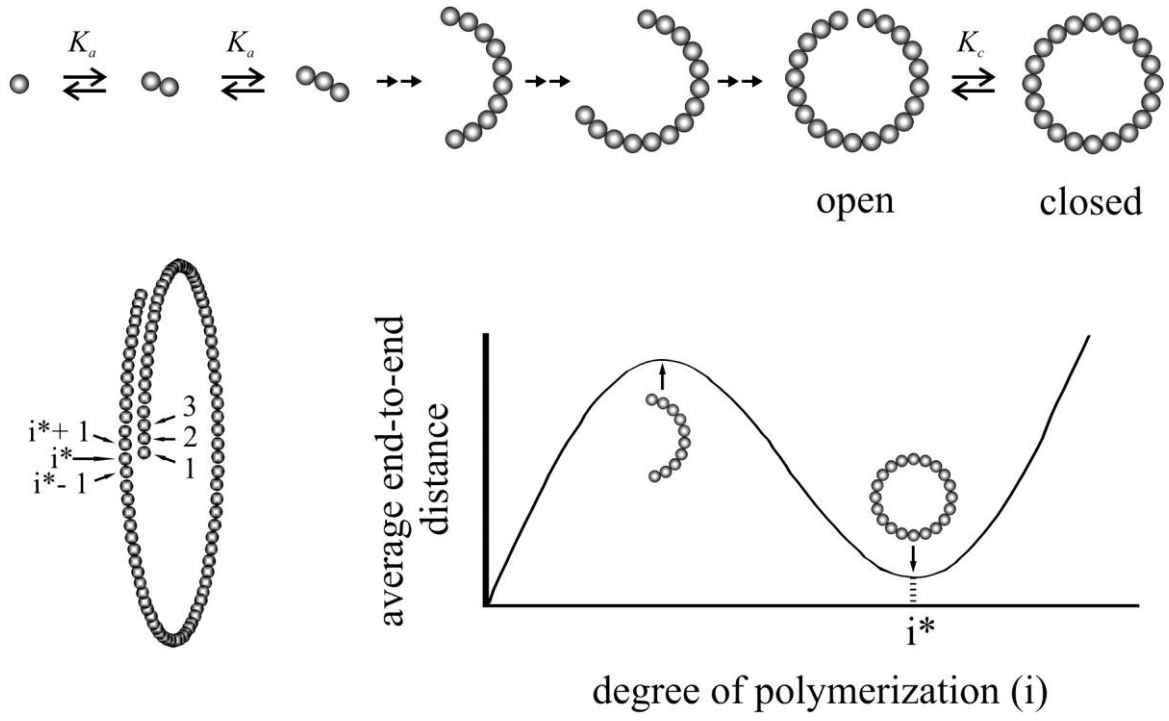

Figura 5. Representación esquemática del modelo de asociación isodésmica + ciclación. Implicaba un crecimiento isodésmico del polímero seguido de una ciclación preferencial. La ciclación, se produce cuando la cadena polimérica tiene suficiente longitud [36].

La polimerización de FtsZ para formar proto-filamentos, está acoplada a la hidrólisis de GTP, coincidiendo la desaparición de los polímeros con el agotamiento del GTP [38]. Los factores que influyen en la velocidad de hidrólisis de GTP, son los cationes K^+ y Mg^{2+}, que afectan también a la estabilidad de los polímeros [32, 37 - 39]. FtsZ a pH neutro, requiere la presencia conjunta de Mg^{2+} y K^+ para el ensamblaje, pero la dependencia del

ensamblaje con la concentración de estos cationes, no ha sido estudiada en detalle anteriormente hasta el trabajo presentado en esta tesis doctoral (Capítulos I y II).

De esta manera, en función de las condiciones experimentales, los polímeros de FtsZ pueden adoptar gran variedad de estructuras, como son, filamentos sencillos, dobles, cintas, círculos, etc [27, 37, 40 - 43]. En la figura 6 se muestran algunas de estas estructuras mediante micrografías de microscopía electrónica de transmisión.

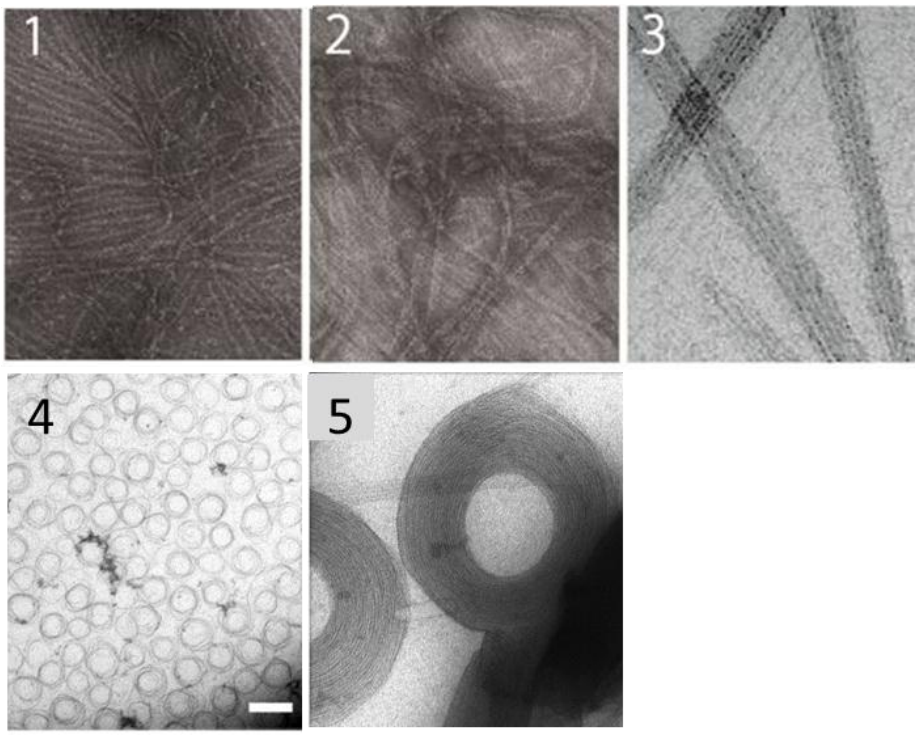

Figura 6. Plasticidad estructural de FtsZ. En función de las condiciones experimentales se pueden encontrar formando: (1) filamentos sencillos, (2) filamentos dobles, (3) haces de filamentos o cintas, (4) círculos, (5) toroides [27, 37, 40 - 43].

A modo de resumen, la Figura 7 muestra la gran cantidad de procesos de asociación y ensamblaje en los que puede estar involucrada FtsZ. Además cada uno de éstos procesos de ensamblaje-desensamblaje, puede estar modulado por efectos de agentes de aglomeración molecular, concentración de diferentes cofactores y efectos de pH.

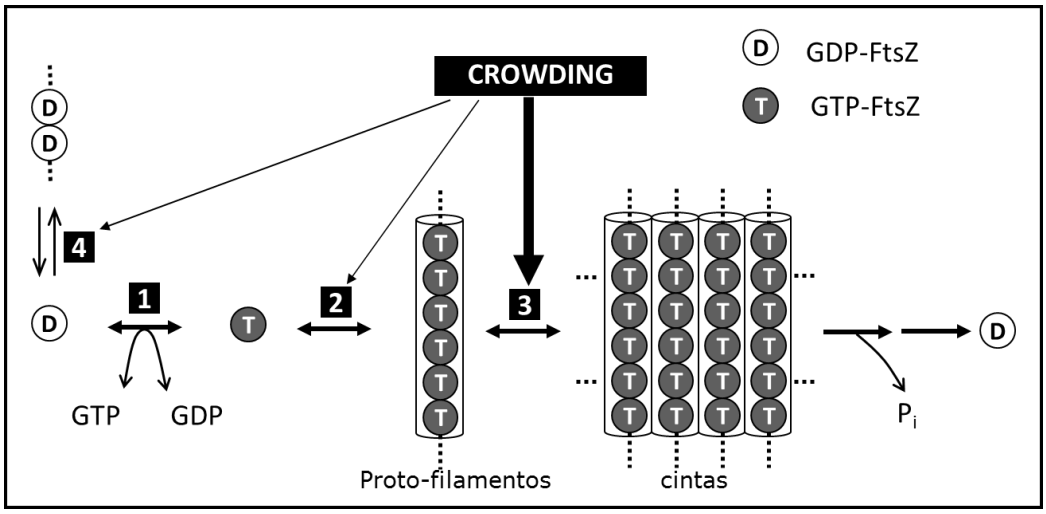

Figura 7. Esquema de la diversidad de procesos de ensamblaje y desensamblaje que puede sufrir FtsZ. Cada una de las reacciones puede estar modulada por efectos de agentes de aglomeración molecular, concentración de diferentes cofactores y efectos de pH.

1.3.-Interacción entre elementos del proto-anillo: FtsZ y ZipA

Como se ha descrito anteriormente, el primer complejo multiproteico que inicia el proceso de división en *Escherichia coli,* es el proto-anillo. Esta compuesto por las proteínas FtsZ, ZipA y FtsA, y ensamblado en a la membrana citoplasmática. La formación del proto-anillo, es esencial para la formación del divisoma maduro, y por tanto, para hacer posible el proceso de división [44, 45]. En el proto-anillo, los proto-filamentos de FtsZ, están anclados a la membrana interna a través de su dominio C-terminal y el dominio C-terminal de ZipA, además de FtsA. En condiciones normales, ZipA, es imprescindible para la formación del proto-anillo, estabiliza los polímeros de FtsZ tanto *in vitro* como *in vivo* y es capaz de inducir la formación de haces de polímeros de FtsZ [46 - 48]. La naturaleza de la interacción entre FtsZ y ZipA se ha estudiado extensamente mediante técnicas genéticas y estructurales, pero el mecanismo de la asociación todavía es desconocido [23, 24, 49 - 52].

Los únicos estudios cuantitativos sobre la afinidad de la formación de complejos FtsZ-ZipA fueron proporcionados por dos trabajos. En el primero de ellos, estudiaban la afinidad mediante la utilización de biosensores ópticos, por Mosyak *et al* (2000) [9]. En el segundo trabajo, Martos *et al.* (2010) [25] (ver Apendice 2), llevaron a cabo el estudio

cuantitativo de la interacción mediante dispersión de luz estática en gradiente de concentración y equilibrio de sedimentación. En ambos casos se determina que la interacción es de baja afinidad (del orden de micromolar). En el segundo trabajo mencionado, además, se establece que la naturaleza de la interacción es subestequiométrica, de manera que un sólo monómero de ZipA es capaz de unirse a oligómeros de FtsZ independientemente de su tamaño, según el esquema que proponen los autores (Figura 8).

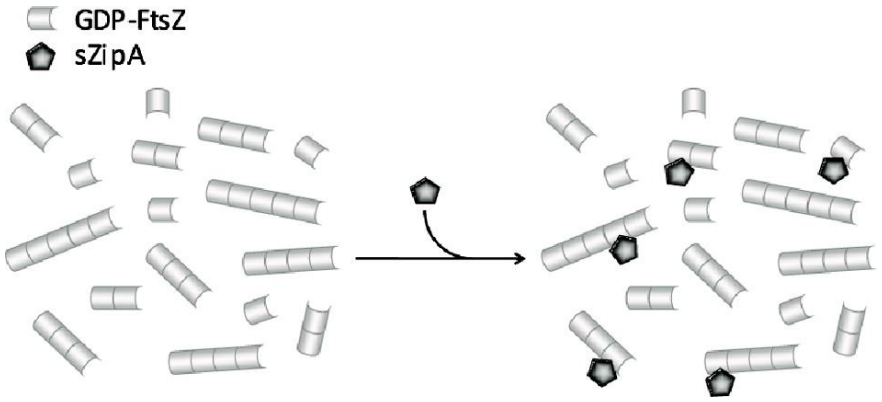

Figura 8. Representación esquemática de Martos *et al* (2010) [25], donde se puede observar la naturaleza subestequiométrica de la interacción, de manera que un monómero de ZipA es capaz de unirse a oligómeros de FtsZ independientemente del tamaño de los últimos.

1.4.- Reconstitución en sistemas biomiméticos de membrana

La reconstitución de sistemas biológicos a partir de sus componentes aislados, es una poderosa herramienta enfocada al estudio de los procesos biológicos. La principal ventaja de estos sistemas, es que podemos controlar con gran precisión, los parámetros bioquímicos y biofísicos experimentales.

Los sistemas reconstituidos *in vitro,* proporcionan información del sistema fuera de la complejidad del entorno celular, apoyándose, además, en la información derivada de los estudios en disolución. Los sistemas complejos, pueden reconstituirse en sistemas más

sencillos, y por tanto, abordar el estudio en diferentes subsistemas. Están limitados espacio-temporalmente, además, el número de variables se reduce significativamente respecto al sistema *in vivo*, por eso, son tan útiles para el desarrollo de modelos simplistas que describan el comportamiento del sistema [53].

El estudio de los sistemas reconstituidos en sistemas modelo de membrana es esencial, ya que la membrana, constituye la frontera que permite, no sólo separar, sino también, poner en comunicación diferentes compartimentos en el interior de la célula y a la propia célula con el exterior. La membrana, es el medio donde tienen lugar las reacciones de gran variedad de procesos biológicos esenciales. Además, la mayoría de dianas en el desarrollo de nuevos fármacos, está relacionada con las interacciones entre proteínas y sus receptores de membrana [54 - 56]. Según el modelo de Mosaico Fluido (45), la totalidad de la membrana es fluida, las moléculas lipídicas se desplazan fácilmente dentro de cada cara de la bicapa mientras que las proteínas, que suponen, en el caso de *Escherichia coli*, cerca del 70% en peso de la membrana, se mueven también con facilidad dentro de toda la bicapa [57, 58].

La composición fosfolipídica de las membranas citoplasmáticas de *Escherichia coli* consta principalmente de fosfatidiletanolamina (PE) en aproximadamente un 67%, fosfatidilglicerol (PG) entorno a un 23% y una pequeña porción cercana al 10% de difosfatidilglicerol (DPG) o cardiolipina (CL) [59].

En nuestro laboratorio, hemos puesto a punto la reconstitución y ensamblaje de algunas proteínas del divisoma en ambientes que mimetizan el entorno de la membrana. Los principales sistemas reconstituidos que utilizamos en nuestro laboratorio, se representan esquemáticamente en la figura 9 (Nanodiscos, microesferas, bicapas soportadas y vesículas). En esta tesis, nos centraremos en la utilización de microesferas como soporte para la reconstitución (ver Apéndice 2), además, como se describe en el capítulo III, nos servirán de base para la fabricación de sustratos ultrasensibles en espectroscopía Raman aumentada por superficie (SERS).

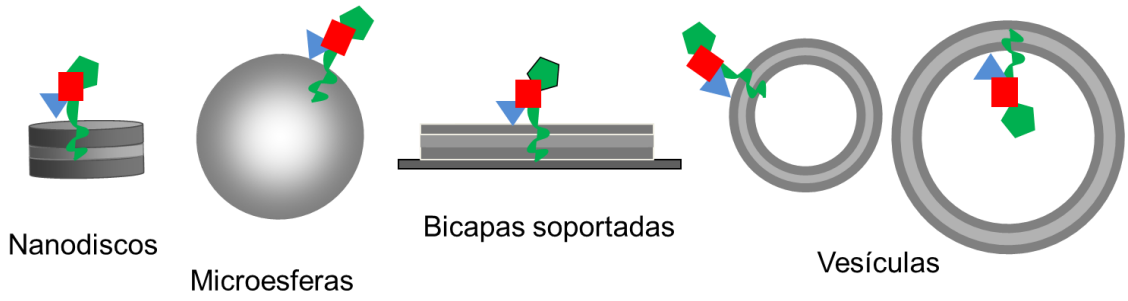

Figura 9. Representación esquemática de la reconstitución del proto-anillo (ZipA (verde), FtsZ (rojo) y FtsA (azul)) en algunos sistemas modelo de membrana. En función de su geometría, podemos clasificarlos en nanodiscos, microesferas, bicapas soportadas y vesículas. Las variables químico-físicas de estos sistemas reconstituidos son fácilmente controlables. Permiten trabajar *in vitro* con sistemas de membrana fuera de la complejidad del citoplasma celular.

Las microesferas proporcionan un soporte rígido, químicamente y físicamente estable. Tienen superficie y curvatura uniformes, además, proporcionan un entorno topológicamente definido y restringido necesario para el estudio químico-físico de las interacciones objeto de nuestro trabajo. Son comerciales, pueden ser de composición y tamaño deseado, y son susceptibles de ser funcionalizadas superficialmente de diversas maneras.

Los trabajos más llamativos hasta el momento tratan sobre la reconstitución del polímero de actina sobre microesferas de poliestireno [60, 61]. Además existen algunos trabajos en los que se describe el recubrimiento de microesferas de diferentes materiales y tamaños con material lipídico, lo cual supone un buen ejemplo de sistemas de membrana reconstituidos [62 - 66]. La reconstitución de sistemas de membrana en microesferas, es un caso particular de bicapas soportadas con condiciones topológicamente restringidas.

La reconstitución de sistemas de membranas en la superficie de microesferas, se produce, gracias a las propiedades anfifílicas de las moléculas lipídicas. Las interacciones hidrofóbicas entre las moléculas anfifílicas y la tendencia del agua a reducir su contacto con las cadenas hidrocarbonadas, proporcionan la fuerza impulsora que hace que

termodinámicamente sea posible la formación y el mantenimiento de estas estructuras, y por tanto, la deposición homogénea de vesículas unilamelares pequeñas en la superficie de las esferas. Las moléculas de fosfolípido se estructuran, en función de su lipofilicidad, en forma de una bicapa dinámica, fluida y continua de espesor variable [67].

Por otro lado, las microesferas, juegan un papel muy importante como soporte para el desarrollo de sensores y materiales compuestos con propiedades ópticas avanzadas. La aplicación de estos materiales avanzados, es entre otras, la clave en el desarrollo de sistemas miniaturizados de diagnóstico rápido, sistemas de detección ultrasensibles, así como sistemas de *screening* de alto rendimiento en condiciones ambientalmente y biológicamente relevantes [68, 69].

En el trabajo llevado a cabo en esta tesis doctoral, concretamente en el capítulo III, combinamos por primera vez, la fabricación de materiales nanoestructurados con propiedades avanzadas para la detección ultrasensible mediante espectroscopía SERS, con la reconstitución del sistema de división bacteriana.

Referencias

1. Vicente M, Rico AI, Martínez-Arteaga R, Mingorance J. Septum enlightenment: assembly of bacterial division proteins. J. Bacteriol.188.1.19–27.2006.

2. Goehring NW, Beckwith J. Diverse paths to midcell: assembly of the bacterial cell division machinery. Current Biology, Vol. 15, R514–R526, 2005.

3. Sun Q, Margolin W. Influence of the nucleoid on placement of FtsZ and MinE rings in Escherichia coli. J Bacteriol. 2001 Feb;183(4):1413-22.

4. Woldringh CL, Mulder E, Valkenburg JA, Wientjes FB, Zaritsky A, Nanninga N. Role of the nucleoid in the toporegulation of division. Res Microbiol. 1990 Jan;141(1):39-49.

5. Meinhardt H, de Boer PA. Pattern formation in Escherichia coli: a model for the pole-to-pole oscillations of Min proteins and the localization of the division site. Proc Natl Acad Sci U S A. 2001 Dec 4;98(25):14202-7.

6. Hu Z, Mukherjee A, Pichoff S, Lutkenhaus J. The MinC component of the division site selection system in Escherichia coli interacts with FtsZ to prevent polymerization. Proc Natl Acad Sci U S A. 1999 Dec 21;96(26):14819-24.

7. Haney SA, Glasfeld E, Hale C, Keeney D, He Z, de Boer P. Genetic analysis of the Escherichia coli FtsZ.ZipA interaction in the yeast two-hybrid system. Characterization of FtsZ residues essential for the interactions with ZipA and with FtsA. J. Biol. Chem. 276:11980–11987. 2001.

8. Ma X, Margolin W. Genetic and functional analyses of the conserved C-terminal core domain of Escherichia coli FtsZ. J. Bacteriol. 181:7531–7544. 1999.

9. Mosyak L, Zhang Y, Glasfeld E, Haney S, Stahl M, Seehra J, Somers WS. The bacterial cell-division protein ZipA and its interaction with an FtsZ fragment revealed by X-ray crystallography. EMBO J. 19:3179–3191. 2000.

10. Erickson HP. FtsZ, a prokaryotic homolog of tubulin?. Cell 80(3): p. 367-370. 1995.

11. Löwe J, Amos LA. Crystal structure of the bacterial cell-division protein FtsZ. Nature 391(6663): p. 203-6. 1998.

12. Mukherjee A, Dai K, Lutkenhaus J. Escherichia coli cell division protein FtsZ is a guanine nucleotide binding protein. Proc Natl Acad Sci U S A 90(3): p. 1053-7. 1993.

13. Romberg L, Levin PA. Assembly dynamics of the bacterial cell division protein FTSZ: poised at the edge of stability. Annu Rev Microbiol, 2003. 57: p. 125-54.

14. Nogales E. When cytoskeletal worlds collide. Proc Natl Acad Sci USA, 2010 vol. 107 no. 46 19609-19610.

15. Mingorance J, Rivas G, Vélez M, Gómez-Puertas P, Vicente M. Strong FtsZ is with the force: mechanisms to constrict bacteria. Trends in Microbiology 18 (2010) 348–356.

16. Niu L, Yu J. Investigating intracellular dynamics of FtsZ cytoskeleton with photoactivation single-molecule tracking. Biophys. J. 95, 2009–2016.

17. Awasthi D, Kumar K, Ojima I.Therapeutic potential of FtsZ inhibition: a patent perspective. Expert Opin Ther Pat. 2011 21(5):657-79.

18. Margalit DN, Romberg L, Mets RB, Hebert AM, Mitchison TJ, Kirschner MW, RayChaudhuri D. Targeting cell division: small-molecule inhibitors of FtsZ GTPase perturb cytokinetic ring assembly and induce bacterial lethality. Proc Natl Acad Sci U S A, 2004. 101(32): p. 11821-6.

19. Wang J, Galgoci A, Kodali S, Herath KB, Jayasuriya H, Dorso K, Vicente F, González A, Cully D, Bramhill D, Singh S. Discovery of a small molecule that inhibits cell division by blocking FtsZ, a novel therapeutic target of antibiotics. J Biol Chem, 2003. 278(45): p. 44424-8.

20. Läppchen T, Hartog AF, Pinas VA, Koomen GJ, den Blaauwen T. GTP analogue inhibits polymerization and GTPase activity of the bacterial protein FtsZ without affecting its eukaryotic homologue tubulin. Biochemistry, 2005. 44(21): p. 7879-84.

21. Beuria TK, Santra MK, Panda D. Sanguinarine blocks cytokinesis in bacteria by inhibiting FtsZ assembly and bundling. Biochemistry, 2005. 44(50): p. 16584-93.

22. Margolin W. Themes and variations in prokaryotic cell division. FEMS Microbiol Rev, 2000. 24(4): p.531-48.

23. Hale CA, de Boer PA. Direct binding of FtsZ to ZipA, an essential component of the septal ring structure that mediates cell division in E. coli. Cell, 1997. 88(2): p. 175-85.

24. Ohashi T, Hale CA, de Boer PA, Erickson HP. Structural evidence that the P/Q domain of ZipA is an unstructured, flexible tether between the membrane and the C-terminal FtsZ-binding domain. J. Bacteriol, 2002. 184(15): p. 4313-5.

25. Martos A, Alfonso C, López-Navajas P, Ahijado-Guzmán R, Mingorance J, Minton AP, Rivas G. Characterization of self-association and heteroassociation of bacterial cell division proteins FtsZ and ZipA in solution by composition gradient-static light scattering. Biochemistry, 2010. 49(51): p.10780–10787.

26. Rivas G, López A, Mingorance J, Ferrándiz MJ, Zorrilla S, Minton AP, Vicente M, Andreu JM. Magnesium-induced linear self-association of the FtsZ bacterial cell division protein monomer. The primary steps for FtsZ assembly. J Biol Chem, 2000. 275(16): p. 11740-9.

27. de Pereda JM, Leynadier D, Evangelio JA, Chacón P, Andreu JM. Tubulin secondary structure analysis, limited proteolysis sites, and homology to FtsZ. Biochemistry. 1996 Nov 12;35(45):14203-15.

28. Rivas G, Fernández JA, Minton AP. Direct observation of the enhancement of noncooperative protein self-assembly by macromolecular crowding: indefinite linear self-association of bacterial cell division protein FtsZ. Proc Natl Acad Sci U S A. 2001 13;98(6):3150-5.

29. Caplan MR, Erickson HP. Apparent cooperative assembly of the bacterial cell division protein FtsZ demonstrated by isothermal titration calorimetry. J Biol Chem. 2003 18;278(16):13784-8.

30. Huecas S, Andreu JM. Energetics of the cooperative assembly of cell division protein FtsZ and the nucleotide hydrolysis switch. J Biol Chem. 2003 14;278(46):46146-54.

31. Mukherjee A, Lutkenhaus J. Dynamic assembly of FtsZ regulated by GTP hydrolysis. EMBO J. 1998 15;17(2):462-9.

32. Mukherjee A, Lutkenhaus J. Analysis of FtsZ assembly by light scattering and determination of the role of divalent metal cations. J Bacteriol. 1999 181(3):823-32.

33. White EL, Ross LJ, Reynolds RC, Seitz LE, Moore GD, Borhani DW. Slow polymerization of Mycobacterium tuberculosis FtsZ. J Bacteriol. 2000 182(14):4028-34.

34. Oosawa, F., and S. Asakura. 1975. Thermodynamics of the polymerization of Protein. Academic Press, London. 41-5 1.

35. Romberg L, Simon M, Erickson HP. Polymerization of Ftsz, a bacterial homolog of tubulin. is assembly cooperative?. J Biol Chem. 2001 Apr 13;276(15):11743-53.

36. González JM, Vélez M, Jiménez M, Alfonso C, Schuck P, Mingorance J, Vicente M, Minton AP, Rivas G. Cooperative behavior of Escherichia coli cell-division protein FtsZ assembly involves the preferential cyclization of long single-stranded fibrils. Proc Natl Acad Sci USA, 2005. 102(6): p. 1895-1900.

37. Yu XC, Margolin W. Ca2+-mediated GTP-dependent dynamic assembly of bacterial cell division protein FtsZ into asters and polymer networks in vitro. EMBO J, 1997. 16(17): p. 5455-63.

38. Mukherjee A, Lutkenhaus J. Purification, assembly, and localization of FtsZ. Methods Enzymol. 1998;298:296-305.

39. Mingorance J, Rueda S, Gómez-Puertas P, Valencia A, Vicente M. Escherichia coli FtsZ polymers contain mostly GTP and have a high nucleotide turnover. Mol Microbiol. 2001 Jul;41(1):83-91.

40. González JM, Jiménez M, Vélez M, Mingorance J, Andreu JM, Vicente M, Rivas G. Essential cell division protein FtsZ assembles into one monomer-thick ribbons under conditions resembling the crowded intracellular environment. J Biol Chem, 2003. 278(39): p. 37664-71.

41. Popp D, Iwasa M, Narita A, Erickson HP, Maéda Y. FtsZ condensates: an in vitro electron microscopy study. Biopolymers, 2009. 91(5): p. 340-50.

42. Erickson HP, Taylor DW, Taylor KA, Bramhill D. Bacterial cell division protein FtsZ assembles into protofilament sheets and minirings, structural homologs of tubulin polymers. Proc Natl Acad Sci USA 1996. 93: p. 519-523.

43. González JM, Vélez M, Jiménez M, Alfonso C, Schuck P, Mingorance J, Vicente M, Minton AP, Rivas G. Cooperative behavior of Escherichia coli cell-division protein FtsZ assembly involves the preferential cyclization of long single-stranded fibrils. Proc Natl Acad Sci USA, 2005. 102(6): p. 1895-1900.

44. Vicente M, Rico AI. The order of the ring: assembly of Escherichia coli cell division components. Molecular microbiology 61, 5-8. 2006.

45. Adams DW, Errington J. Bacterial cell division: assembly, maintenance and disassembly of the Z ring. Nature reviews 7, 642-653. 2009.

46. Hale CA, Rhee AC, de Boer PA. ZipA-induced bundling of FtsZ polymers mediated by an interaction between C-terminal domains. J Bacteriology 182, 5153-5166, 2000.

47. RayChaudhuri D. ZipA is a MAP-Tau homolog and is essential for structural integrity of the cytokinetic FtsZ ring during bacterial cell division. EMBO J, 1999 18, 2372-2383.

48. Hale CA, de Boer PA. Recruitment of ZipA to the septal ring of Escherichia coli is dependent on FtsZ and independent of FtsA. J. Bacteriol. 181:167–176. 1999.

49. Erickson HP. The FtsZ protofilament and attachment of ZipA--structural constraints on the FtsZ power stroke. Current opinion in cell biology 2001, 13, 55-60.

50. Hale CA, de Boer PA. ZipA is required for recruitment of FtsK, FtsQ, FtsL, and FtsN to the septal ring in Escherichia coli. J bacteriol 2002, 184, 2552-2556.

51. Moreira IS, Fernandes PA, Ramos MJ. Detailed microscopic study of the full zipA:FtsZ interface. Proteins 63, 811-821. 2006.

52. Moy FJ, Glasfeld E, Mosyak L, Powers R. Solution structure of ZipA, a crucial component of Escherichia coli cell division. Biochemistry 39, 9146-9156. 2000.

53. Liu AP, Fletcher DA. Biology under construction: in vitro reconstitution of cellular function. Nat Rev Mol Cell Biol. 2009 10(9):644-50.

54. Yildirim MA, Goh KI, Cusick ME, Barabási AL, Vidal M. Drug-target network. Nat Biotechnol. 2007 Oct;25(10):1119-26.

55. Drews J. Drug discovery: a historical perspective. Science. 2000 Mar 17;287(5460):1960-4.

56. Galush WJ, Shelby SA, Mulvihill MJ, Tao A, Yang P, Groves JT. A nanocube plasmonic sensor for molecular binding on membrane surfaces. NANO LETTERS 2009 Vol. 9, No. 5 2077-2082.

57. Singer SJ, Nicolson GL. The fluid mosaic model of the structure of cell membranes. Science. 1972 Feb 18;175(4023):720-31.

58. Devaux PF, Seigneuret M. Specificity of lipid-protein interactions as determined by spectroscopic techniques. Biochim Biophys Acta, 1985. 822(1): p. 63-125.

59. Avanti Polar Lipids Inc. (http://avantilipids.com/)

60. Bugyi B, Didry D, Carlier MF. How tropomyosin regulates lamellipodial actin-based motility: a combined biochemical and reconstituted motility approach. EMBO J. 2010 Jan 6;29(1):14-26. Epub 2009 Nov 5.

61. Akin O, Mullins RD.Capping protein increases the rate of actin-based motility by promoting filament nucleation by the Arp2/3 complex. Cell, 2008. 133(5): p. 841-51.

62. Linseisen FM, Hetzer M, Brumm T, Bayerl TM. Differences in the physical properties of lipid monolayers and bilayers on a spherical solid support. Biophys. J. 72, 1997 1659-1667.

63. Ahmed S, Wunder SL. Effect of high surface curvature on the main phase transition of supported phospholipid bilayers on SiO2 nanoparticles. Langmuir. 2009 Apr 9;25(6):3682-91.

64. Tsuda K, Furuta N, Inaba H, Kawai S, Hanada K, Yoshimori T, Amano A. Functional analysis of alpha5beta1 integrin and lipid rafts in invasion of epithelial cells by

Porphyromonas gingivalis using fluorescent beads coated with bacterial membrane vesicles. Cell Struct Funct. 2008;33(1):123-32.

65. Lim YT, Lee KY, Lee K, Chung BH. Immobilization of histidine-tagged proteins by magnetic nanoparticles encapsulated with nitrilotriacetic acid (NTA)-phospholipids micelle. Biochemical and Biophysical Research Communications 344 (2006) 926–930.

66. Gopalakrishnan G, Rouiller I, Colman DR, Lennox RB. Supported bilayers formed from different phospholipids on spherical silica substrates. Langmuir. 2009 May 19;25(10):5455-8.

67. Nollert P, Kiefer H, Jähnig F. Lipid vesicle adsorption versus formation of planar bilayers on solid surfaces. Biophys. J. 1995, 69:1447-1455.

68. Tsoutsi D, Montenegro JM, Dommershausen F, Koert U, Liz-Marzán LM, Parak WJ, Álvarez-Puebla RA. Quantitative surface-enhanced Raman scattering ultradetection of atomic inorganic ions: the case of chloride. ACS Nano. 2011 Sep 27;5(9):7539-46.

69. Liu R, Lin S, Rallo R, Zhao Y, Damoiseaux R, Xia T, Lin S, Nel A, Cohen Y. Automated phenotype recognition for zebrafish embryo based in vivo high throughput toxicity screening of engineered nano-materials. PLoS One. 2012;7(4):e35014.

2.-OBJETIVOS

Esta Tesis Doctoral se ha centrado en dos objetivos principales:

- Caracterización de los mecanismos de oligomerización y polimerización de FtsZ y dependencia con sus cofactores.

- Desarrollo de métodos rápidos para la detección de la interacción FtsZ-ZipA en sistemas reconstituidos de membrana.

Los resultados obtenidos se han estructurado en tres capítulos redactados en formato manuscrito, y tres apéndices, seguidos de una discusión integradora y unas conclusiones finales:

Capítulo 1. Análisis biofísico de la polimerización de FtsZ en las formas GTP y GMPCPP: dependencia con la concentración de Mg^{2+}. Determinación de la masa molecular de los polímeros. Implicaciones en el mecanismo de ensamblaje.

Apéndice 1. Análisis biofísico de la oligomerización de FtsZ en la forma GDP: dependencia con la concentración de $Mg^{2+.}$

Capítulo 2. Análisis biofísico de la polimerización de FtsZ en las formas GTP y GMPCPP: dependencia con la fuerza iónica.

Capítulo 3. Estudio de las interacciones entre FtsZ y otros elementos del proto-anillo de división en sistemas de membrana soportados sobre microesferas funcionalizadas con sensores plasmónicos: detección mediante espectroscopía Raman aumentada por superficie (SERS).

Apéndice 2. Reconstitución de los elementos del proto-anillo en microesferas.

Apéndice 3. Caracterización de la interacción entre ZipA y FtsZ en su forma GDP mediante dispersión de luz estática en gradiente de concentración.

3.-MÉTODOS

En este apartado se pretende proporcionar una breve introducción de las técnicas empleadas en este trabajo. Las condiciones concretas, el tipo de análisis de datos, así como los modelos de ajuste utilizados en cada experimento se especifican en el apartado de materiales y métodos de cada capítulo individual.

3.1.-Dispersión de luz estática

Mediante esta técnica es posible obtener la masa molecular promedio de especies macromoleculares en disolución. La dispersión de luz estática, o dispersión Rayleigh, es la luz dispersada por las moléculas en una disolución, con la misma longitud de onda que la radiación incidente. La radiación electromagnética incidente es capaz de polarizar las moléculas que componen la muestra, desplazando sus electrones e induciendo la formación de un dipolo oscilante. Este dipolo oscilante inducido actúa como emisor de luz dispersada que radia en todas direcciones del plano de detección [(1)].

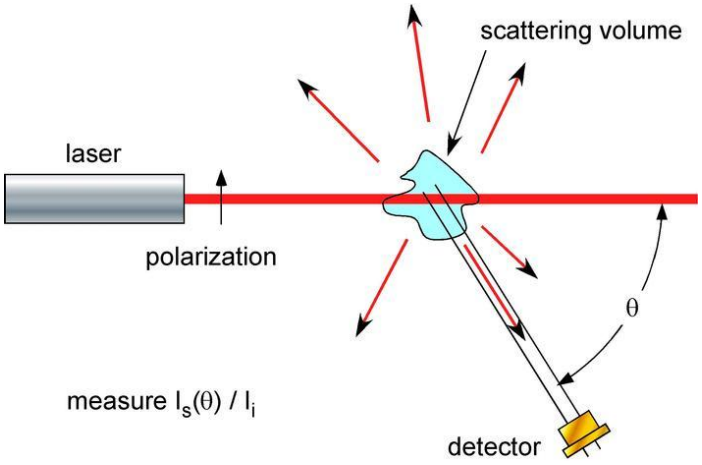

Figura 5. Diagrama esquemático del sistema de luz dispersada (2).

La dispersión de luz es proporcional a la masa molecular de las especies que compongan la muestra y a su concentración. Conociendo la concentración inicial y los ángulos a los cuales se mide, se puede relacionar la intensidad de luz dispersada para cada ángulo de medida con la masa molecular promedio de las especies en disolución. De esta manera se obtienen los valores de exceso de dispersión Rayleigh debida a la proteína, *R(θ,{w})*,

$$\frac{R(\theta, w_{tot})}{K} = \sum_{i=0}^{i_{max}} \sum_{j=1}^{j_{max}} C_{ij} \left[sen^2(\theta/2) \right]^i w_{tot}^j \qquad [1]$$

donde *{w}* representa la concentración de las especies presentes en la disolución, *i* y *j* indican la dependencia de la intensidad de luz dispersada con el ángulo y con la concentración total de especie, w_{tot}, C_{ij} es la masa de las especies, *K* es la constante óptica, definida por[3]:

$$K = \frac{4\pi^2 n_o^2}{\lambda^4 N_A} \left(\frac{dn}{dw_n} \right)^2 = K' \left(\frac{dn}{dw_n} \right)^2 \qquad [2]$$

donde, n_o, es el índice de refracción del tampón, λ es la longitud de onda de la luz dispersada en condiciones de vacío (690nm) y N_A es el número de Avogadro.

Se puede definir disolución ideal, con partículas isotrópicas, donde el exceso de luz dispersada Rayleigh a ángulo 0º esta definido por Stacey [4] según:

$$\langle R(0,\{w\}) \rangle = K' \sum_n \left(\frac{dn}{dw_n} \right)^2 M_n w_n \qquad [3]$$

donde, w_n, es la concentración de cada una de las *n* especies y viene dada en unidades de peso/volumen, (dn/dw_n), es la variación del índice de refracción con la concentración de cada una de las *n* especies presentes en la disolución y M_n es la masa molecular de cada una de las *n* especies. Proteínas sin grupos prostéticos, tienen generalmente $(dn/dw_n)=0.185\ ml/g$ constante a la longitud de onda y temperatura de trabajo (690nm) y 20^{o}C.

Cuando las especies responsables de la dispersión tienen la misma composición química, se puede asumir que la variación del índice de refracción con la concentración para cada una de las *n* especies va a ser constante. Por tanto, la ecuación 3 se simplifica de la siguiente forma:

$$\langle R_{\theta=0}(w_{tot})\rangle = K\sum_n M_n w_n = K w_{tot} M_{w,aver} \qquad [4]$$

donde $M_{w,aver}$, es la masa molar promedio de las especies presentes [3].

Ejemplos concretos de análisis y su desarrollo teórico se encuentra detallado en la referencia 3. En el capítulo 1 se puede encontrar el análisis aplicando un modelo de asociación isodésmico. En el capítulo 2, además, se puede encontrar el caso de especies angularmente dependientes.

3.2.-Dispersión de luz dinámica

La dispersión de luz dinámica, es una técnica que permite calcular los coeficientes de difusión. Para ello, se enfoca un láser sobre una pequeña región de la muestra. La mayoría de la luz atraviesa la muestra, pero una pequeña proporción de la luz incidente es dispersada y detectada a un ángulo de 90^{o}, en este caso, respecto de la dirección del haz incidente. El movimiento browniano de las moléculas en la disolución produce fluctuaciones (en la escala de los microsegundos a los milisegundos) en la intensidad de la

luz dispersada como consecuencia de la entrada y salida de estas partículas de la región por la que pasa el haz. La frecuencia de estas fluctuaciones en la intensidad de la luz dispersada, está relacionada con la difusión de las moléculas [5]. El análisis de las fluctuaciones en la intensidad de luz dispersada, se realiza mediante la obtención de la función de autocorrelación. Esta función, describe la correlación entre las intensidades de luz dispersada a tiempo t y las intensidades a un tiempo posterior $t + \tau$, donde τ es el tiempo de correlación [6]. La intensidad de luz dispersada, depende de la posición de las partículas en el volumen analizado. Por ello, a tiempos cortos, la correlación es alta, porque la posición de las partículas está muy relacionada con la posición que tenían anteriormente. A tiempos largos, la correlación es menor, y por ello la función de autocorrelación decae con el tiempo. La relación entre ambas propiedades se establece en la siguiente ecuación:

$$g(t) = 1 + e^{-Dq^2 t} \qquad [5]$$

donde $g(t)$ es la función de autocorrelación, D es el coeficiente de difusión de la molécula, t el tiempo, q es el vector de dispersión de luz,

$$q = \frac{4\pi n}{\lambda} \, sen \frac{\theta}{2} \qquad [6]$$

donde n es el índice de refracción del disolvente, λ la longitud de onda de la luz incidente, y θ el ángulo de dispersión de la luz [6].

En el capítulo 1, 2 y 3 se pueden encontrar ejemplos de la utilización de esta técnica y su análisis.

3.3.-Velocidad de sedimentación

Mediante el uso de esta técnica, las especies presentes en la disolución se fraccionan en función de su masa, forma y densidad. Por tanto podemos obtener un perfil de las especies presentes y su concentración relativa. Durante un experimento de velocidad de sedimentación las moléculas están sometidas a un elevado campo centrífugo. Esto provoca que la fuerza centrífuga supere a la de difusión, produciéndose un transporte neto de materia en el sistema. El flujo de sedimentación en disolución de una especie molecular *i* que se encuentra girando con una velocidad angular ω viene descrito por la ecuación de Lamm:

$$J_i = s_i w_i \omega^2 - D_i \frac{dw_i}{dr} \qquad [7]$$

donde J_i es el flujo de la especie *i* en unidades de masa/(área · tiempo), w_i es su concentración (peso/volumen), ω es la velocidad angular del rotor (radianes/segundo), *r* es la posición radial s_i y D_i y son los coeficientes de sedimentación y difusión traslacional de la especie molecular respectivamente, siendo ambos coeficientes propiedades de la especie molecular en un determinado disolvente. El coeficiente de sedimentación viene dado por:

$$s_i = \frac{M_i(1-\nu_i\rho_0)}{N_A f_{sed,i}} = \frac{M_i^*}{N_A f_{sed,i}} \qquad [8]$$

donde, M_i , v_i y $f_{sed,i}$ y son respectivamente, la masa molecular, el volumen específico parcial y el coeficiente de fricción para la sedimentación de la especie *i*, ρ_o es la densidad

del disolvente y N_A es el número de Avogadro. El producto $M_i (1-v_i \rho_o)$ se denomina masa molecular de flotación, M_i^*. A su vez, el coeficiente de difusión viene dado por:

$$D_i = \frac{RT}{N_A f_{dif,i}} \qquad [9]$$

donde R es la constante de los gases ideales, T es la temperatura absoluta y $f_{dif,i}$ el coeficiente de fricción para la difusión.

Los coeficientes de fricción definidos son función del tamaño y de la forma de la macromolécula, así como de su interacción con el disolvente y con otras moléculas de soluto. En el límite de idealidad, estos dos coeficientes, $f_{sed,i}$ y $f_{dif,i}$ son iguales [6]. Por tanto, combinando las ecuaciones 8 y 9 se llega a la siguiente expresión, la ecuación de Svedberg:

$$\frac{s_i}{D_i} = \frac{M_i^*}{RT} \qquad [10]$$

El análisis de los perfiles de sedimentación obtenidos a intervalos de tiempo regulares se realiza mediante el ajuste directo de las soluciones a la ecuación de Lamm (ecuación [7]) con el programa SEDFIT [7, 8].

En los capítulos 1, 2 y 3 se muestran diversos ejemplos de análisis por velocidad de sedimentación.

3.4.-Equilibrio de sedimentación

Mediante esta técnica podemos obtener información termodinámica acerca de la masa molecular promedio, estequiometría y afinidad de unión de las proteínas estudiadas, estableciéndose por tanto una complementareidad entre la información aportada por los experimentos de equilibrio de sedimentación y los de CG-SLS.

Dada una disolución uniforme, que se somete a una fuerza centrífuga moderada se establece un equilibrio entre el proceso de sedimentación de las macromoléculas hacia el fondo de la celda, y el proceso de difusión que se opone al anterior. El equilibrio se alcanza cuando, transcurrido un tiempo, los dos procesos se igualan y como resultado el transporte neto se anula ($J_i=0$); llegado este punto, las macromoléculas estarán distribuidas formando un gradiente de concentración creciente hacia el fondo de la celda que no variará con el tiempo.

Para una situación de equilibrio $J_i=0$, combinando las ecuaciones 7 y 10 se obtiene la ecuación:

$$\frac{d\mathrm{Ln}\, w_i}{dr^2} = \frac{M_i^* w^2}{2RT} \qquad [11]$$

Donde *w* es la concentración y *r* es el radio de la celda de medida. Si esta expresión es integrada respecto a r^2, obtendremos la ecuación de equilibrio para la sedimentación de un soluto ideal.

$$w_i(r) = w_i(r_0)^{\left(\frac{M_i^* w^2}{2RT}(r^2 - r_0^2)\right)} \qquad [12]$$

Donde r_0 indica la posición de referencia donde empieza el gradiente. El gradiente en el equilibrio, se caracteriza fundamentalmente porque es invariante con el tiempo, es independiente de las propiedades hidrodinámicas del soluto, y depende únicamente de la masa molecular de flotación (M_i^*). En los experimentos de equilibrio de sedimentación, el tiempo necesario para alcanzar el equilibrio depende de la velocidad utilizada, del tamaño

de la macromolécula y de la longitud de la columna que es la distancia desde el menisco hasta el fondo de la celda.

Con el ajuste de la ecuación 12 al gradiente obtenido en el equilibrio, mediante el software Heteroanalisys, obtenemos la masa molecular aparente de flotación [9]. El volumen específico parcial de las proteínas se calcula como el promedio en peso de los valores de volumen específico parcial de los aminoácidos de la proteína mediante el programa SEDNTERP.

3.5.-Espectroscopía de correlación de Fluorescencia (FCS)

Mediante la técnica de espectroscopia de correlación de fluorescencia, se miden las fluctuaciones temporales aleatorias de moléculas fluorescentes cuando atraviesan un pequeño volumen de observación. De esta manera, podemos determinar parámetros químico-físicos característicos de la proteína fluorescente para descifrar procesos de dinámica molecular como la difusión o fluctuaciones conformacionales. Se utiliza un laser pulsado (Ti:Zafiro) que se enfoca al limite de difracción. Moléculas fluorescentes difundiéndo en el medio pueden pasar por el volumen iluminado. A través del proceso de excitación de dos fotones, las moléculas que difunden dentro del volumen, generan un fotón. Este fotón, es capturado por la misma óptica que enfoca al láser y es transmitido a detectores a través de filtros ópticos. Finalmente, el fotón es detectado por un diodo de avalancha.

Si se observa el volumen por un tiempo largo, del orden de segundos, a altas frecuencias de adquisición (GHz), se pueden capturar miles de fotones. El vector de tiempos de la llegada de los fotones se puede promediar para generar una señal analógica. Las fluctuaciones con respecto al promedio de la intensidad de este nuevo vector, dependen del tamaño de la iluminación y el coeficiente de difusión. Si las moléculas se desplazan en el volumen de observación, la intensidad de fluorescencia a un tiempo t estará correlacionada a un tiempo $t + \tau$. De esta manera el método de correlación, analiza la intensidad de fluorescencia media $F(t)$ autocorrelacionando las fluctuaciones alrededor del valor medio de fluorescencia $\langle F(t) \rangle$ en un periodo finito de tiempo. El análisis de la

función de autocorrelación puede proveer información acerca del coeficiente de difusión y concentración absoluta.

La función de autocorrelación se define como:

$$G(\tau) = \frac{\langle \delta F(t) \delta F(t+\tau) \rangle}{\langle F(t) \rangle^2} = \frac{\langle F(t) F(t+\tau) \rangle}{\langle F(t) \rangle^2} - 1 \qquad [13]$$

Donde $\delta F(t) = F(t) - \langle F(t) \rangle$. El promedio de intensidad esta dado por:

$$\langle F(t) \rangle = \frac{1}{T} \int_0^T F(t) dt \qquad [14]$$

Donde T es el tiempo total de observación [10].

3.6.-Espectroscopía Raman aumentada por superficie (SERS)

La espectroscopia de dispersión Raman aumentada por superficie (*surface-enhanced Raman scatering*, SERS) es una técnica espectroscópica que combina la espectroscopia láser con las propiedades ópticas (plasmones localizados) características de las nanoestructuras metálicas. Esta interacción láser-plasmón da como resultado un enorme aumento de la señal Raman proveniente de sistemas moleculares situados en la proximidad de dichas nanoestructuras. Este aumento puede llegar hasta 14 órdenes de magnitud respecto a la señal obtenida mediante dispersión Raman convencional. El espectro obtenido es esencialmente un espectro de vibración y, por tanto, contiene toda la información estructural del sistema molecular estudiado [11, 12]. Estas capacidades se combinan para tener la posibilidad de elucidar no sólo la estructura, sino también, la reactividad de los sistemas moleculares bajo estudio. Esta espectroscopia, es por tanto,

una técnica versátil que permite su aplicación analítica en campos tan diversos como la ciencia de materiales, química analítica, biomedicina o ciencias medioambientales [13].

En la dispersión Raman (Raman scattering, RS) convencional, la intensidad de la dispersión Stokes $P^{RS}(\nu_S)$ es proporcional a la sección eficaz Raman σ^R_{free}, a la intensidad del láser de excitación $I(\nu_L)$, y al número de moléculas *N* contenidas en el volumen irradiado:

$$P^{RS}(\nu_S) = N\sigma^R_{free} I(\nu_L) \qquad [15]$$

El efecto SERS se debe fundamentalmente a dos efectos, por una parte, un mecanismo electromagnético (EM), según el cual, la señal aumenta debido al acoplamiento de la molécula, con los campos electromagnéticos locales generados por las nanoestructuras metálicas cuando son excitados con un haz de fotones. Este primer mecanismo es esencial en SERS, y supone incrementos de intensidad de la señal de 5-7 órdenes de magnitud respecto a RS. Por otro lado, la proximidad de la molécula a la nanoestructura, genera transferencia de carga entre los orbitales HOMO-LUMO de la molécula y la banda de conducción del metal. Este fenómeno se conoce como mecanismo químico o de transferencia de carga (CT). El mecanismo químico no es esencial para obtener SERS, sin embargo, los límites de detección necesarios para detectar una sola molécula, sólo se alcanzan cuando ambos mecanismos actúan conjuntamente. Para que ocurra transferencia de carga, es necesario un contacto intimo molécula-nanoestructura, por ese motivo, la aparición del segundo mecanismo sólo se produce en la primera capa quimisorbida o fisisorbida. De acuerdo con los dos mecanismos descritos, la ecuación 15 toma la siguiente forma:

$$P^{SERS}(\nu_S) = N'\sigma^R_{ads}|A(\nu_L)|^2|A(\nu_S)|^2 I(\nu_L) \qquad [16]$$

donde, $A(v_L)$ y $A(v_S)$ definen los factores de aumento para el láser y para la RS, respectivamente; σ^R_{ads} describe la sección eficaz aumentada del nuevo proceso Raman de la molécula adsorbida y *N'* es el número de moléculas que están involucradas en el proceso SERS y puede ser menor que el número de moléculas *N* [14-17].

En muchos casos, los sustratos activos en SERS están formados por un grupo de nanopartículas de oro y/o plata, tales como agregados de partículas o películas delgadas que contienen islas metálicas. En estos agregados, los dipolos oscilantes (plasmones) individuales de cada una de las partículas que los forman, se acoplan entre sí, generando modos plasmónicos para el agregado en un intervalo amplio de frecuencias, que abarcan desde la región del visible hasta el infrarrojo cercano (NIR). Hay que tener en cuenta, sin embargo, que la excitación del campo no está distribuida uniformemente sobre el conjunto del agregado, sino que tiende a estar localizada espacialmente en las denominadas "zonas o puntos calientes" (*hot spots*). El tamaño de los *hot spots* suele ser pequeño, del orden de unos pocos nanómetros y su localización depende fuertemente de la geometría del agregado, de la longitud de onda de excitación y de la polarización de los campos. Cuando la excitación óptica está localizada en *hot spots* pequeños, el aumento electromagnético SERS es extremadamente elevado [16, 11, 18].

Referencias

1. Técnicas de caracterización de polímeros, Miguel Ángel Llorente Uceta, Arturo Horta Zubiaga, Publicaciones UNED, ISBN: 8436226100 ISBN-13: 9788436226102 (1990)

2. http://www.wyatt.com/

3. Attri AK, Minton AP. New methods for measuring macromolecular interactions in solution via static light scattering: basic methodology and application to nonassociating and self-associating proteins. Analytical Biochemistry 337 (2005) 103–110.

4. K.A. Stacey, Light-Scattering in Physical Chemistry, Academic Press, New York, 1956.

5. Murphy RM. Static and dynamic light scattering of biological macromolecules: what can we learn?. Curr Opin Biotechnol. 1997 Feb 1;8(1):25-30.

6. van Holde, K.E., Johnson, W.C. y Ho, P.S. (1998) Principles of Physical Biochemistry. Prentice-Hall, Inc., Upper Saddle River, New Jersey.

7. Schuck P, Rossmanith P. Determination of the sedimentation coefficient distribution by least-squares boundary modeling. Biopolymers. 2000 Oct 15;54(5):328-41.

8. Schuck P. Some statistical properties of differencing schemes for baseline correction of sedimentation velocity data. Analytical Biochemistry 401 (2010) 280–287

9. Cole JL. Analysis of heterogeneous interactions. Meth. Enzym. 384 212-232.(2004).

10. Elliot L. Elson, Douglas Magde. Fluorescence correlation spectroscopy. I. Conceptual basis and theory. Biopolymers, 13, 1–27. 1974.

11. Katrin Kneipp, Yang Wang, Harald Kneipp, Lev T. Perelman, Irving Itzkan, Ramachandra R. Dasari, and Michael S. Feld. Single Molecule Detection Using Surface-Enhanced Raman Scattering (SERS). Physical Review Letters, (1997) 78, 1667.

12. Nie S, Emory SR. Probing Single Molecules and Single Nanoparticles by Surface-Enhanced Raman Scattering. Science (1997) 275, 1102.

13. Katrin Kneipp[1], Harald Kneipp, Irving Itzkan, Ramachandra R Dasari and Michael S Feld. Surface-enhanced Raman scattering and biophysics. Journal of Physics Condensed Matter, (2002) 14, R597.

14. Martin Moskovits. Surface-enhanced spectroscopy. Reviews of Modern Physics, (1985) 57, 783.

15. R.F. Aroca, R.A. Alvarez-Puebla, N. Pieczonka, S. Sanchez-Cortez, J.V. Garcia-Ramos. Surface-enhanced Raman scattering on colloidal nanostructures. Advances in colloid and interface science, (2005) 116, 45.

16. K. Kneipp, H. Kneipp, P. Corio, S. D. M. Brown, K. Shafer, J. Motz, L. T. Perelman, E. B. Hanlon, A. Marucci, G. Dresselhaus, and M. S. Dresselhaus. Surface-Enhanced and Normal Stokes and Anti-Stokes Raman Spectroscopy of Single-Walled Carbon Nanotubes. Physical Review Letters, (2000) 84, 3470.

17. E. Hesse and J. A. Creighton. Investigation by Surface-Enhanced Raman Spectroscopy of the Effect of Oxygen and Hydrogen Plasmas on Adsorbate-Covered Gold and Silver Island Films. Langmuir (1999) 15, 3545.

18. Kneipp, Katrin; Kneipp, Harald; Kartha, V. Bhaskaran; Manoharan, Ramasamy; Deinum, Geurt; Itzkan, Irving; Dasari, Ramachandra R.; Feld, Michael S. Detection and identification of a single DNA base molecule using surface-enhanced Raman scattering (SERS). Physical Review E: Statistical Physics, Plasmas, Fluids, and Related Interdisciplinary Topics, (1998) 57, R6281.

CHAPTER I

Mg^{2+}-linked self-assembly of FtsZ in the presence of GTP or a GTP analog involves the concerted formation of a narrow distribution of oligomeric species

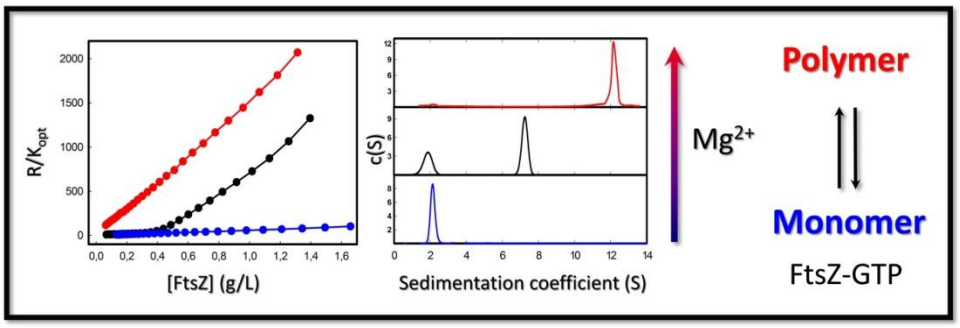

The assembly of the bacterial cell division FtsZ protein in the presence of constantly replenished GTP was studied as a function of Mg^{2+} concentration (at neutral pH and 0.5 M potassium) under steady-state conditions by sedimentation velocity, concentration-gradient light scattering, fluorescence correlation spectroscopy and dynamic light scattering. Sedimentation velocity measurements confirmed previous results indicating cooperative appearance of a narrow size distribution of oligomeric species with increasing protein concentration. The concentration dependence of light scattering and diffusion coefficients independently verified the cooperative appearance of a narrow size distribution of oligomeric species, and in addition provided a measurement of the average size of these species, which corresponds to 100 ± 20 FtsZ protomers at millimolar Mg^{2+} concentration. Parallel experiments on solutions containing GMPCPP, a slowly hydrolysable analog of GTP, in place of GTP, likewise indicated the concerted formation of a narrow size distribution of stable oligomers with a larger average mass (corresponding to 160 ± 20 FtsZ monomers). The closely similar behavior of FtsZ in the presence of both GTP and GMPCPP suggests that the observations reflect equilibrium rather than non-equilibrium steady-state properties of both solutions and exhibit parallel manifestations of a common association scheme.

INTRODUCTION

FtsZ is an essential protein required for septation in most bacteria, in archaea and in some organelles. It is an early septum component, forms a ring at midcell and it is thought to be responsible for initiating and driving cell constriction [1-3]. FtsZ shares structural, but not sequence, homology with eukaryotic tubulin, as well as its GTPase activity and its capacity to polymerize. Unlike tubulin, FtsZ requires binding of nucleotide and divalent cations for folding. These properties suggest the two proteins have different modes of action [3]. The self-association of FtsZ in the presence of GDP and its polymerization in the presence of GTP have been studied extensively [3, 4]. While the mechanism of GDP-FtsZ oligomer formation is relatively well understood, that is not the case for the GTP-linked FtsZ polymerization. In the presence of GTP, FtsZ polymerizes in an apparently cooperative manner to form single stranded protofilaments that, depending upon solution and working conditions (buffer composition, temperature, protein density, surface effects, excluded volume and electrostatic non-specific effects of macromolecular additives, specific effects of other cell division proteins) can adopt a variety of supramolecular structures: flexible single and multi-stranded fibers, circles, ribbons, bundles and toroids [1, 3, 5-8]. This polymorphism is due to the structural plasticity of FtsZ polymers: it would take only a very small free energy perturbation to change the structural organization of the intermolecular interface and bring about large changes in the geometry of the fibers [9].

Erickson and co-workers have established that FtsZ polymers are highly dynamic both *in vivo* [10] and *in vitro* [11]. In the former study, they bleached part of a fluorescent Z-ring in a bacterium that has been engineered to produce fluorescent FtsZ, and observed that the fluorescence recovers in ca. 10-30 seconds [10]. While this finding establishes a dynamic exchange of FtsZ between the Z-ring and the cytoplasm, the implications for the kinetics or pseudo-equilibria governing fiber or Z-ring assembly are not at all clear. The dynamic character of FtsZ polymers linked to the GTPase activity of the protein constitutes an additional challenge to study FtsZ assembly in the presence of GTP, which requires special procedures for the maintenance of polymer stability throughout the duration of a typical biochemical and biophysical experiment [6]. The variety of quantitative techniques that have been applied to study FtsZ assembly is consequently low compared to the variety of techniques utilized to study other protein assembly systems. Moreover, different research groups have studied assembly

under differing solution conditions (pH, ionic strength, buffer composition). These facts may in part explain disagreements that have arisen during the last years regarding the mechanism of FtsZ polymerization in the presence of GTP [5, 9].

The dependence on protein concentration of the sedimentation coefficient distribution of FtsZ in the presence of GTP and Mg^{2+} was measured by sedimentation velocity [9]. In that study an enzymatic GTP regenerating system (GTP-RS) was added to the solutions to avoid GTP depletion, and hence polymer disassembly, during sufficient time to perform the sedimentation velocity measurements reported under steady-state conditions. The data clearly showed a system consisting of a well separated slowly sedimenting fraction and a rapid species. With increasing total protein concentration, the abundance of the slowly sedimenting fraction was reduced while the amount of the fast species increased. The rapid fraction corresponded to a finitely sized distribution of species with an *s*-value of around 13 S, which did not grow indefinitely upon increasing protein concentration. This behavior resembled a condensation reaction in which the condensed species was soluble and with a relatively narrow size distribution.

The motivation of this work is to confirm and extend the previous experimental observations, to obtain a model-free estimate of the oligomer size and the dependence of oligomer size upon Mg concentration, to verify the existence of a phase transition-like cooperativity of oligomer formation on the assembly pathway, and to test whether this concerted transition reflects or not a quasi-equilibrium behavior, and does not derive from a precarious balance of competing hydrolytic and nucleotide exchange reactions far from equilibrium. With these goals, we have carried out parallel studies of FtsZ assembly using a combination of biophysical methodologies (sedimentation velocity, concentration gradient static and dynamic light scattering, and fluorescence correlation spectroscopy) to more clearly elucidate the nature of the self-assembly process under a well-defined set of experimental conditions, close to physiological (neutral pH, 0.5 M potassium). These studies were done over a broad range of Mg and protein concentrations under working conditions comparable to those utilized in previous work [9]. Experiments were first performed with FtsZ under steady-state conditions in the presence of GTP and the GTP-RS. To assess the possible contribution of effects arising from GTP hydrolysis and nucleotide exchange on the behavior of the system, parallel experiments were

conducted in the presence of GMPCPP, a GTP analog which is hydrolyzed at a rate that is only 4% that of FtsZ-catalyzed hydrolysis of GTP under the conditions of our experiments [14].

EXPERIMENTAL PROCEDURES

Materials. Guanine nucleotides were from Jena. Other analytical grade chemicals were from Sigma. Even if not specifically mentioned, in all the GTP-induced assembly experiments the GTP was regenerated using a GTP-regenerating system (1 unit/mL acetate kinase, 15 mM acetyl phosphate) as previously described [6] to maintain FtsZ polymers at steady-state during the time scale of the experiments.

FtsZ purification and labeling. *E. coli* FtsZ was purified by the Ca^{2+}-induced precipitation method as described [4] and stored at -80^{o}C in the ionic exchange elution buffer. Immediately before use, FtsZ was dialyzed in the working buffer (50 mM Tris-HCl, pH 7.5, 500 mM KCl) supplemented with the specified concentrations of $MgCl_2$. Protein labeling with Alexa 488 carboxylic acid succinimidyl ester dye was performed in polymeric form as described in detail elsewhere [15, 16], rendering labeled FtsZ that behaves as the unlabeled protein in terms of polymerization [6, 16]. The Alexa 488 dye was selected for being highly photo-stable, very bright and quite hydrophilic. The degree of labeling of FtsZ, estimated from the molar absorption coefficients of the fluorophore and the protein, was 30-50%.

Sedimentation velocity (SV). The experiments were carried out in a Beckman Optima XL-I ultracentrifuge (Beckman-Coulter) equipped with interference optics that allows monitoring FtsZ sedimentation at physiological (mM) GTP concentrations. FtsZ (0.5 – 1 g/L) was equilibrated in working buffer (over a broad range of Mg^{2+} concentrations) and, just before the sedimentation experiment, supplemented with millimolar GTP or GMPCPP. FtsZ samples were centrifuged at 30000 rpm and 25^{o}C using an An50Ti eight-hole rotor and double-sector Epon-charcoal centerpieces. Differential sedimentation coefficient distributions *c(s)* were calculated by least-squares boundary modeling of the experimental data using SEDFIT [17].

Static light scattering (CG-SLS)

Multi-angle light scattering. Measurements of angular dependence of scattering over a broad range of FtsZ concentrations were carried out in a DAWN-EOS multi-angle light scattering photometer equipped with a Calypso system (Wyatt Technology Corp, Santa Barbara) consisting of a software-controlled multiple syringe pump used to create the concentration gradient and an Optilab rEX differential refractometer configured to collect data in parallel from the incoming sample stream. All components of the GTP-RS or GMPCPP were supplemented at each gradient step to maintain constant concentration of these components throughout FtsZ gradient. Data were collected at 20^{o}C with 1% sensitivity of the detectors. The raw data acquired consist of the time-dependent scattering intensity at fourteen scattering angles and the time-dependent differential refractive index. The Rayleigh ratio was calculated from the raw scattering intensity, and the w/v concentration of protein, *w*, calculated from the differential refractive index as described in [18, 19], except that an empirical constant of proportionality between *dRI* and *w* was used to calculate the w/v concentration as a function of time. The results are expressed as the concentration and angle-dependent Rayleigh ratio $R(w,\theta)$ in units of an optical constant

$$K_{opt} = \frac{4\pi^2 n_0^2}{N_A \lambda_0^4}\left(\frac{dn}{dw}\right)^2 \qquad [1]$$

where n_0, N_A and λ_0 denote the solvent refractive index, Avogadro's number and the vacuum wavelength of incident light (690 nm), respectively, and dn/dw is the specific refractive index increment of the protein, taken as 0.185 cm^3/g [19].

90^{o} Static Light Scattering. Measurements of the dependence of scattering intensity at 90^{o} upon FtsZ concentration were performed in a modified mini-DAWN light scattering photometer (Wyatt Technology Corp., Santa Barbara) using an automated dilution protocol as described [20]. The composition of the sample solution and the dilution buffer were the same to maintain constant concentration of all the components present in the GTP and GMPCPP solutions throughout the process of FtsZ dilution. Preliminary measurements of scattering intensity established that FtsZ species formed in the presence of GTP plus GTP-RS or GMPCPP were stable over periods of time far exceeding the

duration of a dilution experiment. Concentration of protein at each dilution step was calculated from the initial concentration and raw scattering intensity data was converted to the scaled Rayleigh ratio $R(w,90^o)/K_{opt}$ as described in [20].

Dynamic light scattering assays (DLS). DLS experiments were carried out in a Protein Solutions DynaPro MS/X instrument (Protein Solutions, Piscataway, NJ) at 25°C using a 90° light scattering cuvette. Previous to measurements, samples were filtered twice with 0.1 µm Anotop 10 Plus filters (Whatman) and subsequently centrifuged during 30 minutes at 100000 × *g* and 4°C. Data were collected and exported as text files with Dynamics V6 Software, and analyzed using user-written scripts and functions in MATLAB (Ver. 7.10, MathWorks, Natick, MA). Data correspond to a minimum of two independent measurements each of which was the average of at least 7 replicates.

DLS data are reported in the form of an autocorrelation function describing the time-dependence of the correlation between scattering intensity at any given time and the intensity at a subsequent increment of time τ. For a single scattering species, the auto-correlation function is given by [21]

$$ACF(\tau) = ACF_{\infty} + \left(ACF_0 - ACF_{\infty}\right)\exp(-2Dq^2\tau) \qquad [2]$$

where

$$q = \frac{4\pi n_0}{\lambda_0}\sin\left(\frac{\pi}{4}\right)$$

ACF_0 and ACF_{∞} respectively denote the values of ACF in the short and long time limits, q denotes the scattering vector at 90°, n_0 and λ_0 are the solvent refractive index and the wavelength of incident light, and D is the translational diffusion coefficient of the scattering species. In the present work, the scattering arises from an as-yet-undefined mixture of scattering species, and in this case the autocorrelation function is more appropriately described by an empirical exponential function of the kind used for analysis of the slowly sedimenting component of fibrinogen fibrin and protofibrils [22].

$$ACF = ACF_{\infty} + (ACF_0 - ACF_{\infty})\exp\left[-\left(D_{app}q^2\tau\right)^{\beta}\right]^2 \qquad [3]$$

where D_{app} represents an apparent average diffusion coefficient, and β is a parameter that decreases from unity with the width of the distribution of diffusion coefficients. For each set of experimental conditions, equation [3] was fit to experimental autocorrelation functions via nonlinear least squares to obtain the best-fit value of the apparent diffusion coefficient, which was then corrected to a standard temperature and solvent viscosity (20º C, water) for comparison with the results obtained by other techniques. Since D_{app} is an average, it may vary with total protein concentration when the protein is undergoing equilibrium self-association.

Fluorescence correlation spectroscopy (FCS) assays. FCS measurements were carried out under two-photon excitation on a MicroTime 200 system (PicoQuant, Berlin, Germany) with the setup described elsewhere [16]. 5-10 autocorrelation curves were acquired for each sample during 1 minute each at 21°C and globally analyzed with the FFS Data processor software (Scientific Software Technologies Center, Belarus) [23] using the following expression, in which it is assumed that the samples are excited by a three dimensional Gaussian beam:

$$G(\tau) = 1 + G(0)\sum_i \left[f_i \left(1 + \tau / \tau_{Di} \right)^{-1} \left(1 + \tau / S^2 \tau_{Di} \right)^{-1/2} \right] \qquad [4]$$

where *G(0)* is the amplitude of the autocorrelation function. *S* is a structure parameter ($S = z_0/r_0$ where r_0 and z_0 are the lateral and axial dimensions of the effective detection volume), which varied from 3 to 6 as determined by calibration with fluorescein or rhodamine 110 solutions. τ_{Di} is the translational diffusion time of the fluorescent particle *i* ($\tau_{Di} = r_0^2/8D_i$, for two-photon excitation, where D_i is the translational diffusion coefficient). The r_0 value was estimated from the calibration assuming *D* of 400 $\mu m^2/s$ and 435 $\mu m^2/s$ for fluorescein and rhodamine 110, respectively [24-26]. f_i is the fractional contribution of species *i* to the autocorrelation function. A two species model was fit to the autocorrelation curves for samples containing unpolymerized FtsZ-Alexa 488 [16], the faster one indicating the presence of minor fractions (~10-20%) of free dye in the samples and the other one corresponding to the unassembled protein. The fast component was also found in the solutions containing assembled FtsZ and its translational diffusion time was fixed to that measured for Alexa 488

in the same buffer (corresponding to a D ~400 $\mu m^2/s$). Preparations of labeled protein containing different amounts of free dye rendered translational diffusion coefficients equivalent within the error for the polymer. To fit the autocorrelation traces obtained in the presence of GTP or GMPCPP, two other components corresponding to the slowly diffusing polymeric species and to unassembled protein were required (*16*). The translational diffusion time of the unpolymerized protein was fixed to that obtained for FtsZ in the absence of GTP or GMPCPP (corresponding to a D ~50 $\mu m^2/s$) and its contribution varied depending on the total FtsZ concentration in the solution and on the buffer conditions. Slight variations in the fraction of unassembled FtsZ (for a given buffer and protein concentration) were observed depending on the preparation of labeled protein used, which, however, did not have any effect on the translational diffusion coefficient retrieved for the polymeric species. D values given here were normalized to standard conditions (20°C, water) and represent the average of at least 3 independent measurements.

The concentration of FtsZ-Alexa 488 was typically 0.006 g/L (150 nM) and the final protein concentration was achieved by adding unlabeled protein. No significant changes in the spectral properties of the Alexa 488 dye were observed upon incorporation of the protein to the polymers [16], and equivalent autocorrelation curves were obtained at different distances (from 10 to 30 μm) from the cover-slip surface. Some measurements of the translational diffusion coefficient of assembled FtsZ were also performed using fluorescein or tetramethylrhodamine labeled FtsZ with the same result as reported here for the Alexa 488 labeled protein.

Estimate of molar mass of FtsZ polymers from hydrodynamic measurements. The apparent molar mass of a single sedimenting solute species, M, may be calculated using measured values of the sedimentation coefficient s and the diffusion coefficient D according to the Svedberg equation [27]

$$M = \frac{RT}{(1-\bar{v}\rho)} \frac{s_{20,w}}{D_{20,w}} \qquad [5]$$

where T, R and ρ respectively denote the absolute temperature, the universal gas constant and the density of the solution and $\bar{v}$ the partial specific volume of the solute. It is stressed that since the frictional coefficients for sedimentation and diffusion cancel in the derivation of equation [5], the estimate of molar mass obtained via this relation is valid independent of the structure of the

sedimenting/diffusing species. As described in the results section, at high magnesium concentration both sedimentation and diffusion measurements indicate the presence of a narrow size distribution of oligomeric species. We assume that the Svedberg relation holds approximately for such a distribution [28], and utilize the average value of *s* obtained from analysis of sedimentation velocity and the average of the *D* values obtained from analysis of dynamic light scattering and fluorescence correlation spectroscopy.

RESULTS

Sedimentation velocity

Distributions of sedimentation coefficients, obtained from SEDFIT analysis of the sedimenting boundaries, are plotted in **Figure 1** for 1 g/L solutions prepared at different Mg^{2+} concentrations in the presence of millimolar GTP supplemented with the GTP-regenerating system. At millimolar magnesium, > 95% of the protein sedimented with an experimental *s*-value of around 13 S, while the corresponding GDP-form of FtsZ sedimented as a mixture of monomers and dimers, with s-values around 3 and 4 S, confirming our previous observations [9]. The sedimentation coefficient distribution of GTP-FtsZ polymers changed dramatically upon lowering the Mg^{2+} concentration. At cation concentrations between 10-100 µM, the sedimentation data were well described by two main sedimenting species with *s*-values around 2.5 and 6-7 S, respectively. The relative concentration of these two species changed with Mg^{2+} (the 2.5 S species predominating at lower Mg^{2+}), a characteristic feature of Mg^{2+}-linked self-association reactions [4]. In the presence of EDTA, the protein sedimented as a single peak with *s*-value of 2.5 S, compatible with a protein monomer whose shape deviates from the expected behavior of a globular protein.

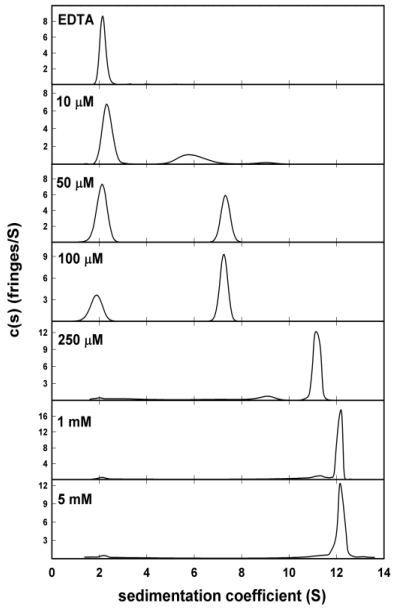

Figure 1. Mg^{2+} dependence of FtsZ sedimentation velocity in the presence of 1 mM GTP + GTP-RS: Sedimentation profiles of 1 g/L FtsZ equilibrated in working buffer at the magnesium concentrations specified in the figure.

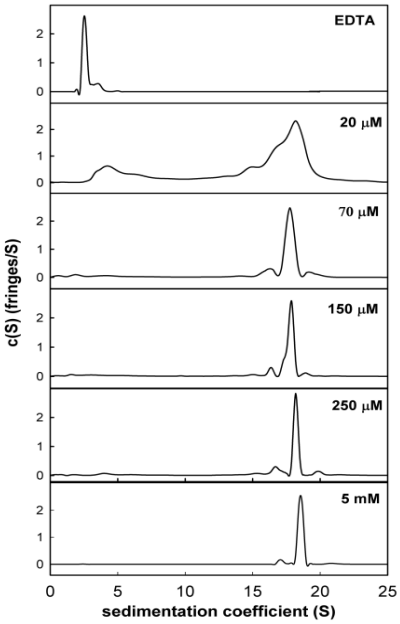

Figure 2. Sedimentation velocity analysis of FtsZ in the presence of 1 mM GMPCPP at variable Mg^{2+} concentration: Sedimentation profiles of 0.5 g/L FtsZ equilibrated in working buffer at the magnesium concentrations specified in the figure.

The sedimentation velocity data obtained at a protein concentration of 0.5 g/L at various magnesium concentrations (**Figure 2**) qualitatively resemble those obtained with GTP, indicating a highly concerted formation of FtsZ polymers. At millimolar Mg^{2+}, the distribution of sedimentation coefficients is quantitatively described by a single sharp sedimenting boundary with an average *s*-value of 18-19 S, significantly higher than that characterizing the sedimentation of FtsZ polymers in the presence of GTP. This difference in *s*-value could in principle be attributed to differences in average mass and/or conformation, but additional data to be described below will indicate that the difference may be attributed exclusively to differences in average mass. The *c(s)* distributions at intermediate Mg^{2+} showed that below 70 μM Mg^{2+} polymers induced by GMPCPP sedimented primarily as a mixture of rapidly sedimenting (18-19 S) and slowly sedimenting (~3 S) species, with only minor contribution from intermediate species. This difference in *s*-value could in principle be attributed to differences in average mass and/or conformation, but additional data to be described below will indicate that the difference may be attributed exclusively to differences in average mass. The *c(s)* distributions at intermediate Mg2+ showed that below 70 μM Mg2+ polymers induced by GMPCPP sedimented primarily as a mixture of rapidly sedimenting (18-19 S) and slowly sedimenting (~3 S) species, with only minor contribution from intermediate species. The most remarkable difference with GTP-FtsZ polymers regarding the effect of magnesium is that, in the presence of GMPCPP, the observed sedimentation coefficient of rapidly sedimenting protein remained invariant through the whole Mg^{2+} concentration range assayed (i.e. at 20 μM and above). In the presence of EDTA, FtsZ sedimented as a main single species with *s*-value around 2.5 S, similar to the value obtained under the same conditions but in the presence of GTP instead of GMPCPP (see above). Hence the presence of EDTA, under our conditions, precluded the formation of polymers irrespective of the nucleotide triggering polymerization.

Concentration-dependent 90^{o} static light scattering

In **Figure 3A** the relative intensity of 690-nm light scattered at 90º recorded in a typical experiment is plotted as a function of time for a set of serial dilutions for FtsZ equilibrated in working buffer with 5 mM Mg^{2+} (black) or EDTA (grey) in the presence of 1 mM GTP supplemented with GTP-RS. The

calculated concentration dependence of scattering intensity, expressed as the scaled Rayleigh ratio (see experimental procedures) measured at different Mg^{2+} concentrations over a broad range of FtsZ concentrations (0.1-1.5 g/L) is plotted in **Figure 3B**. The results of corresponding measurements of the dependence of the 90^o static light scattering of FtsZ upon the concentration of protein in the presence of GMPCPP and various concentrations of Mg^{2+} are plotted in **Figure 3C**. The outstanding qualitative feature of the measured dependence of scattering intensity upon concentration at fixed Mg^{2+} in both nucleotides is a concerted transition between a region at low concentration with a low slope and a second region at higher concentration with a substantially greater slope. These data may be used to test the hypothesis that below a certain "critical concentration" comparable to a solubility, w_{sol}, the protein exists primarily as a single species or narrow distribution of low molecular weight scatterers, $M_{w,low}$, and that all protein in excess of the critical concentration exists as a single species or narrow distribution of high molecular weight scatterers, the mean size of which is approximately independent of the amount of scatterer. As we assume that for a given concentration of Mg^{2+} the size of the large scatterers is approximately independent of total concentration, we can define an apparent molar mass, $M_{w,high}^{apparent}$, equal to the product of the true molar mass times a constant attenuation factor equal to the ratio of the intensity of scattering at 90^o to that at 0^o, which will be subsequently shown to be of the order of one-third. We then propose that the concentration dependence may be approximately described by the following two-state model:

$$\frac{R\left(w,90^o\right)}{K_{opt}} = w_{low}M_{w,low} + w_{high}M_{w,high}^{apparent} \qquad [6]$$

where the proportion of low and high molecular weight scatterers is governed by a quasi-first order phase transition. Thus, for $w_{tot} \leq w_{sol}$, $w_{low} = w_{tot}$, and $w_{high} = 0$, and for $w_{tot} > w_{sol}$, $w_{low} = w_{sol}$ and $w_{high} = w_{tot} - w_{sol}$. Equation [6] was fit to the combined data for each nucleotide at each Mg^{2+} concentration. The best fit of this equation to each data set is plotted together with the data in **Figures 3B** and **3C**, and the best-fit parameter values are presented in **Table 1**.

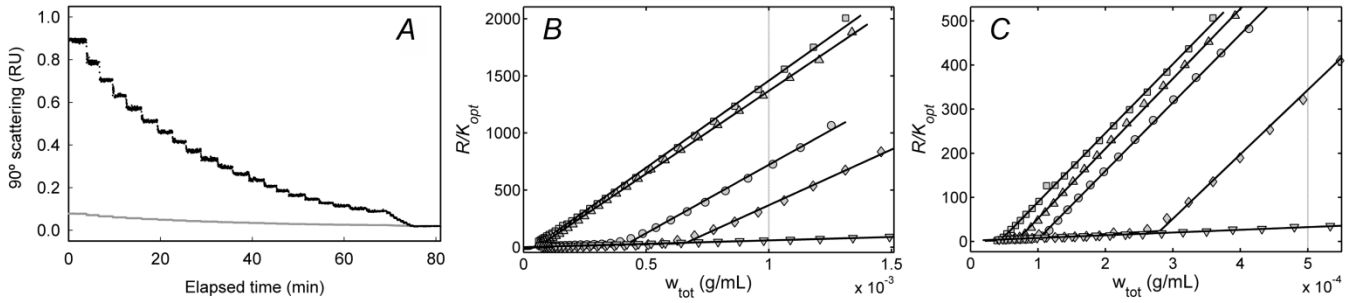

Figure 3. Mg^{2+} dependence of FtsZ composition gradient light scattering (90°, 690 nm). *A*. Light scattering of a FtsZ solution (initial concentration around 1 g/L) in working buffer in the presence of 1 mM GTP (black) or EDTA (grey), both supplemented with GTP-RS, plotted as a function of the elapsed time through a dilution experiment. *B* and *C*. Concentration dependence of GTP-FtsZ and GMPCPP-FtsZ static light scattering at 90º, respectively. From top to bottom, Mg^{2+} content was 5 mM, 300 µM, 100 µM and 20 µM (*B*) and 5 mM, 100 µM, 50 µM and 20 µM (*C*). Scattering profiles showing only a small dependence of scattering upon concentration were obtained from solutions containing 2 mM EDTA. Curves represent best-fits of the solubility model to each data set, calculated using equation [6] with best-fit parameter values given in **Table 1**. Vertical dashed lines depict the FtsZ concentrations at which sedimentation velocity experiments in **Figures 1** and **2** were conducted.

Table 1. Values of best-fit parameters obtained by fitting equation [6] to the 90° scattering data plotted in Figure 3B and C

Nucleotide	[Mg^{2+}]	w_{sol} (g/L)	$M_{w,high}^{apparent}$
GTP	0 (EDTA)	--	--
	20 μM	0.66	9.8×10^5
	100 μM	0.42	1.2×10^6
	300 μM	0.058	1.45×10^6
	5 mM	0.044	1.52×10^6
GMPCPP	0 (EDTA)	--	--
	20 μM	0.28	1.46×10^6
	50 μM	0.10	1.55×10^6
	100 μM	0.07	1.59×10^6
	5 mM	0.045	1.56×10^6

Values of M_{low} were determined in the presence of EDTA, 60000 for GTP and 61500 for GMPCPP, and subsequently used as constrained parameters for the fits in the presence of the different magnesium concentrations.

Concentration-dependent multi-angle light scattering

The normalized scattering intensity of a solution of FtsZ in 1 mM GTP + RS + 5 mM Mg is plotted as a function of concentration and $\sin^2(\theta/2)$ in **Figure 4A**, and data obtained from a solution of FtsZ in 0.4 mM GMPCPP + 5 mM Mg is plotted in **Figure 4B**. In both cases the angular dependence of scattering is evident. These data were analyzed in the context of the solubility model described above, modified to allow empirically for the dependence of the scattering of high molecular weight species upon θ [29]:

$$\frac{R(w_{tot},\theta)}{K_{opt}} = w_{low}M_{w,low} + w_{high}M_{w,high}\left(1 + A_1 g + A_2 g^2 + A_3 g^3\right) \quad [7]$$

where $g = \sin^2(\theta/2)$. A surface calculated according to the best least-squares fit of equation [7] to the combined data, using the best-fit parameter values given in the figure caption, is plotted together with the data in **Figures 4A** and **4B**.

According to the results obtained by fitting the solubility model to the data obtained from solutions containing GMPCPP + 5 mM Mg, the "solubility" of low molecular weight scatterer is too low to be distinguishable from zero with current experimental precision. The data are compatible with a value of $M_{w,high}$ between 5.7 and 7.0 x 10^6, corresponding to a mean oligomer stoichiometry between 145 and 175 monomers.

According to the results obtained by fitting the solubility model to the data obtained from solutions containing GTP + RS + 5 mM Mg, the "solubility" of low molecular weight scatterer is too low to be distinguishable from zero with current experimental precision. The data are compatible with a value of $M_{w,high}$ between 4.2 and 4.8 x 10^6, corresponding to a mean oligomer stoichiometry between 105 and 120 monomers.

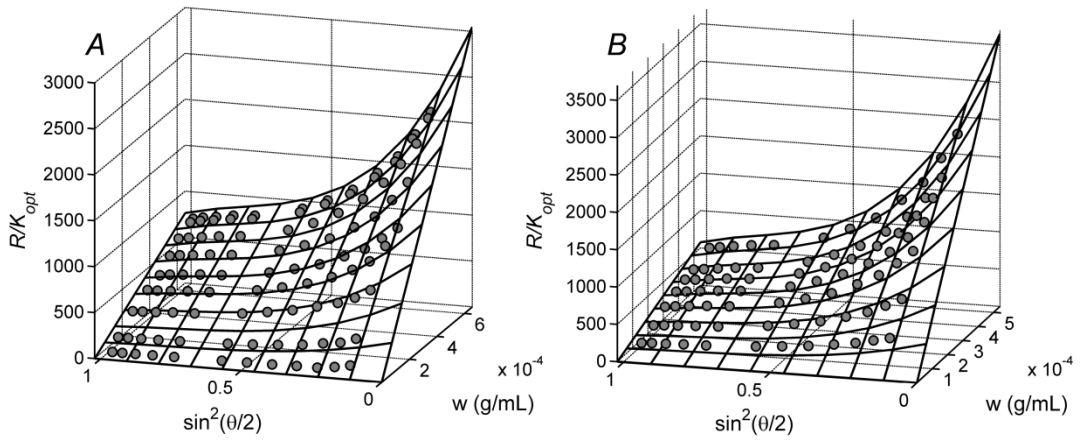

Figure 4. Angular and concentration dependence of scattering of FtsZ polymers in 5 mM Mg and GTP + RS (*A*) or GMPCPP (*B*). Scattering intensity plotted as a function of the w/v FtsZ concentration and $\sin^2(\theta/2)$. Black mesh surface is the best fit of the solubility model to the experimental data (symbols), calculated using equation [7] with the following best-fit parameter values. For GTP + RS, w_{sol} = 0, $M_{w,high}$ = 4.6 (± 0.4) x 10^6, A_1 = -2.32, A_2 = 2.67, and A_3 = -1.09. For GMPCPP, w_{sol} = 0, $M_{w,high}$ = 6.7 (± 0.7) x 10^6, A_1 = -2.62, A_2 = 3.0, and A_3 = -1.21.

Fluorescence correlation spectroscopy

Fluorescence autocorrelation functions obtained at constant protein concentration and various Mg concentrations in the presence of GTP + RS are plotted in **Figure 5A**. Comparable data obtained in the presence of GMPCPP are plotted in **Figure 5B**. In both panels the shift toward longer relaxation times with increasing Mg is evident, and may be attributed to the increasing abundance of larger species with smaller diffusion coefficients. The data were fitted to within experimental precision by equation [4] with three fluorescent species: a rapidly diffusing free dye, a more slowly diffusing labeled monomeric FtsZ, and a very slowly diffusing labeled polymeric FtsZ. In the presence of GTP + RS, the autocorrelation function becomes essentially independent of Mg concentration at concentrations exceeding ~ 0.4 mM (**Figure 5A**), and in the presence of GMPCPP, the autocorrelation function becomes essentially independent of Mg concentration at concentrations exceeding ~ 0.1 mM (**Figure 5B**). These results accord semiquantitatively with the Mg dependence of polymer formation monitored by sedimentation velocity (**Figures 1** and **2**) and 90^{o} light scattering (**Figures 3B** and **C**). The best fit value of the diffusion coefficient of polymer at 5 mM Mg was $4.1 \pm 0.3 \times 10^{-8}$ cm^2/s in GTP + RS and $3.1 \pm 0.4 \times 10^{-8}$ cm^2/s in CMPCPP (**Figure 5E**).

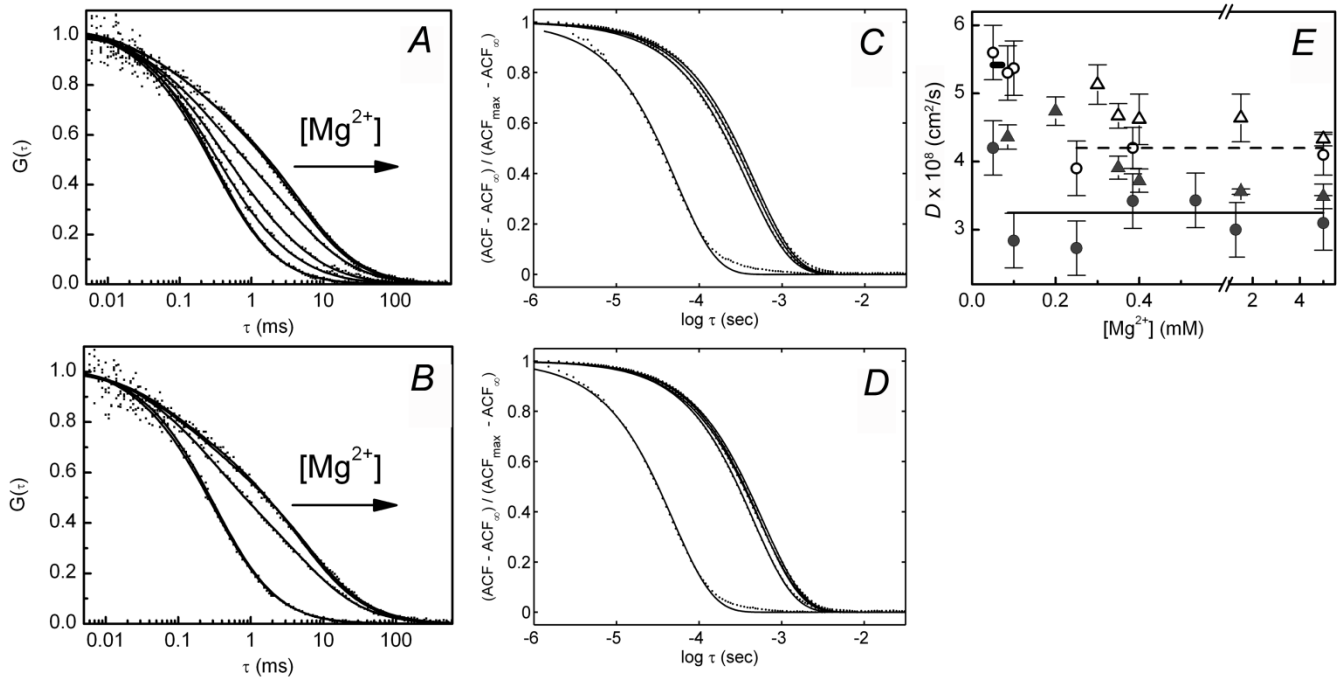

Figure 5. Dependence with $MgCl_2$ concentration of translational diffusion properties of FtsZ polymers formed in GTP + GTP-RS or GMPCPP. *A* and *B*. Normalized FCS autocorrelation curves of GTP-FtsZ and GMPCPP-FtsZ polymers, respectively. From faster to slower diffusion, $MgCl_2$ content was 0, 50, 100, 250, 385 µM and 5 mM (*A*, GTP, the last two indistinguishable) and 0, 50, 250 µM and 5 mM (*B*, GMPCPP, the last two indistinguishable). Samples without Mg^{2+} contain 1 mM EDTA and overlap with unassembled FtsZ-Alexa488 (no GTP or GMPCPP added). The fraction of unassembled FtsZ with GTP was 15-20% (1 mM-385 µM), 32% (250 µM), 53% (100 µM) and 67% (50 µM $MgCl_2$), and with GMPCPP 15-20% (5 mM-250 µM) and 29% (50 µM $MgCl_2$). Solid lines are the fits of the models indicated in the main text. Concentration of FtsZ-Alexa 488 was 0.006 g/L and unlabeled FtsZ was added up to 1 g/L. *C* and *D*. Normalized DLS autocorrelation curves of GTP-FtsZ (1 g/L FtsZ) and GMPCPP-FtsZ (0.5 g/L FtsZ) polymers, respectively. From faster to slower diffusion, $MgCl_2$ content was 0, 300, 350 µM and 5 mM (*C*, GTP, those with Mg^{2+} similar within error) and 0, 200, 300 µM, 1.5 and 5 mM (*D*, GMPCPP, last three similar within error). Samples without Mg^{2+} contain 1 mM EDTA. Solid lines are the fits to the model indicated in the main text. *E*. Dependence of the normalized translational diffusion coefficient of GTP- (open) and GMPCPP-FtsZ polymers (solid) determined by DLS (triangles) and FCS (circles). Data are the average of at least three independent experiments ± SD. Horizontal traces depict the average diffusion values calculated over the concentration independent range, 4.2×10^{-8} (GTP) and 3.2×10^{-8} cm^2/s (GMPCPP).

Fluorescence autocorrelation functions obtained for different protein concentrations in the presence of 5 mM Mg and GTP + RS are plotted in **Figure 6A**, and comparable data obtained in the presence of GMPCPP are plotted in **Figure 6B**. In both cases the autocorrelation functions become almost independent of protein concentration at concentrations exceeding ~ 0.5 g/L, indicating that at these concentrations almost all of the protein exists as high molecular weight species of constant size. The limiting values of the diffusion coefficients of polymer in GTP + RS and in GMPCPP are the same as

obtained from analysis of Mg dependence as described above (**Fig 6E**) to within the uncertainties specified above. Interestingly, early detection of polymers in the presence of GTP occurred at concentrations slightly above 0.05 g/L coinciding with the critical concentration of polymerization of FtsZ under these conditions [6, 9, 16]. In the presence of EDTA and GTP or GMPCPP, the fluorescence autocorrelation curves overlap with those obtained for the unassembled protein.

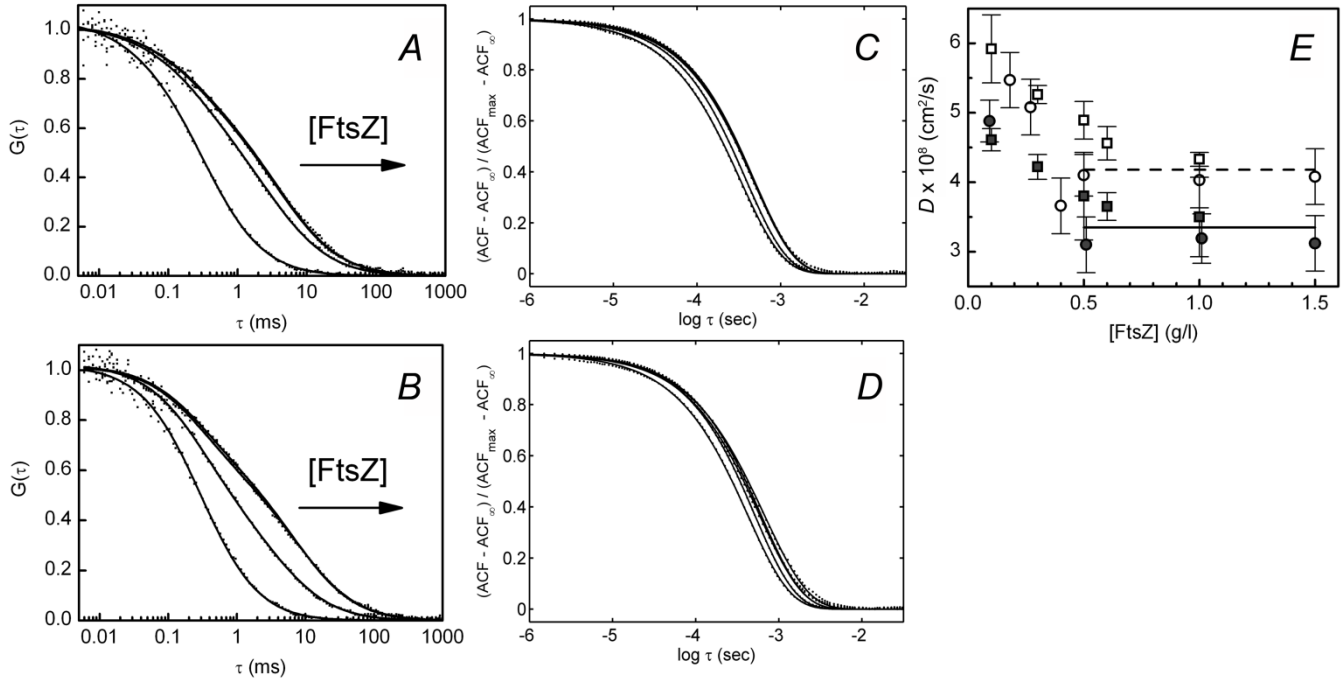

Figure 6. Concentration dependence of translational diffusion of GTP and GMPCPP FtsZ polymers. *A* and *B*. Normalized FCS autocorrelation curves of FtsZ polymers formed in the presence of 1 mM GTP or 0.4-1mM GMPCPP, respectively. From faster to slower diffusion, 0.006, 0.18, 0.5 and 1.5 g/L FtsZ (A, GTP, last two overlap) and 0.006, 0.09, 0.5 and 1 g/L FtsZ (B, GMPCPP, last two superimposable). The fraction of unassembled FtsZ with GTP was ~10% (1.5-0.5 g/L) and 24% (0.18 g/L), and with GMPCPP ~10% (0.5-1 g/L) and 40% (0.09 g/L). Concentration of FtsZ-Alexa 488 was 0.006 g/L and additional unlabeled FtsZ was added up to the final concentration specified. *C* and *D*. Normalized DLS autocorrelation curves of FtsZ polymers formed in the presence of 1 mM GTP or 0.4 mM GMPCPP, respectively. From faster to slower diffusion: 0.1, 0.3, 0.5, 0.6 and 1.0 g/L FtsZ. Profiles at 0.5 - 1.0 g/L overlap for GTP and are similar, within error, for GMPCPP. *E*. Dependence with FtsZ concentration of the normalized apparent diffusion coefficient of GTP- (open) and GMPCPP-FtsZ polymers (solid) determined by DLS (squares) and FCS (circles). Horizontal lines indicate the average diffusion value of the concentration independent polymeric species, 4.2×10^{-8} (GTP) and 3.2×10^{-8} cm^2/s (GMPCPP).

Dynamic light scattering and estimate of molar masses from hydrodynamic measurements

Autocorrelation functions obtained at a constant concentration of protein showed a significant shift to longer times with increasing Mg concentration both in the presence of GTP + RS and GMPCPP (**Figures**

5C and **D**). In accordance with FCS data, GTP-FtsZ polymers showed a significant increase of the translational diffusion coefficient of assembled FtsZ with decreasing Mg^{2+} concentrations (**Figure 5C**), while GMPCPP-FtsZ polymers existed as a defined species with a translational diffusivity that did not depend on Mg^{2+} concentration above 20-50 μM (**Figure 5D**), also in good agreement with the sedimentation velocity and static light scattering results (**Figures 1-3**). The translational mobility of FtsZ polymers in GMPCPP, according to the *D*-values measured both by FCS and DLS, was systematically slower than that previously measured for FtsZ in GTP under the same conditions (**Figure 5**), in agreement with a larger size for the 19 S species that FtsZ forms in the presence of GMPCPP at high Mg^{2+}. The data were fitted to within experimental precision by equation [3] rendering best fit values of the diffusion coefficients of polymer in the high Mg concentration limit of 4.3 ± 0.4 x 10^{-8} cm^2/s in GTP + RS and 3.4 ± 0.2 x 10^{-8} cm^2/s in CMPCPP (**Figure 5E**).

DLS autocorrelation functions obtained at different FtsZ concentrations with 5 mM Mg and GTP + RS or GMPCPP are plotted in **Figure 6C** and **D**, respectively. As observed by FCS, profiles become almost independent of protein concentration above ~ 0.5 g/L FtsZ, verifying our previous findings that the concentration dependence of the *c(s)* distribution of GTP-FtsZ was compatible with the concerted formation of a narrow distribution of favored oligomers (13 S) whose apparent size does not increase between 0.4 and 1.5 g/L FtsZ (*9*).

The apparent molar masses calculated from the diffusion values, average of FCS and DLS, and sedimentation coefficients according to Equation [6] are 3.4 x 10^6 g (~85 FtsZ molecules/oligomer) for the GTP-FtsZ polymer and 6.0 x 10^6 g (~150 FtsZ molecules/oligomer) for the GMPCPP-FtsZ polymer. Although the diffusion coefficients from DLS data account for the diffusing properties of all species in solution, it should be noted that the measured autocorrelation function will be mainly contributed by the bigger species. Therefore, under conditions at which polymers are formed, translational diffusion coefficients obtained by DLS should be directly comparable to those obtained by FCS for the slowly diffusing polymeric FtsZ, since the contribution of unassembled species (given their low concentration and much smaller size) is negligible. This might be also the case for the intermediate GTP-FtsZ species formed at micromolar Mg^{2+} (~40 FtsZ subunits as calculated from *D* and *s* via the Svedberg equation).

DISCUSSION

Comparison of the results obtained by measurement of sedimentation velocity and 90^{o} light scattering provides a consistent and unequivocal picture of the mechanism of FtsZ self-assembly in the presence of GTP. The results shown in **Figure 1** (GTP + RS) were obtained from solutions containing 1 g/L protein, indicated by a dashed vertical line in **Figure 3B.** In the presence of EDTA the scattering signal is consistent with an average molecular weight corresponding to a mixture of monomeric and dimeric FtsZ, in qualitative agreement with sedimentation velocity results. In the presence of 100 μM Mg^{2+}, the scattering data indicate a mixture of approximately 40% low molecular weight species and 60% high molecular weight species, again in good agreement with the distribution of sedimentation coefficients shown in **Figure 1**. In the presence of 5 mM Mg^{2+} almost complete (>95%) conversion of protein to an even higher molecular weight species occurs, once again in qualitative agreement with the distribution of sedimentation coefficients shown in **Figure 1**. Taken together, the scattering data indicate that the mean size of the high molecular weight species is approximately independent of protein concentration, but gradually increases with increasing Mg^{2+} concentration, apparently attaining a maximum size between 350 μM and 1 mM, again in qualitative agreement with the results shown in **Figure 1**.

The results shown in **Figure 2** (GMPCPP) were obtained from solutions containing 0.5 g/L protein, indicated by a dashed vertical line in **Figure 3C.** In the absence of Mg^{2+}, the scattering profile is consistent with an average molecular weight between that of monomeric and dimeric FtsZ, consistent with the results shown in **Figure 2**. In the presence of 20 μM Mg^{2+}, the scattering profile is consistent with the presence of comparable amounts of both low and high molecular weight species, in qualitative accord with the distribution of sedimentation coefficients obtained from sedimentation velocity experiments. At higher Mg^{2+} concentrations, the scattering profile suggests the presence of predominantly high molecular weight scatterers, the mean size of which is insensitive to changes in Mg^{2+} concentration. This last result, which differs from that found in the presence of GTP-RS, is once again in qualitative accord with distribution of sedimentation coefficients obtained from the sedimentation velocity experiments.

Taken together, the sedimentation velocity data and 90^{o} scattering data provide strong evidence for a highly concerted transition, thermodynamically similar to a second-order phase transition, between a paucidisperse size distribution of low molecular weight oligomers, and a paucidisperse size distribution of high molecular weight oligomers. Both of these observations, together with the results of angle-dependent static light scattering, dynamic light scattering, and fluorescence autocorrelation spectroscopy, rule out mechanisms based solely upon incremental growth of oligomer via sequential addition of monomers, and any scheme leading to unbounded polymer size. The control experiments conducted in the presence of the slowly hydrolysable analog of GTP exhibit identical qualitative behavior, indicating that the observed growth scheme is not attributable in essence to a non-equilibrium steady-state reaction cycle involving GTP hydrolysis and GTP-GDP exchange, although these factors are likely to modulate the observed behavior, as discussed below.

The mean size of polymer in 5 mM Mg was estimated to be 115 ± 8 in GTP + RS and 165 ± 15 in GMPCPP on the basis of a two-state analysis of angle- and concentration-dependent light scattering. The mean size of polymer was also independently estimated from approximate analyses of the results of measurements of the sedimentation and diffusion coefficients by means of equation [5]. The values obtained from this relation for the stoichiometry of polymers in GTP and GMPCPP are 85 ± 7 and 150 ± 10 respectively. The difference between the values obtained by the two different approaches may be attributed at least in part to the fact that both analyses depend upon two-state approximations applied in rather different contexts. This approximation is probably more realistic when applied to FtsZ self-assembly in GMPCPP than in GTP.

Although the self-assembly of FtsZ in GTP qualitatively resembles that in GMPCPP, significant quantitative differences are present. (*a*) The average size of polymer varies with Mg concentration in GTP, whereas it does not in GMPCPP. (*b*) The cooperative transition between low and high molecular weight distributions appears to be sharper and more similar to a first-order phase transition in the presence of GMPCPP than in GTP. (*c*) The average size of polymer in the presence of high Mg is significantly greater in GMPCPP than in GTP. It is clear that non-equilibrium steady-state effects arising from GTP hydrolysis and GTP-GDP exchange cannot be responsible for the concerted nature of the transition between low and high molecular weight species observed in the presence of both GTP +

RS and GMPCPP, since the cooperativity of the transition is more pronounced in the presence of the much more slowly hydrolysable GTP analog.

Fragmentation certainly can limit the size of fibrillar oligomers, but by itself cannot elicit a highly concerted formation of a narrow distribution of favored polymers in a manner resembling a phase transition, as we observe here. The results clearly indicate that there is no significant amount of material existing as oligomers intermediate between a low molecular weight distribution consisting mainly of monomers and dimers, and a narrow high molecular weight oligomeric species of stoichiometry between 80 and 180 (depending upon the nucleotide used to promote FtsZ assembly). The major consequence of fragmentation and annealing of fibrils would be to accelerate the approach to equilibrium. The rapid exchange of FtsZ subunits when mixing donor-labeled and acceptor-labeled FtsZ fibrils in the FRET experiments done by Erickson and co-workers [(11)] does not require the disappearance of fibrils, merely transient breakage and closure along the length of a fibril. The essential point is that without a mechanism for formation of a discrete oligomer or narrow molecular weight distribution of oligomers in a highly cooperative fashion, nucleation + fragmentation alone will not account for the data.

In summary, the combined results reported above support the following two major conclusions:

1. *The self-assembly of FtsZ under the conditions of this study proceeds by a concerted transition, thermodynamically resembling a second order phase transition, between a paucidisperse distribution of low molecular weight species, consisting primarily of monomer and dimer, and a paucidisperse distribution of high molecular weight species (polymer), the size of which is independent of total protein concentration, and, in the presence of GMPCPP, is independent of magnesium concentration. It should be kept in mind that this mode of self-assembly may not necessarily apply under other experimental conditions, as it is well known that the structure of non-covalent oligomers/polymers formed by proteins in general, and FtsZ in particular, may vary considerably depending upon solution conditions (see, for example, (5) and references therein).*

2. In the limit of high magnesium concentration, the average size of polymer is estimated to lie between 80 and 120 FtsZ protomers in the presence of GTP + RS, and between 140 and 180 FtsZ protomers in the presence of GMPCPP.

The purpose of the present report is not to advocate any particular molecular model for oligomer formation, but to present a substantial body of experimental data obtained via several biophysical methods that is self-consistent and, in our opinion, must be taken into account in any future attempt to formulate a mechanistic scheme for FtsZ self-assembly.

We do not attribute physiological significance to the narrow size distribution of oligomeric species, indicated by our data, since the system studied here is highly simplified and lacks the companion proteins and surfaces required to assemble the septal ring *in vivo*. However, the characterization of FtsZ solution behavior provides information that will ultimately be integrated into more complex schemes describing systems containing the additional elements referred to above.

References

1. Adams, D. W., and Errington, J. (2009) Bacterial cell division: assembly, maintenance and disassembly of the Z ring, *Nat Rev Microbiol 7*, 642-653.

2. Margolin, W. (2000) Organelle division: Self-assembling GTPase caught in the middle, *Curr Biol 10*, R328-330.

3. Mingorance, J., Rivas, G., Vélez, M., Gómez-Puertas, P., and Vicente, M. (2010) Strong FtsZ is with the force: mechanisms to constrict bacteria, *Trends Microbiol 18*, 348-356.

4. Rivas, G., López, A., Mingorance, J., Ferrándiz, M. J., Zorrilla, S., Minton, A. P., Vicente, M., and Andreu, J. M. (2000) Magnesium-induced linear self-association of the FtsZ bacterial cell division protein monomer. The primary steps for FtsZ assembly, *J Biol Chem 275*, 11740-11749.

5. Erickson, H. P., Anderson, D. E., and Osawa, M. (2010) FtsZ in bacterial cytokinesis: cytoskeleton and force generator all in one, *Microbiol Mol Biol Rev 74*, 504-528.

6. González, J. M., Jiménez, M., Vélez, M., Mingorance, J., Andreu, J. M., Vicente, M., and Rivas, G. (2003) Essential cell division protein FtsZ assembles into one monomer-thick ribbons under conditions resembling the crowded intracellular environment, *J Biol Chem 278*, 37664-37671.

7. Mingorance, J., Tadros, M., Vicente, M., González, J. M., Rivas, G., and Vélez, M. (2005) Visualization of single Escherichia coli FtsZ filament dynamics with atomic force microscopy, *J Biol Chem 280*, 20909-20914.

8. Popp, D., Iwasa, M., Narita, A., Erickson, H. P., and Maeda, Y. (2009) FtsZ condensates: an in vitro electron microscopy study, *Biopolymers 91*, 340-350.

9. González, J. M., Vélez, M., Jiménez, M., Alfonso, C., Schuck, P., Mingorance, J., Vicente, M., Minton, A. P., and Rivas, G. (2005) Cooperative behavior of Escherichia coli cell-division protein FtsZ assembly involves the preferential cyclization of long single-stranded fibrils, *Proc Natl Acad Sci U S A 102*, 1895-1900.

10. Stricker, J., Maddox, P., Salmon, E. D., and Erickson, H. P. (2002) Rapid assembly dynamics of the Escherichia coli FtsZ-ring demonstrated by fluorescence recovery after photobleaching, *Proc Natl Acad Sci U S A 99*, 3171-3175.

11. Chen, Y., and Erickson, H. P. (2009) FtsZ filament dynamics at steady state: subunit exchange with and without nucleotide hydrolysis, *Biochemistry 48*, 6664-6673.

12. Erickson, H. P. (2009) Modeling the physics of FtsZ assembly and force generation, *Proc Natl Acad Sci U S A 106*, 9238-9243.

13. Huecas, S., Llorca, O., Boskovic, J., Martín-Benito, J., Valpuesta, J. M., and Andreu, J. M. (2008) Energetics and geometry of FtsZ polymers: nucleated self-assembly of single protofilaments, *Biophys J 94*, 1796-1806.

14. Salvarelli, E., Krupka, M., Rivas, G., Vicente, M., and Mingorance, J. (2011) Independence between GTPase active sites in the Escherichia coli cell division protein FtsZ, *FEBS Lett*.

15. Jiménez, M., Martos, A., Vicente, M., and Rivas, G. (2011) Reconstitution and organization of Escherichia coli proto-ring elements (FtsZ and FtsA) inside giant unilamellar vesicles obtained from bacterial inner membranes, *J Biol Chem 286*, 11236-11241.

16. Reija, B., Monterroso, B., Jimenez, M., Vicente, M., Rivas, G., and Zorrilla, S. (2011) Development of a homogeneous fluorescence anisotropy assay to monitor and measure FtsZ assembly in solution, *Anal Biochem 418*, 89-96.

17. Schuck, P. (2000) Size-distribution analysis of macromolecules by sedimentation velocity ultracentrifugation and lamm equation modeling, *Biophys J 78*, 1606-1619.

18. Attri, A. K., and Minton, A. P. (2005) Composition gradient static light scattering: a new technique for rapid detection and quantitative characterization of reversible macromolecular hetero-associations in solution, *Anal Biochem 346*, 132-138.

19. Kameyama, K., and Minton, A. P. (2006) Rapid quantitative characterization of protein interactions by composition gradient static light scattering, *Biophys J 90*, 2164-2169.

20. Fernández, C., and Minton, A. P. (2008) Automated measurement of the static light scattering of macromolecular solutions over a broad range of concentrations, *Anal Biochem 381*, 254-257.

21. Schmitz, K. S. (1990) *An introduction to dynamic light scattering by macromolecules (Chapter 2)*, Academic Press, Boston.

22. Kita, R., Takahashi, A., Kaibara, M., and Kubota, K. (2002) Formation of fibrin gel in fibrinogen-thrombin system: static and dynamic light scattering study, *Biomacromolecules 3*, 1013-1020.

23. Skakun, V. V., Hink, M. A., Digris, A. V., Engel, R., Novikov, E. G., Apanasovich, V. V., and Visser, A. J. (2005) Global analysis of fluorescence fluctuation data, *Eur Biophys J 34*, 323-334.

24. Bacia, K., and Schwille, P. (2007) Practical guidelines for dual-color fluorescence cross-correlation spectroscopy, *Nat Protoc 2*, 2842-2856.

25. Culbertson, C. T., Jacobson, S. C., and Michael Ramsey, J. (2002) Diffusion coefficient measurements in microfluidic devices, *Talanta 56*, 365-373.

26. Gendron, P. O., Avaltroni, F., and Wilkinson, K. J. (2008) Diffusion coefficients of several rhodamine derivatives as determined by pulsed field gradient-nuclear magnetic resonance and fluorescence correlation spectroscopy, *J Fluoresc 18*, 1093-1101.

27. Svedberg, T., and Pedersen, K. O. (1940) *The Ultracentrifuge.* Oxford, Clarendon Press.

28. Reisler, E., Cheung, P., and Borochov, N. (1986) Macromolecular assemblies of myosin, *Biophys J 49*, 335-342.

29. Zimm, B. H. (1948) The dependence of the scattering of light on angle and concentration in linear polymer solutions, *J Phys Colloid Chem 52*, 260-267.

30. Tanford, C. (1961) *Physical chemistry of macromolecules*.

SUPLEMENTARY MATERIAL

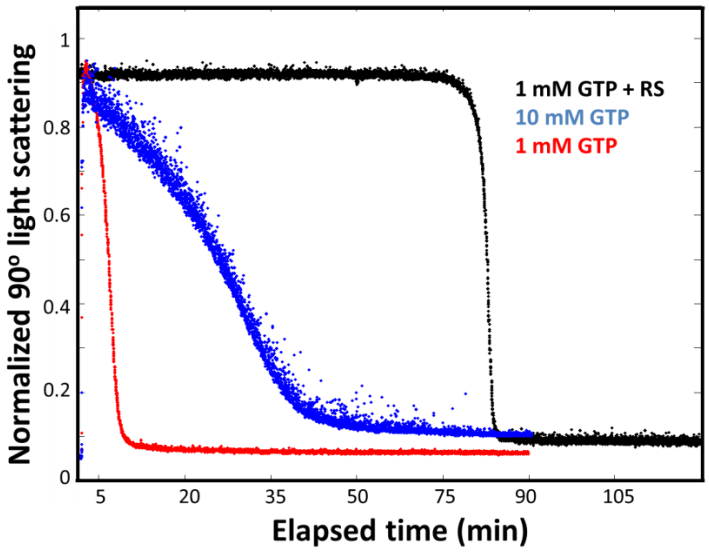

Figure S1. Normalized 90° light scattering as a function of time of FtsZ at 12 µM polymerized in the presence of 1 mM GTP (red), 10 mM GTP (blue) and 1 mM GTP supplemented with GTP regenerating system (black). We observe that polymers formed are stable in these conditions long enough time to perform the assays.

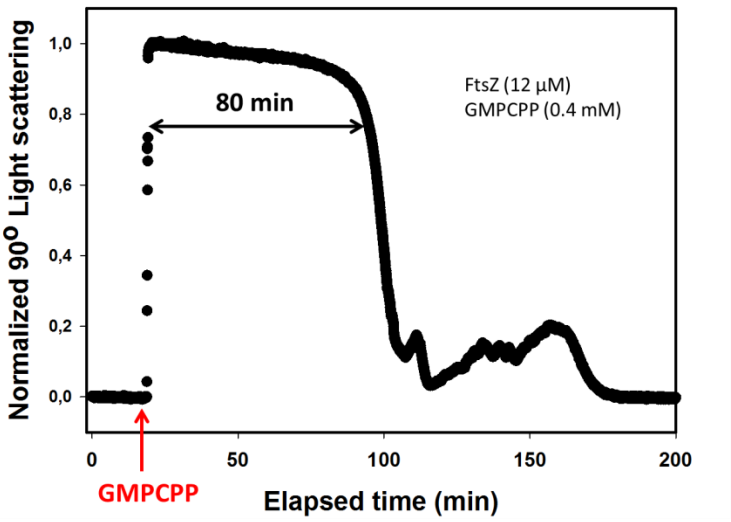

Figure S2. Normalized 90° light scattering of FtsZ at 12 µM polymerized in the presence of 0.4 mM of GMPCPP as a function of time. We observe that polymers formed are stable in these conditions long enough time to perform the assays.

APENDIX 1

BIOPHISICAL CHARACTERIZATION OF FtsZ IN ITS GDP-BOUND STATE (GDP-FtsZ). Regulation by Mg^{2+} concentration of the protein association state.

The effect of submillimolar Mg^{2+} concentrations in the self-association of FtsZ in its GDP-bound state (GDP-FtsZ) was analyzed using composition gradient static light scattering (CG-SLS), dynamic light scattering (DLS) and sedimentation velocity and equilibrium. Experiments were carried out at high ionic strength (500mM KCl) and buffer was supplemented with different amounts of $MgCl_2$ (from 10 μM to 5 mM) or 2mM EDTA. FtsZ self-associated from monomer to dimer or small oligomers in a non-cooperative fashion. Experimental data were quantitatively described by an equilibrium model which takes into account significant contributions of monomer and dimer and some contribution of other small oligomers.

EXPERIMENTAL PROCEDURES

All the assays described in this Apendix were done as described in experimental section of Chapter I and supplemented with 0.1 mM of GDP. Static light scattering data were processed as previously described by Attri and Minton [1, 2]. The composition dependence of R/K_{opt} is modeled in the context of equilibrium scheme described in Apendix 3 [5], Model 1 (*Isodesmic model for self-association of GDP-FtsZ*), that specify the molar masses of all significant scattering species, and the dependence of concentrations of *i* species, c_i, upon postulated equilibrium association constants and the total concentrations of protein.

RESULTS

Magnesium induces oligomerization of FtsZ. The effect of magnesium was studied in a wide range of magnesium and FtsZ concentrations. The dependence of the dimerization was carried out by sedimentation velocity and gradient-concentration-static light scattering (GC-SLS) and dynamic light scattering (DLS).

The magnesium effect in physiologic high ionic strength conditions (500 mM KCl) was studied in detail by GC-SLS in a wide range of FtsZ concentrations from around 1 mg/mL (25 μM) to 0.04 mg/mL (1 μM) (see **Figure 2**, panel A) and by sedimentation velocity at FtsZ concentrations of 37.5 and 10 μM. Distributions of sedimentation coefficients of FtsZ solutions prepared at different Mg^{2+} concentrations in the presence of 0.1 mM GDP (**Figure 1**), were obtained by analysis of the experimental sedimenting boundaries with SEDFIT program [3]. When FtsZ concentration was 10 μM the predominant species sedimented with an S-value of 2.5 at all studied magnesium conditions except in the presence of millimolar concentration of magnesium, where was also present other specie with an S-value around 3.7 (**Figure 1**, right panel). This two main species have a sedimentation coefficient compatible with an FtsZ monomer and dimer according with Gonzalez *et al* (2005) [4]. At high FtsZ concentration of 37.5 μM the protein evolves with a similar behavior (**Figure 1**, left panel). In the presence of EDTA and in the absence of Mg^{2+}, the protein sedimented as a single specie with *S*-value around 2.5 S. At magnesium concentrations between 10 and 100 μM, the sedimentation data were well described by a main sedimenting species with S-value around 2.5 S and a very small amount of higher order species (dimer, trimer…). In these range of concentrations of magnesium chloride GC-SLS experiments show a displacement of the equilibrium to the formation of small amount of dimeric species. Finally, at millimolar magnesium concentrations the protein sediments as a two main species with an experimental *s*-values of 2.5 and around 3.5-3.9 S, this last species was compatible with the dimer.

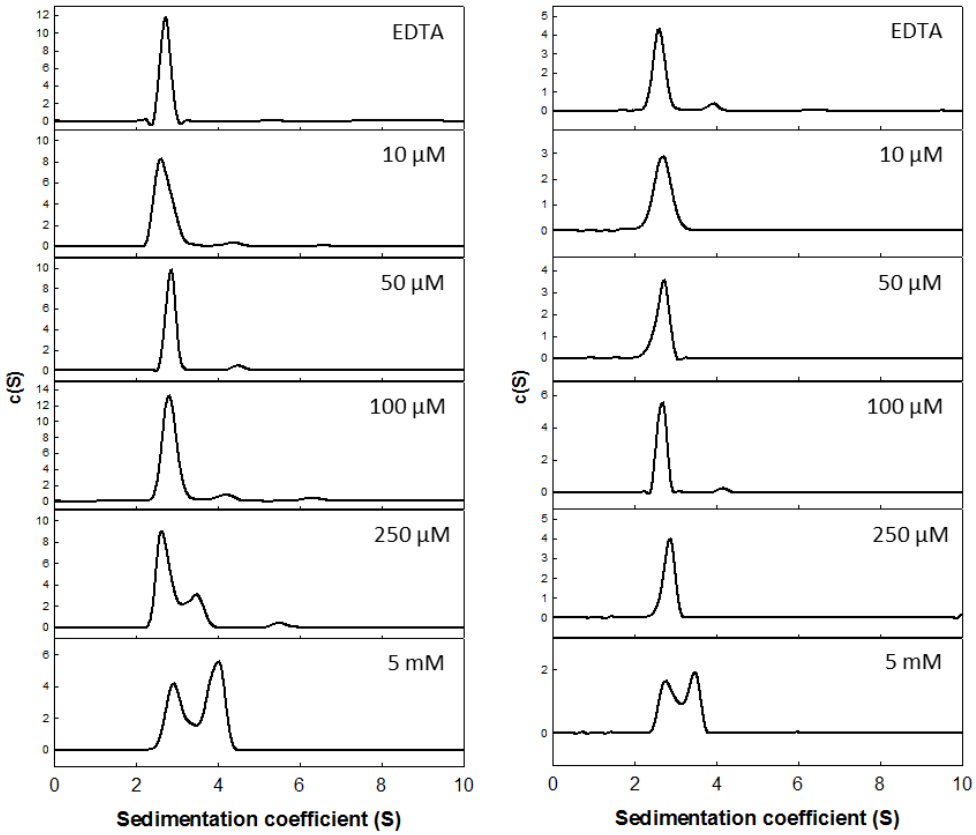

Figure 1. Mg^{2+} dependence of FtsZ in the presence of 0.1 mM GDP. Sedimentation profiles of 37.5 (left) and 10 µM (right) FtsZ equilibrated in working buffer at the magnesium concentrations specified in the figure.

Similar result was obtained by GC-SLS experiments, plotted in **Figure 2** (Panel A), where in the total absence of Mg^{2+} and in presence of 2 mM EDTA, experimental data fitted well to a single species in all range of protein concentrations with an average molecular mass of 43.0 ± 0.3 kDa. Beside this, we observe a small amount of higher order oligomers as described before [5]. In this range of magnesium concentrations GC-SLS experiments are in good agreement with the evolution of the system toward the formation of dimeric and a small amount of larger species. Isodesmic model described in Apendix 3 or reference [5] (Model 1) were fitted to static light scattering data (**Figure 2**) in order to obtain the best parameters that describes the equilibrium process.

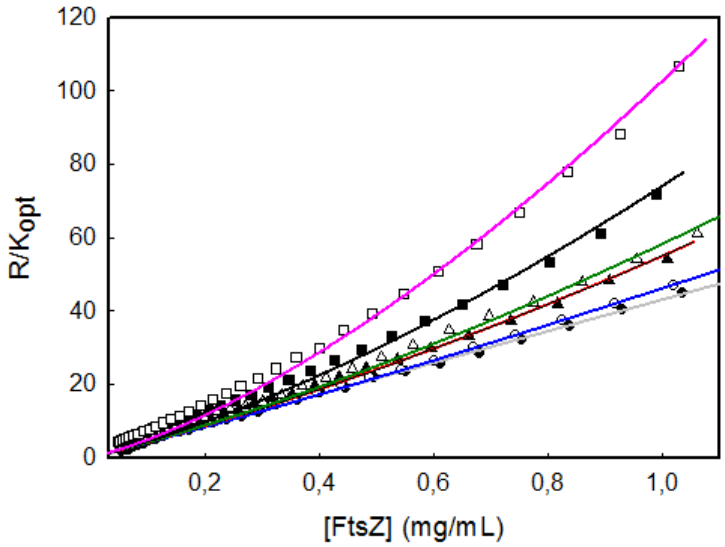

Figure 2. Mg^{2+} dependence of FtsZ. Composition gradient light scattering (90º, 690 nm) of a FtsZ solution (initial concentration around 1 g/L) in working buffer in the presence of 0.1 mM GDP. From top to bottom, Mg^{2+} content was 5 mM, 1 mM, 100 µM, 30 µM, 10 µM and absence of Magnesium (2mM EDTA). Solid curves represent best-fits of the isodesmic model to each data set (*Isodesmic model for self-association of GDP-FtsZ described in Apendix 3*). Calculated equilibrium constants are in **Table 1**.

Table 1: $M_{w,\,aver}$ and Log K_{iso} obtained from GC-SLS data.

$[Mg^{2+}]$ (mM)	$M_{w,\,aver}$ (kDa)	Log $K_{iso\ CG\text{-}SLS}$
0 (EDTA)	43.0±0.1	-
0.01	46.3 ± 0.5	3.6 ± 0.1
0.05	51.9 ± 0.6	4.2 ± 0.1
0.1	56.4 ± 0.7	4.5 ± 0.1
1	66.5 ± 1.1	4.4 ± 0.1
5	95.7 ± 2.4	4.7 ± 0.1

The effect of protein concentration in the oligomerization of FtsZ. The dependence of oligomerization with protein concentration was studied in a wide range. The effect of FtsZ concentration in the dimerization has been analyzed by sedimentation velocity and GC-SLS. In the presence of millimolar concentrations of magnesium (5 mM) and high ionic strength (500 mM KCl) the experiments show a mixture of monomer and dimer. A set of sedimentation velocity assays of FtsZ in a wide range of concentrations show two main different species with sedimentation coefficients around 2.5 and 3.9 S respectively (see **Figure 3**). The equilibrium is clearly shifted toward dimer formation with increasing the concentration of FtsZ. The GC-SLS experiments verify this tendency (see **Figure 2,** pink curve and **Table 1**).

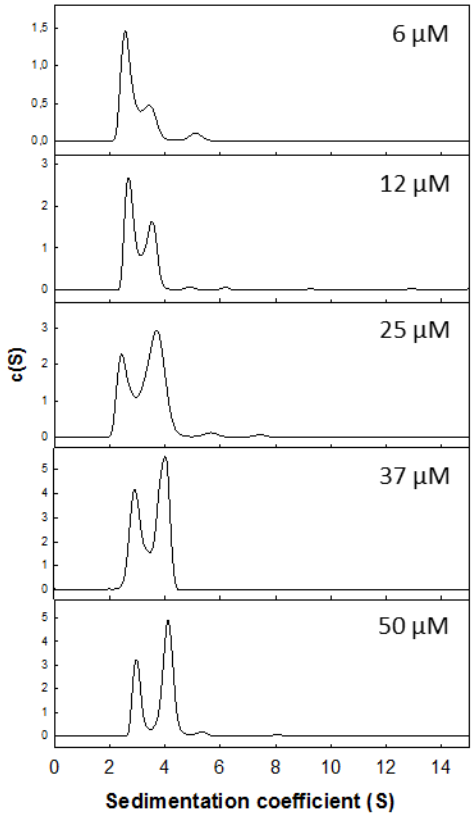

Figure 3. Concentration dependence of FtsZ sedimentation velocity in the presence of 0.1 mM GDP and 5 mM Mg^{2+}. Sedimentation profiles in a wide range of FtsZ concentrations shown the shift to dimer formation with increasing the concentration of protein.

DISCUSION

Previous work shows the stability of GDP-FtsZ in absence of Mg^{2+}, and in the presence of moderate or high ionic strength. Although it was well known that Mg^{2+} is involved in oligomerization processes of GDP-FtsZ that is disadvantaged in high ionic strength, was not determined before the dependence of oligomerization in high ionic strength of GDP-FtsZ with the micromolar concentrations of Mg^{2+} [6, 7, 8].

In order to describe the first steps in the oligomerization of GDP-FtsZ and their dependence on Mg^{2+} concentration, sedimentation velocity and gradient concentration static light scattering scattering were employed. This study required the use of Mg^{2+} concentration in the range from nanomolar to millimolar.

The obtained results from employed techniques were in good agreement to confirm that the oligomerization of GDP-FtsZ in high ionic conditions is very sensitive to the variation of concentration of Mg^{2+}. The analysis of the results show that there were two main species at physiologic millimolar concentrations of Mg^{2+}, monomer and dimer, but small amount of higher order species were also present in good agreement with the isodesmic model proposed before [5, 8]. At micromolar concentration of Mg^{2+} the main species was the monomer but we also found the presence of dimer and a very small amount of other larger species. In total absence of Mg^{2+}, in the presence of EDTA, we found that monomer was the only present species. In the other hand, we saw that the oligomerization of GDP-FtsZ in the presence of millimolar concentrations of Mg^{2+} was also protein concentration dependent. If we increase the concentration of protein the equilibrium was shifted to the formation of dimer and larger species.

The static light scattering data were fitted to a previously described isodesmic self-association model [5]. Comparing GDP-FtsZ with GTP-FtsZ, described in Chapter I, and their dependence with the concentration of Mg^{2+}, we found that in both cases in the range of micromolar concentrations of Mg^{2+} the oligomerization and polymerization were triggered. In the case of GTP-FtsZ the polymerization was much more sensitive to Mg^{2+} than in the case of GDP-FtsZ. In the absence of Mg^{2+}, in both cases the protein is essentially a monomer.

References

1. Attri, A. K., and Minton, A. P. (2005) Composition gradient static light scattering: a new technique for rapid detection and quantitative characterization of reversible macromolecular hetero-associations in solution, Analytical biochemistry 346, 132-138.
2. Attri, A. K., and Minton, A. P. (2005) New methods for measuring macromolecular interactions in solution via static light scattering: basic methodology and application to nonassociating and self-associating proteins, Analytical biochemistry 337, 103-110.
3. Schuck P.Size-distribution analysis of macromolecules by sedimentation velocity ultracentrifugation and lamm equation modeling. Biophys J. 2000 Mar;78(3):1606-19.
4. González JM, Vélez M, Jiménez M, Alfonso C, Schuck P, **Mingorance** J, , Minton AP, Rivas G . Cooperative behavior of Escherichia coli cell-division protein FtsZ assembly involves the preferential cyclization of long single-stranded fibrils. Proc Natl Acad Sci U S A. 2005 Feb 8;102(6):1895-900.
5. Martos A, Alfonso C, López-Navajas P, Ahijado-Guzmn R, Mingorance J, Minton AP, Rivas G. Characterization of self-association and heteroassociation of bacterial cell division proteins FtsZ and ZipA in solution by composition gradient-static light scattering. Biochemistry. 2010 Dec 28;49(51):10780-7. Epub 2010 Dec 3.
6. Rivas, G., Fernandez, J. A., and Minton, A. P. (2001) Direct observation of the enhancement of noncooperative protein self-assembly by macromolecular crowding: indefinite linear self-association of bacterial cell division protein FtsZ, Proceedings of the National Academy of Sciences of the United States of America 98, 3150-3155.

7. Rivas, G., Lopez, A., Mingorance, J., Ferrandiz, M. J., Zorrilla, S., Minton, A. P., Vicente, M., and Andreu, J. M. (2000) Magnesium-induced linear self-association of the FtsZ bacterial cell division protein monomer. The primary steps for FtsZ assembly, J Biol Chem 275, 11740-11749.

8. Minton AP. Alternative strategies for the characterization of associations in muticomponent solutions via measurements of sedimentation equilibrium. Prog Colloid Polymer Sci 1997;107:11-19.

CHAPTER II

Different Response of GTP- and GMPCPP-FtsZ Polymers to KCl Concentration.

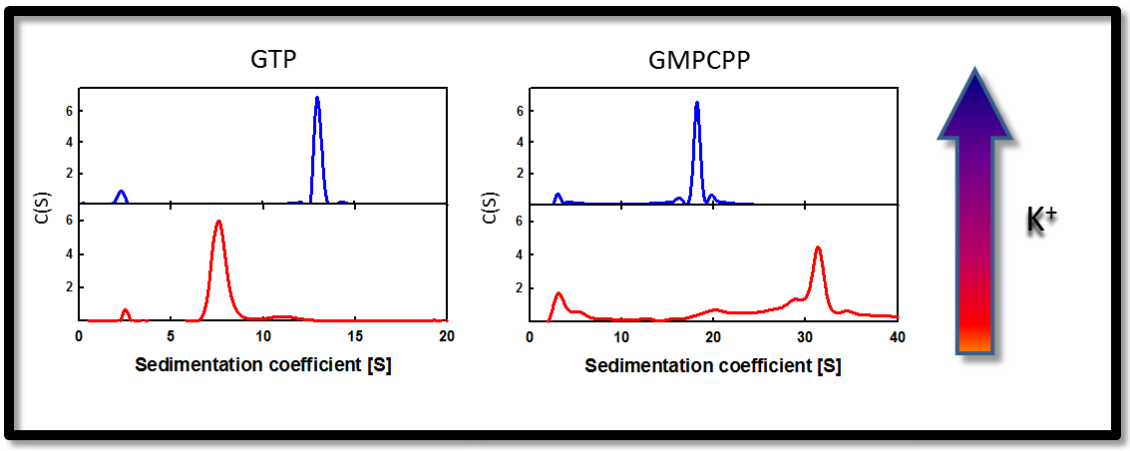

FtsZ polymers are flexible structures with the ability to arrange adopting different morphologies depending upon the experimental conditions, as observed by electron microscopy. The aim of this work was to check the possible effect of salt content on those polymers in solution, and confirm whether the apparent differences in size (number of monomers forming the polymer) also observed by EM correlate with the measurements in solution. Sedimentation velocity, light scattering and fluorescence correlation spectroscopy were used to determine the effect of potassium chloride or acetate. KCl has opposite effects on the strength of FtsZ assembly and on the size and diffusion of the fibrils formed in the presence of GTP or GMPCPP. Lowering KCl concentrations rendered polydisperse and larger GMPCPP-FtsZ polymers, while resulted in smaller GTP-FtsZ fibrils consistently behaving as a narrow distribution of preferred species. Potassium acetate has effects comparable to KCl on size distribution of GTP-FtsZ species in the presence of Mg^{2+}. However, in the absence of the cation (i.e. with EDTA) resulted in the formation of large aggregates of FtsZ that, otherwise, remains mainly monomeric. Our results highlight the modulation of the state of association of FtsZ polymers by solution conditions and physiological ligands, which may be a reflection of the fine-tuning of Z ring formation.

INTRODUCTION

FtsZ is probably the most ubiquitous prokaryotic division protein, being an essential component of the bacterial cell division machinery. It is structurally similar to tubulin although their sequences are different. Like tubulin, FtsZ is a GTPase able to form GTP-dependent polymers whose assembly/disassembly, linked to GTP hydrolysis, is crucial for the formation of the dynamic division ring [1]. *E. coli* FtsZ has been shown to polymerize in dilute physiological buffers into one subunit thick protofilaments behaving as a narrow distribution of preferred fibrils [2-5], thought to be the basic entity conforming the Z-ring. The polymorphic nature of FtsZ polymers, enlightened by their capacity to group adopting different levels of organization *in vitro* depending on the experimental conditions as shown by AFM and EM [4, 6, 7], is a reflect of the sensitivity of FtsZ assembly to the environment.

Besides the nucleotide requirement for FtsZ assembly, monovalent and divalent cations seem to play a determinant role [8]. K^+ binding is indispensable for polymerization of *E. coli* FtsZ at physiological pH and, although assembly can also be triggered by other monovalent cations, it is unlikely they play a physiological role given their low affinity for FtsZ [8, 9]. The interaction of FtsZ with monovalent cations has been proposed to be responsible for the dynamic behavior of the polymers, and it has been shown that K^+ concentration affects both the GTPase activity and morphology of FtsZ polymers [8, 10, 11]. On the other hand, the role of Mg^{2+} in FtsZ assembly remains controversial. Thus, it has been suggested that Mg^{2+} is not required for FtsZ assembly but for GTP hydrolysis, since assembly has been found to occur in solutions containing EDTA [11, 12]. However, we have found that removal of Mg^{2+} precludes FtsZ polymerization at neutral pH in the presence of KCl and GTP or GMPCPP, a slowly hydrolysable GTP analog [5].

Here we present a comprehensive study of the effect of KCl concentration on the behavior of FtsZ polymers induced by GTP or GMPCPP using a combination of biophysical methodologies including sedimentation velocity (SV), fluorescence correlation spectroscopy (FCS), dynamic light scattering (DLS) and concentration gradient light scattering (CG-SLS). After a brief description of the materials and methods, the KCl

dependence of the size and homogeneity of both kinds of FtsZ polymers is presented and the differences are emphasized. Next, the effect of replacing KCl by potassium acetate (KAc), particularly in EDTA containing solutions, on FtsZ assembly was addressed. The manuscript concludes with a comparison of the behavior of the GMPCPP and GTP-FtsZ polymers with respect to their modulation by KCl.

MATERIALS AND METHODS

FtsZ purification and labeling: FtsZ was purified and labeled with Alexa 488 as described previously [13-15]. Experiments were performed in working buffer (50 mM Tris-HCl, pH 7.5) supplemented with the specified concentration of KCl (or KAc) and Mg^{2+} or EDTA. GTP-FtsZ polymers were stabilized by an enzymatic regenerating system added immediately before starting measurements [16].

Sedimentation velocity: Experiments were conducted in a Beckman Optima XL-I ultracentrifuge (Beckman-Coulter) with interference optics, following the experimental procedure described before [5]. Differential sedimentation coefficient distributions *c(s)* were obtained from SEDFIT analysis of the sedimenting boundaries [17].

***Composition-gradient static light scattering (CG-SLS)* -** The dependence of 90^{o} scattering intensity with FtsZ concentration was monitored in a modified mini-DAWN light scattering photometer (Wyatt Technology Corp., Santa Barbara) using an automated dilution protocol as previously described [18, 5]. Protein concentration at each dilution step was calculated from the initial concentration and raw scattering intensity data converted to the scaled Rayleigh ratio R/K_{opt} [18] that, although in this case is not a direct function of the composition of macromolecular solutes because of the angular dependence in the scattering of FtsZ polymers [5], is here shown as representative for comparison of different solution properties depending on the composition.

Fluorescence correlation spectroscopy: FCS measurements were carried out on a MicroTime 200 instrument with two-photon excitation as previously described [15]. Data traces were globally analyzed with the software FFS Data processor (SSTC, Belarus) [19] considering a two species model (10-20% free dye and unassembled protein) for

unpolymerized FtsZ-Alexa 488 and a three species model (a single polymeric species, 10-20% unassembled protein with D~50 $\mu m^2/s$ and 10-20% free dye with D~400 $\mu m^2/s$) for FtsZ assembled in the presence of GTP or GMPCPP as described in detail elsewhere [5].

Dynamic light scattering: DLS experiments were carried out with a Protein Solutions DynaPro MS/X instrument (Protein Solutions, Piscataway, NJ) preparing the samples as described in [5]. Data were collected and exported with Dynamics V6 Software and analyzed using user-written scripts and functions in MATLAB (Ver. 7.10, MathWorks, Natick, MA). The obtained autocorrelation functions were analyzed to get the apparent diffusion coefficient, D_{app} [5].

Estimate of molar mass from hydrodynamic measurements: The apparent molar mass of FtsZ polymers was calculated according to the Svedberg equation which requires no assumptions of a specific geometry, using the average standard *s*-values obtained from analysis of sedimentation velocity and the average of the standard *D*-values obtained from analysis of dynamic light scattering and fluorescence correlation spectroscopy, as described in detail in Monterroso *et al*. 2012 [5].

RESULTS

Lowering KCl concentration reduces the size of FtsZ polymers in the presence of GTP: Distributions of sedimentation coefficients is plotted in **Figure 1A** for 1 mg/ml solutions of FtsZ in 1 mM GTP in the presence of the GTP regenerating system and milimolar Mg^{2+} at different KCl concentrations. At 500 mM KCl, the 13 S species was the main sedimenting material, confirming our original observations [4, 5]. The sedimentation coefficient distribution changed considerably upon lowering KCl concentration. At 100 mM KCl, the sedimentation data were well described by a single sedimenting species with s-value around 9 S. This behavior was related to ionic strength and not to specific K^+ effects as verified by control experiments in the presence of 100 mM KCl and 400 mM NaCl that yielded an s-value of 12.5 S similar to the 13 S found in 500 mM KCl.

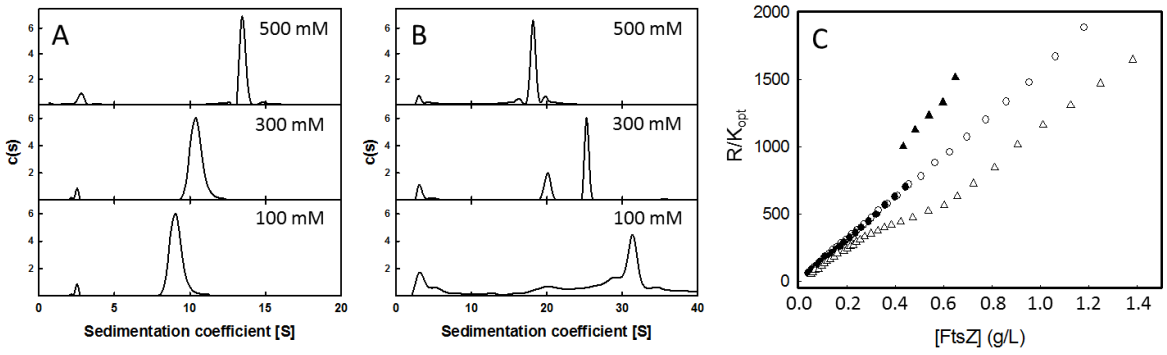

Figure 1. Effect of KCl on FtsZ assembly: Sedimentation velocity and static light scattering analysis. Panels A, B: Sedimentation coefficient distributions of FtsZ (1 mg/ml) in the presence of 1 mM GTP (A) or GMPCPP (B) equilibrated in working buffer with the KCl concentrations specified in the graphs. **Panel C:** Concentration dependence of FtsZ scattering at 90º in GTP and GMPCPP containing buffers at different KCl concentrations. For GTP species (open), KCl was 500 (circles) and 100 mM (triangles), while for GMPCPP species (solid), KCl was 500 (circles) and 100 mM (triangles).

These results were confirmed by CG-SLS experiments: the concentration dependence of scattering intensity at 90^{o} (expressed as normalized Rayleigh ratio R/K_{opt}, see methods and reference 18) decreased as KCl is lowered (**Figure 1C**). In the absence of angular dependence of scattering, R/K_{opt} is directly proportional to protein mass [(20)]. These findings were in good agreement with the translational diffusion coefficients for GTP-FtsZ determined by FCS and DLS, which varied from ~4 to ~5 $\mu m^2/s$ when KCl was lowered from 500 and 100 mM KCl (**Figure 2)**. The faster diffusion and slower sedimentation observed for FtsZ in 100 mM KCl yielded an apparent mass (via Svedberg equation) for these species which is equivalent to protofilaments of 30-40 monomers, in very good agreement with electron microscopy determinations under the same experimental conditions [2, 3, 21]. These values are 2-3 fold lower than the 100 ± 15 monomers estimated for FtsZ protofilaments at 500 mM KCl [5]. Interestingly, taken together, the different experimental techniques favor the presence of a narrow distribution of oligomeric FtsZ species, whose apparent size is inversely proportional to KCl concentration.

FtsZ polymers formed in the presence of GMPCPP become larger and more heterogeneous upon lowering KCl concentration: The dependence on KCl of the sedimentation coefficient distributions of FtsZ in the presence of GMPCPP (a slowly-hydrolyzable GTP analog) and milimolar Mg^{2+} are plotted in **Figure 1B**. In 100 mM KCl, the distribution of FtsZ was quantitatively described by main species with s-values larger than 30 S, significantly higher that the s-value (18 S) that characterized the sedimentation of GMPCPP-FtsZ in 500 mM KCl of 18 S [5]. Therefore the effect of KCl on the sedimentation behavior of GMPCPP-FtsZ was the opposite than the observed for the GTP system.

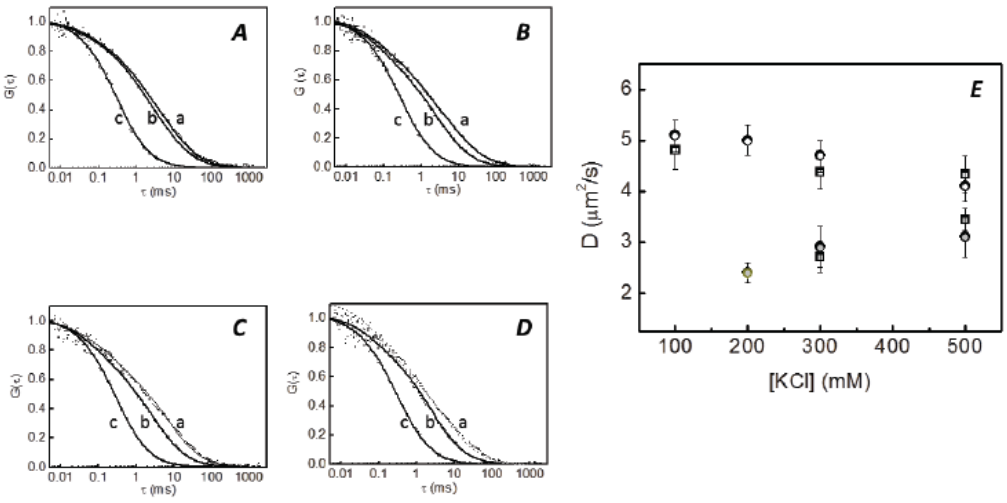

Figure 2. Effect of KCl on FtsZ assembly: Fluorescence correlation and dynamic light scattering analysis. *A*-*D*: Normalized FCS autocorrelation curves of GTP-FtsZ (*b*) and GMPCPP-FtsZ polymers (*a*) in the presence of 500 (***A***), 300 (***B***), 200 (***C***) and 100 mM KCl (***D***). Fits of the models described in reference 5 appear as solid lines. The fit of the GMPCPP-FtsZ profile at 200 mM KCl is shown (faint line) to indicate its low quality, while that of the GMPCPP-FtsZ curve at 100 mM KCl was unacceptable and hence is not shown. Autocorrelation curves of unassembled FtsZ-Alexa488 are plotted for comparison (*c*). ***E.*** Dependence of the normalized translational diffusion coefficients of GTP-FtsZ (open) and GMPCPP-FtsZ (solid) as determined by FCS (circles) and DLS (squares). Data obtained for GMPCPP-FtsZ polymers at 200 mM KCl is masked to indicate low quality of the fit. Data are the average of at least three independent experiments ± SD.

These findings were confirmed by measurements of the concentration dependence of scattering intensity of GMPCPP-FtsZ at different KCl concentrations, being the scattering signal at 100 mM KCl considerably larger than at 500 mM KCl (**Figure 1C**). In addition, fluorescence and scattering measurements yielded D-values of ~3 $\mu m^2/s$ at 500 mM KCl and ~2 $\mu m^2/s$ at 200 mM KCl (**Figure 2**). The faster sedimentation and slower diffusion observed for GMPCPP-FtsZ polymers with lower KCl concentrations is compatible with an increase in the average mass of the polymers, which is opposite to the observed for FtsZ in GTP. Interestingly, the heterogeneity of the large sedimenting species of GMPCPP-FtsZ found at low KCl were compatible with the poor quality of the fit to a single-species model of the FCS at 100 mM KCl, also observed in the fitting of the DLS data. This contrasts with the homogeneous appearance of the GTP-FtsZ species independently of KCl.

A cautionary note on the effect of EDTA on E. coli FtsZ assembly: A remarkable observation was obtained when evaluating the assembly behavior of FtsZ in Mg^{2+} free buffers (in the presence of EDTA) containing acetate instead of chloride as the main monovalent anion. The scattering signal measured by CG-SLS was so high that saturated the detector (not shown), meaning that an aggregation process was taking place. To verify this result, we carried out sedimentation velocity analysis of these same samples (**Figure 3A**). At the highest salt concentration (500 mM KAc) and EDTA large part of the loading material precipitated, while the remaining protein sedimented with *s*-values higher than 30 S. The sedimentation behavior was essentially the same at 300 mM, and the protein sedimented slower (*ca*. 14S) at 100 mM KAc. The larger > 30S aggregates found at 500 mM KAc dissociated to a *ca*. 4S species by a tenfold drop in protein concentration (0.1 g/l, inset in **Figure 3A**).

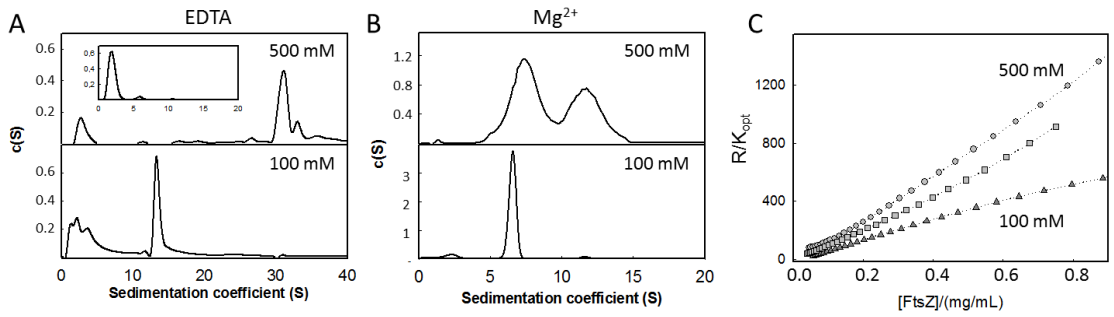

Figure 3. Effect of KAc on FtsZ assembly: sedimentation velocity and static light scattering analysis. Panels A, B: Sedimentation coefficient distributions of FtsZ (1 mg/ml) in the presence of 1 mM GTP equilibrated in working buffer with the KAc concentrations specified in the graphs, with 1 mM EDTA (A) or Mg^{2+} (B). Inset shows dissociation of the 30S aggregate at 500 mM KAc whit dilution of protein concentration to 0.1 g/l. **Panel C:** Concentration dependence of FtsZ scattering at 90^{o} in the presence of GTP at 100 (triangles), 300 (squares) and 500 (circles) mM KAc and 5mM Mg^{2+}.

This behavior contrasts with that observed in Mg-free EDTA/GTP or GMPCPP buffer in the presence of KCl, where no polymers were detected, and most of the protein (95% of the loading material) protein sedimented with an s-value around 2.3 S [5, 15]. It should be noted that the sedimentation velocity (**Figure 3B**) and static light scattering (**Figure 3C**) of FtsZ equilibrated in 5 mM magnesium acetate and 1mM GTP followed essentially the same trend with KAc concentration as in the case of proteins equilibrated in KCl buffers (although the sedimentation distributions are more complex in the KAc system). Therefore, while replacement of chloride by acetate had little effect on the assembly behavior of FtsZ in the presence of Mg^{2+}, in agreement with previous results from several laboratories [11, 12, 16], the FtsZ association behavior in the absence of Mg^{2+} is strikingly different depending on whether KCl or KAc is the main salt in the working buffer.

Table 1. Effect of KCl concentration on sedimentation and diffusion coefficients of FtsZ polymers obtained with GTP and GMPCPP.

[KCl] (mM)	$s_{20,w}$ [a] (S)	$D_{20,DLS}$ ($\mu m^2/s$)	$D_{20,FCS}$ ($\mu m^2/s$)	M_S [b] (g)	monomers/polymer
GTP					
500	14.4 ± 0.1	4.3 ± 0.4	4.1 ± 0.3	3.4×10^6	85 ± 7
300	10.4 ± 0.1	4.4 ± 0.3	4.7 ± 0.3	1.9×10^6	48 ± 5
200	---	---	5.0 ± 0.3	---	---
100	9.0 ± 0.1	4.8 ± 0.4	5.1 ± 0.3	1.7×10^6	43 ± 4
GMPCPP					
500	19.9 ± 0.1	3.4 ± 0.2	3.1 ± 0.4	6.0×10^6	150 ± 10
300	26.8 ± 0.1	2.7 ± 0.3	2.9 ± 0.4	1.0×10^7	240 ± 37
200	---	---	2.4 ± 0.2	---	---
100	> 38	---	---	---	---

Measurements of 0.5 g/L FtsZ in working buffer with 5 mM $MgCl_2$.
[a] Major species when several are present.
[b] Apparent molar mass calculated via the Svedberg equation from the sedimentation coefficient and the average values of the diffusion coefficients obtained by DLS and FCS.

DISCUSSION

Using a variety of hydrodynamic and thermodynamic techniques we have measured the effect of KCl on the size distribution and homogeneity of FtsZ species in the presence of GTP, and in the presence of a slowly hydrolyzable analog, under steady-state conditions. The combined results presented here point clearly that the apparent size of the narrow distribution of polymeric species consistently observed at high KCl [4, 5] was found to decrease upon lowering salt concentration from around 100 (500 mM) to 30-40 monomers (100 mM) per protofilament. This is opposite to the behavior of GDP-containing FtsZ oligomers, in which lowering KCl enhances Mg^{2+}-linked protein self-association [13]. Although the possible functional consequences of these findings are not yet known, they point that the formation of FtsZ oligomers (linked to GDP) and polymers (GTP-driven) do not share the same assembly pathway.

The sizes for the polymers in 500 mM KCl reported here (**Table 1**) and by static light scattering in a previous work [5] are in excellent agreement with those determined by AFM [25], 103 ± 26 subunits for GTP-FtsZ polymers and 137 ± 32 subunits for GMPCPP-FtsZ polymers. Our estimates of sizes from the solution measurements are then in remarkable good agreement with reported data from EM or AFM under equivalent conditions.

In the case of GTP-FtsZ polymers, the differences in size might be related with the suggested tendency of FtsZ polymers to anneal that seems to be enhanced under conditions of lower GTPase activity [11] as those at 500 mM KCl compared to the higher GTPase activity reported for FtsZ polymers at 100 mM KCl [10]. The parallel study of FtsZ in the presence of GMPCPP demonstrate that these FtsZ species responded very different to KCl. The GMPCPP is able to inhibit the GTPase activity [22]. A possible explanation would be that the even lower rate of nucleotide hydrolysis in GMPCPP-FtsZ polymers leads to the formation of larger polymers which size also decreases upon lowering the salt concentration, but that these shorter filaments suffer some kind of electrostatically driven assembly rendering more polydisperse higher order species. With increasing ionic strength, these attractive interactions are screened, and the size of polymer decrease. The sensitivity of FtsZ polymers to the solution conditions seems to be determining not only the structural arrangement of the polymers [4, 7] but their final size, as reflected by the wide range of lengths reported in different EM studies. Thus, at 50-100 mM salt EM depicts polymers of sizes around 50 subunits in KCl [24] and ranging between 20-40 subunits in KAc [2], similar to the 43 ± 4 with 100 mM KCl estimated in this work. Our observation that the size of GTP-FtsZ polymers increases with increasing salt content, whether with KCl or KAc, fully agrees with the work by Chen and Erickson [11] in KAc, where they observed the same trend in the size of the polymers and determined that, in the several assays tested, KCl and KAc gave identical results.

We have observed a remarkable effect on the behavior of GTP-FtsZ at neutral pH in Mg-free buffers containing EDTA depending on the main monovalent anion: replacement of chloride by acetate provokes the aggregation of FtsZ, that otherwise exists as a soluble *ca*. 2.3 S species in Tris-KCl buffer. Very recently, Erickson and co-workers have used KAc buffers to characterize FtsZ filament dynamics at steady state by means of fluorescence-based assays with mutant FtsZ proteins [11]. In their experiments, authors have used EDTA to block the GTPase activity, allegedly altering only polymer dynamics but not the degree of protein assembly [11], i.e. stabilizing them without de-assembly upon GTP depletion. Our experimental observations indicate that Erickson's group statement that FtsZ is able to

polymerize at neutral pH in Mg-free buffers in the presence of EDTA, has to be taken cautiously, since the absence of polymerization in Tris-KCl buffer might not be an exception.

The Z-ring is an essential element of bacterial division responsible for the invagination of the cell membrane that, closely followed by the septation of the cell wall, produces the separation of two daughter cells [1]. Z-ring formation and constriction is known to occur under the control of a concerted downstream reaction modulated by the proteins of the divisome, some of which interact directly with the ring [23]. It is therefore reasonable to think that both the FtsZ pool in the cytoplasm and also the assembled structure are able to react to subtle environmental changes, such as concentration of a certain ligand (GTP/GDP ratio, cation content) or modulators in the membrane with which it interacts (ZipA, FtsN and others), in order to act at a specific moment in the cell cycle. It has been speculated about the polymorphic nature of the FtsZ polymers, able to form very distinct structures depending on the experimental conditions *in vitro* [4, 7], proving its ability to adapt to subtle changes in the surrounding. The results presented here clearly show the plasticity of the Z-ring is reflecting, in turn, the plasticity of the FtsZ species, their main individual constituent polymer, whose structural organization is very much modulated by small physiological ligands and osmolytes. In addition, our results could help to clarify several discrepancies reported on the literature of FtsZ.

References

1. Mingorance J, Rivas G, Vélez M, Gómez-Puertas P, Vicente M. Strong FtsZ is with the force: mechanisms to constrict bacteria. Trends Microbiol. 2010 Aug;18(8):348-56. and references therein.

2. Chen Y, Erickson HP. Rapid in vitro assembly dynamics and subunit turnover of FtsZ demonstrated by fluorescence resonance energy transfer. J Biol Chem. 2005 Jun 10;280(23):22549-54.

3. Romberg L, Simon M, Erickson HP. Polymerization of Ftsz, a bacterial homolog of tubulin. is assembly cooperative? J Biol Chem. 2001 Apr 13;276(15):11743-53. Epub 2001 Jan 4.

4. González JM, Vélez M, Jiménez M, Alfonso C, Schuck P, Mingorance J, Vicente M, Minton AP, Rivas G. Cooperative behavior of Escherichia coli cell-division protein FtsZ assembly involves the preferential cyclization of long single-stranded fibrils. Proc Natl Acad Sci U S A. 2005 Feb 8;102(6):1895-900. Epub 2005 Jan 31.

5. Mg^{2+}-linked self-assembly involves the concerted formation of a narrow distribution of oligomeric species. Begoña Monterroso, Rubén Ahijado-Guzmán, Belén Reija, Carlos Alfonso, Silvia Zorrilla, Allen P. Minton, and Germán Rivas. Biochemistry In press.

6. Mingorance J, Tadros M, Vicente M, González JM, Rivas G, Vélez M.Visualization of single Escherichia coli FtsZ filament dynamics with atomic force microscopy. J Biol Chem. 2005 May 27;280(21):20909-14. Epub 2005 Mar 26.

7. Popp D, Iwasa M, Narita A, Erickson HP, Maéda Y. FtsZ condensates: an in vitro electron microscopy study. Biopolymers. 2009 May;91(5):340-50.

8. Tadros M, González JM, Rivas G, Vicente M, Mingorance J. Activation of the Escherichia coli cell division protein FtsZ by a low-affinity interaction with monovalent cations. FEBS Lett. 2006 Sep 4;580(20):4941-6. Epub 2006 Aug 8.

9. Mingorance J, Rueda S, Gómez-Puertas P, Valencia A, Vicente M. Escherichia coli FtsZ polymers contain mostly GTP and have a high nucleotide turnover. Mol Microbiol. 2001 Jul;41(1):83-91.

10. Lu C, Erickson HP. Purification and assembly of FtsZ. Methods Enzymol. 1998;298:305-13.

11. Chen Y, Erickson HP. FtsZ filament dynamics at steady state: subunit exchange with and without nucleotide hydrolysis. .- Biochemistry. 2009 Jul 21;48(28):6664-73.

12. Erickson HP, Anderson DE, Osawa M. FtsZ in bacterial cytokinesis: cytoskeleton and force generator all in one. Microbiol Mol Biol Rev. 2010 Dec;74(4):504-28.

13. Rivas G, López A, Mingorance J, Ferrándiz MJ, Zorrilla S, Minton AP, Vicente M, Andreu JM. Magnesium-induced linear self-association of the FtsZ bacterial cell division protein monomer. The primary steps for FtsZ assembly. J Biol Chem. 2000 Apr 21;275(16):11740-9.

14. Jiménez M, Martos A, Vicente M, Rivas G. Reconstitution and organization of Escherichia coli proto-ring elements (FtsZ and FtsA) inside giant unilamellar vesicles obtained from bacterial inner membranes. J Biol Chem. 2011 Apr 1;286(13):11236-41. Epub 2011 Jan 21.

15. Reija B, Monterroso B, Jiménez M, Vicente M, Rivas G, Zorrilla S. Development of a homogeneous fluorescence anisotropy assay to monitor and measure FtsZ assembly in solution. Anal Biochem. 2011 Nov 1;418(1):89-96. Epub 2011 Jul 13.

16. González JM, Jiménez M, Vélez M, Mingorance J, Andreu JM, Vicente M, Rivas G. Essential cell division protein FtsZ assembles into one monomer-thick ribbons under conditions resembling the crowded intracellular environment. J Biol Chem. 2003 Sep 26;278(39):37664-71. Epub 2003 Jun 14.

17. Schuck P, Rossmanith P. Determination of the sedimentation coefficient distribution by least-squares boundary modeling. Biopolymers. 2000 Oct 15;54(5):328-41.

18. Fernández C, Minton AP. Automated measurement of the static light scattering of macromolecular solutions over a broad range of concentrations. Anal Biochem. 2008 Oct 15;381(2):254-7. Epub 2008 Jun 27.

19. Skakun VV, Hink MA, Digris AV, Engel R, Novikov EG, Apanasovich VV, Visser AJ. Global analysis of fluorescence fluctuation data. Eur Biophys J. 2005 Jun;34(4):323-34. Epub 2005 Feb 12.

20. K.A. Stacey, Light-Scattering in Physical Chemistry, Academic Press, New York, 1956.

21. Li Z, Trimble MJ, Brun YV, Jensen GJ. The structure of FtsZ filaments in vivo suggests a force-generating role in cell division. EMBO J. 2007 Nov 14;26(22):4694-708. Epub 2007 Oct 18.

22. Salvarelli E, Krupka M, Rivas G, Vicente M, Mingorance J. Independence between GTPase active sites in the Escherichia coli cell division protein FtsZ. FEBS Lett. 2011 Dec 15;585(24):3880-3. Epub 2011 Nov 3.

23. Vicente M, Rico AI, Martínez-Arteaga R, Mingorance J. Septum enlightenment: assembly of bacterial division proteins. J Bacteriol. 2006 Jan;188(1):19-27.

24. Huecas S, Llorca O, Boskovic J, Martín-Benito J, Valpuesta JM, Andreu JM. Energetics and geometry of FtsZ polymers: nucleated self-assembly of single protofilaments. Biophys J. 2008 Mar 1;94(5):1796-806. Epub 2007 Nov 16.

25. Mateos-Gil et al. 2012. In Press

SUPLEMENTARY MATERIAL

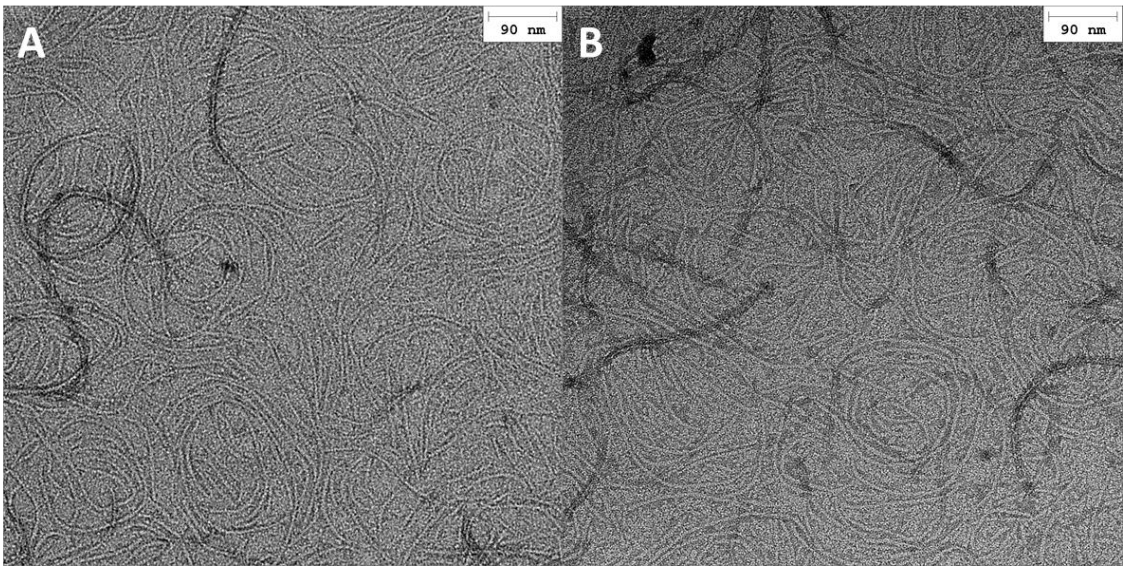

Figure S1. Transmission electron microscopy images of GMPCPP-FtsZ (A) and GTP-FtsZ (B) in the presence of 500 mM KCl and 5 mM Mg^{2+}. The polymerization was induced by addition of nucleotide to a final concentration of 1 mM. After 1 min, a drop of protein solution was applied to carbon-coated, glow-discharged copper grids, blotted, and stained with 2% uranylacetate and air dried and visualized under a Jeol JEM-1230 microscope operated at 100 kV and a nominal magnification of 60,000.

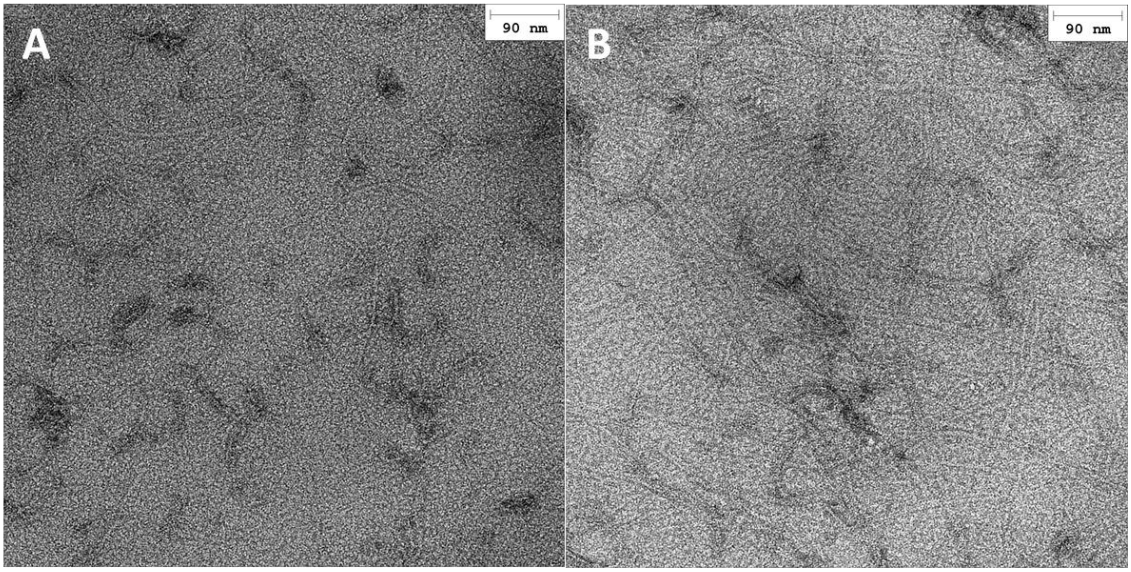

Figure S2. Transmission electron microscopy images of GTP-FtsZ (A) and GMPCPP-FtsZ (B) in the presence of 100 mM KCl and 5 mM Mg^{2+} prepared following description in Figure S1.

CHAPTER III

RECONSTITUTION, SELF-ASSEMBLY AND SERS-BASED DETECTION OF THE INTERACTIONS BETWEEN THE ESSENTIAL DIVISION FtsZ PROTEIN AND BACTERIAL MEMBRANE ELEMENTS

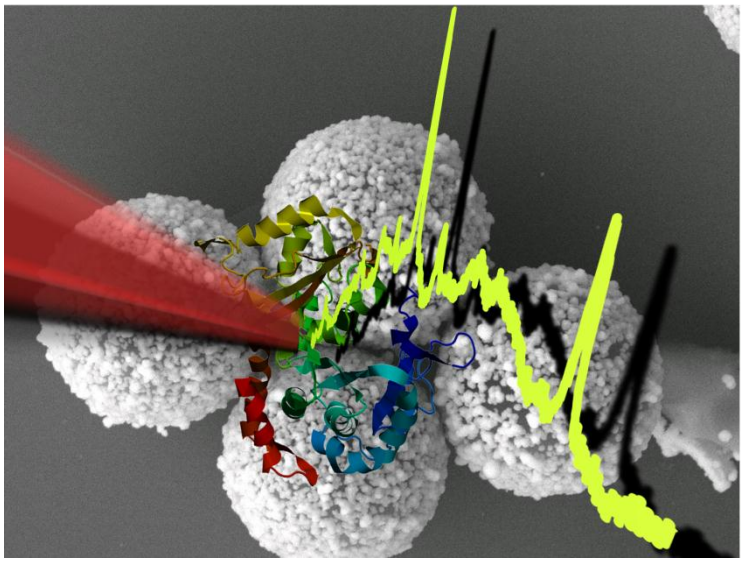

Surface-enhanced Raman scattering spectroscopy (SERS) sensing has been applied to detect the interaction of the FtsZ protein from *Escherichia coli* with membrane-bound elements of the division machinery on the surface of synthetic and natural membranes supported on silver-coated polystyrene micron-sized beads. The engineered micro-beads offer a stable support with a high density of SERS hotspots, allowing the sensing of conformational changes associated to the binding of FtsZ to the membrane. This system can be exploited to develop systematic assays to screen for substances that inhibit FtsZ attachment to the membrane with potential antimicrobial activity.

INTRODUCTION

The detection of interactions between soluble proteins and membrane receptors at the membrane environment is very important to biological and pharmacological research as many biochemical processes involve membranes and, therefore, a significant amount of the successful drugs in the market target membrane-associated proteins. The understanding of these processes is key for the development of new families of therapeutic agents, especially those targeting protein-membrane receptor interactions.[1] The bacterial division machinery is a good example of an essential dynamic macromolecular assembly process that takes place at the membrane.

The first known event during the bacterial division process is the formation of the proto-ring, where the soluble cytoplasmic protein FtsZ interacts with the membrane protein ZipA [2] When FtsZ and ZipA interact, conformational changes occur in the C-terminal domain of ZipA.[3] The understanding of the FtsZ-ZipA interaction within the membrane is of special interest as it is essential for the bacterial cell division process[4] and, consequently, an important target in the development of new families of antibiotics.

ZipA, a membrane protein, is a 328-amino acid protein that is composed of three domains.[5] However, the binding activity toward FtsZ is localized in the C-terminal domain (residues 189−328). Therefore mutagenesis of the ZipA gene, followed by overexpression and purification were carried out by eliminating the part ranging from the N-terminal domain to the P/Q domain of native ZipA (aminoacids 1-188), while preserving the bioactivity[6] and also keeping the hexahistidine-tag, which is known to bind strongly to silver, gold and Ni-NTA groups.[7] In the case of FtsZ, the wild type protein was expressed and purified from *E. coli*.[8] Notably, FtsZ has GTPase activity[9] and, *in vitro*, forms a variety of polymers in a GTP-dependent manner.[10] We designed several experiments of increasing complexity to study by SERS the FtsZ-ZipA interaction that initiates the bacterial division.

High throughput screening devices are strongly dependent on strategies to miniaturize the sensors. Employing particles as nanoscopic reporters offers the possibility to screen the biomolecular interactions on native membranes.[1] On this way,

Nanoplasmonics has been developed sufficiently to provide suitable tools for studying the mechanisms underlying the interaction between biomacromolecules. A key factor is the engineering of a plasmonic surface with sufficient colloidal stability to reproduce the natural conditions that involve the bioproblem. Surface-enhanced Raman scattering (SERS) spectroscopy[11] is a ultrasensitive molecular spectroscopy technique for with detection limits down to the single molecule have been demonstrated.[12] Additionally, SERS is a vibrational spectroscopy, and thus it provides detailed information about the structure, conformation, and environment of the given molecular target and, more important, experiments can be carried out under biological conditions.[13] These features make SERS especially suitable for the characterization of such protein or nucleic acid interactions that induce conformational changes.[14] However, working with plasmonic nanoparticles and proteins, is usually demanding due to either the size of the target analyte as compared with that of the substrate or the need of using solvents or other biological buffers with high ionic strength to avoid protein denaturalization. Thus, to properly address this drawback a considerable effort is required toward the preparation of highly stable while optically active materials, to be used as both supports and optical enhancers. During the last years our group has pioneered the engineering of colloidally stable, optically dense discrete particles comprising a polymeric or inorganic micro- or submicron-particle homogeneously coated with the desired plasmonic nanostructure.[15] Herein we take advantage of these fabrication protocols to engineer polystyrene microparticles coated with gold and silver (PS@Au@Ag), which display high optical activity, for the immobilization of lipid or bacterial inner membrane and the study of the structural behavior of membrane proteins involved in the cell division process.

In this work, the interaction between FtsZ and ZipA was studied by detection of the vibrational changes in the spectra of ZipA supported onto metallic enhancing nanostructure platforms (PS@Au@Ag beads) promoted by the addition of FtsZ. The characterization of this interaction was done at three different levels of complexity regarding the way ZipA was stabilized onto the metallic nanostructure surface. First, interaction of FtsZ with soluble recombinant mutant of ZipA attached through their

hexahistidine tag to the nanostructures was characterized. Results were then compared to those obtained for FtsZ-ZipA interaction with this ZipA mutant within a lipid bilayer environment. Finally, the interaction of FtsZ with wild type ZipA, that is in the *E. coli* inner membrane that includes other division components, was detected.

RESULTS

Engineered microparticles as SERS platform: PS@Au@Ag microparticles were prepared by using slight modifications of the protocols described in previous reports.[15a, 16] A scheme illustrating the different steps involved in the fabrication of the hybrid material, together with their scanning electron microscopy (SEM) characterization, is shown in **Figure 1A**. Briefly, the positively charged surface of the selected support, in this case homogeneous polystyrene beads with 3 μm diameter, was sequentially coated with polyelectrolytes of opposite charge, namely polystyrenesulfonate (PSS, negative), poly(diallyldimethylammoniumchloride) (PDDA, positive), again PSS and finally, poly(allylaminehydrochloride) (PAH, positive), so as to improve the homogeneity of the coating. The outer PAH layer generates a highly positively charged surface (zeta potential +35 mV) that is appropriate for the adsorption of negatively charged gold nanoparticles (zeta potential -40 mV) (step 2). Upon extensive cleaning to ensure that all non-adsorbed gold nanoparticles were removed, those which remained adsorbed were epitaxially overgrown with silver by *in situ* reduction of Ag^+, using salicylic acid in a glycine buffer (pH 9.5), at room temperature (step 3). It is interesting to note that gold seeds are preferred over silver for subsequent silver growth, mainly due to their higher chemical stability.[17] After systematic variation of the amount of added Ag^+ between 0.6 and 2.4 μmol per mg of polymer beads, an Ag^+ concentration of 1.8 μmol per mg of beads was selected as optimal, since lower concentrations did not result in suitable interparticle plasmon coupling, while higher concentrations yielded interconnected particles with localized surface plasmon resonance (LSPR) radiative damping.[18] As a final product, this preparation process resulted in micron-sized hybrid plasmonic particles with a homogeneous coating of interacting silver particles[19] of ca. 50 nm in size.

Optical properties of the material were characterized by UV-Vis-NIR spectroscopy on a dispersion of the silver coated beads showing a maximum centered at 660 nm (**Figure 1B**). The optical enhancing properties of the nanostructured microbeads were tested through SERS measurements using Benzenethiol (BT) as a model molecular probe. The SERS spectra of BT (**Figure 1C**) at different excitation wavelengths were dominated by the vibrational modes of BT corresponding to the ring breathings (999 and 1073 cm^{-1},) and the C-H in-plane bending (1023 cm^{-1}).

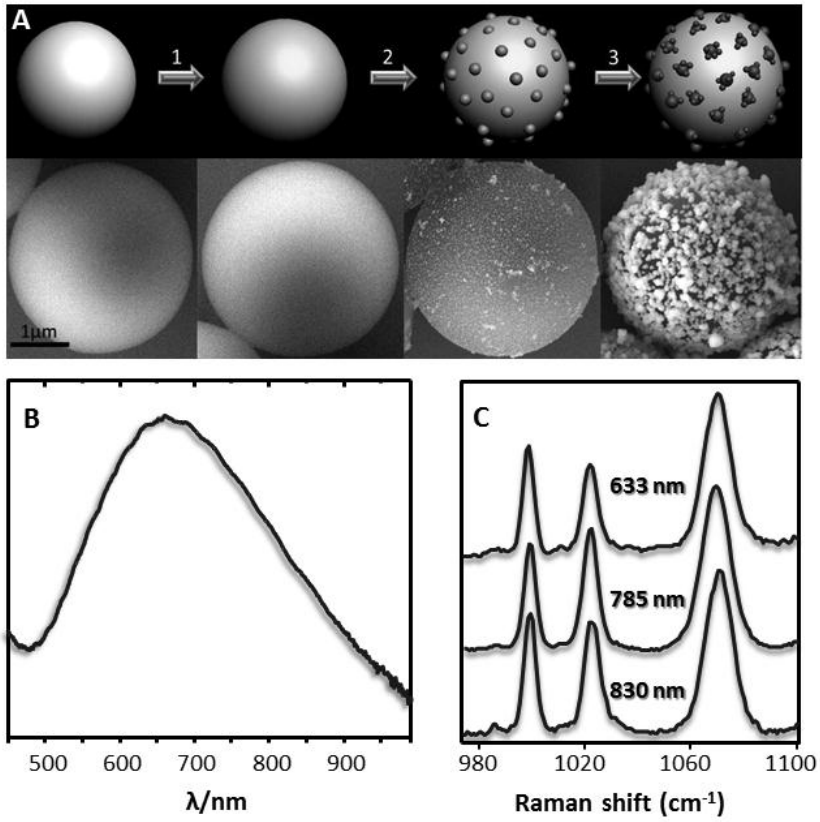

Figure 1. (A) Scheme of the preparation of PS@Au@Ag beads and corresponding SEM characterization. Step 1: micron-sized polystyrene beads were wrapped with polyelectrolytes by sequential LbL self-assembly of PSS, PDDA, PSS, and PAH. Step 2: 15 nm gold nanoparticles were adsorbed onto the functionalized surface of the beads. Step 3: Silver was epitaxially growth on the adsorbed gold nanoparticle surfaces to obtain the final nanocomposite material. (B) UV-Vis-NIR spectrum of the PS@Au@Ag beads in water. (C) SERS spectra of benzenethiol on PS@Au@Ag measured upon excitation with 633, 785 and 830 nm laser lines.

SERS-monitoring FtsZ-ZipA interactions: In a first approach the purified recombinant mutant of ZipA (s2-ZipA, aminoacids 189−328) was directly attached to engineered PS@Ag@Au beads through the hexahistidine-tag. It is worth noting that different amounts of s2-ZipA (5 to 20 µM) were added to maximize the SERS signal, which was found to be best for a concentration of 15 µM in dispersions containing 3.3 mg beads per mL. To investigate the interactions of s2-ZipA with FtsZ, 25 µM of the latter was added to the PS@Ag@Au-s2-ZipA sample, either in the GDP and GTP forms.

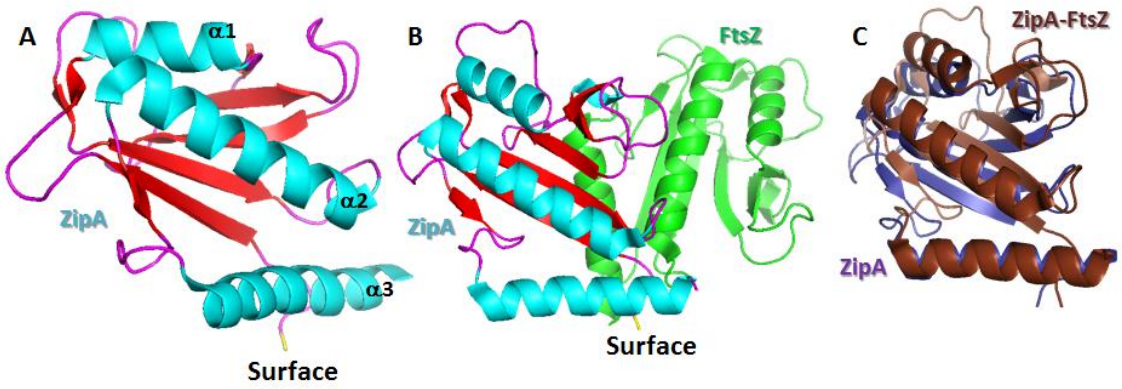

Figure 2. Conformations of s2-ZipA (A); s2-ZipA interacting with FtsZ (B); and overlapped conformations of s2-ZipA (C), before (purple) and after (brown) interaction with FtsZ. Spiral: α-helix; arrow: β-sheet; and, line: random coil. These structures can be accessed free of charge from the Protein Data Bank (access numbers: 1F7W and 1F46). [3, 20]

As an indication, Figure 3 shows the conformations of s2-ZipA,[20] s2-ZipA interacting with FtsZ[3] and the overlapped conformations of s2-ZipA before and after interaction with FtsZ. On the other hand, Figure 4A shows the SERS spectra for s2-ZipA attached to the beads, with and without FtsZ, in the presence and the absence of GTP. The SERS spectrum of s2-ZipA (**Figure 3A**) is dominated by bands that can be assigned to different amino acid residues; for example 1600 cm^{-1} (Phe, Tyr), 1460 cm^{-1} (Ala, Ile, Val, Leu, Tyr), 1319 cm^{-1} (Ala, Lys, Ile, Val, Ser, Gly, Tyr), 1199 cm^{-1} (Phe, Tyr), 1031 cm^{-1} (Phe, Tyr), 1000 cm^{-1} (Phe), 938 cm^{-1} (Leu, Lys, Val), 848 cm^{-1} (Ile, Tyr), 785 cm^{-1} (Ala, Trp, Phe).[21] All these residues, except Phe, are components of the α3-helix (**Figures 2A and 3B**), which is the closest domain (1.2 nm) to the silver surface. The closest Phe residue is around 1.5 nm from the surface (in the α2-helix), however the position of its aromatic ring facing down and almost

normal to the silver surface notably increases its signal, in full agreement with surface selection rules.[22]

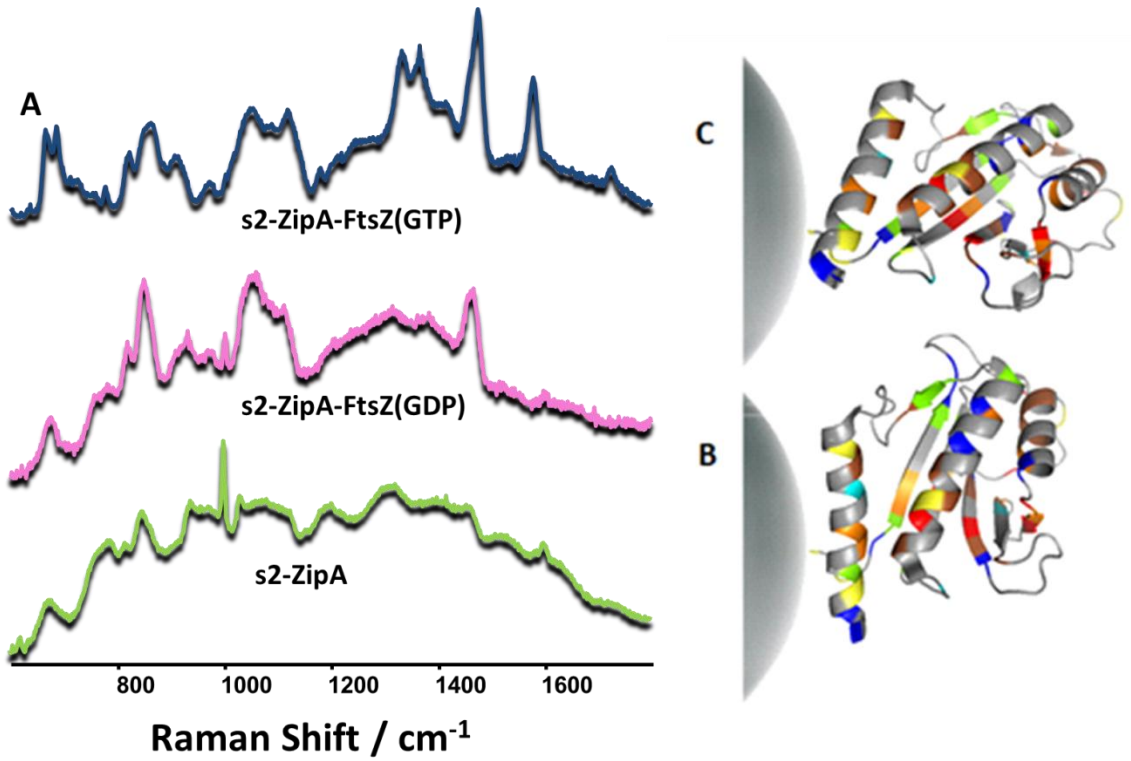

Figure 3. (A) SERS spectra of s2-ZipA on PS@Au@Ag beads, before and after interaction with FtsZ, in the presence and absence of GTP. Samples were illuminated with a 785 nm laser line to avoid damage of the proteins. (B,C) conformation of s2-ZipA on the silver surfaces before and after the interaction with FtsZ, in the absence of GTP. To improve visibility, the residues that are dominant in the vibrational spectra were color-coded as follows: Phe: red, Tyr: cyan, Lys: yellow, Ala: blue, Ile: orange, Leu: brown and Val: green.

When the GDP-FtsZ is added, the cytoplasmic protein self-associates in a non-cooperative fashion yielding oligomers from 1 to 6 units.[6] The SERS spectrum of the complex s2-ZipA-FtsZ(GDP) oligomer resembles that of the s2-ZipA alone but with significant and consistent reproducible differences such as the enhancement of the bands at 1465 cm^{-1} (Ala, Tyr), 1055 cm^{-1} (Ala) and 848cm^{-1} (Tyr) while the ring breathing of Phe 1000 cm^{-1} decreases in intensity. FtsZ interacts specially with the β3-6 sheets (**Figue 3B**), which are relatively far away from the surface (ca. 3 nm). However, the conformational changes of s2-ZipA (**Figure 3C**), produce the subsequent change in its orientation on the metallic surface. Interestingly, the α3-helix, which is almost parallel to the surface when s2-ZipA is free

(**Figure 3B**), gets farther away up to 1.8 nm on one side while approaching on the opposite side upon complexation (**Figure 3C**). This variation leads to positioning the Ala residue perfectly aligned with the silver surface at 0.7 nm, notably increasing its corresponding SERS signal as described by the electromagnetic mechanism.[23] Additionally, the condensed aromatic moiety of Tyr in α3 becomes perpendicular to the surface, contrary to the aromatic ring of Phe, which loses its coupling to the surface vector as the α2-helix opens its angle with respect to the surface. This leads to an increase of the Tyr signal and a decrease of that due to Phe. These variations resemble those reported by monocrystal X-ray diffraction.[3]

In the presence of GTP, FtsZ forms a polymer. Besides the changes appreciated with the oligomeric FtsZ complex (**Figure 3A**), large enhancements of several bands at 1580 cm^{-1} (Tyr), 1366 and 1332 cm^{-1} (Trp, Val), 1115 cm^{-1} (Ala), 909 cm^{-1} (Ala) can be observed indicating a closer distance of the α3-helix to the silver surfaces. Additionally, new SERS bands appear at 1724 cm^{-1} (amide I), 1178 cm^{-1} (Tyr). Although due to the size of the polymeric FtsZ, the interaction of some of their residues within the plasmonic surface cannot be discarded, the difference of both vibrational spectra of s2-ZipA with respect to different forms of FtsZ reveals a different structural conformation of s2-ZipA in the presence of oligomers or polymers. This significant structural difference in s2-ZipA protein is consistent with previous studies revealing a moderate affinity between ZipA and GDP-FtsZ.[6] Observed structural differences might be thus related with the effect exerted by ZipA that, by interactions with GTP-FtsZ polymers, renders polymer bundles that would, induce a heavier structural change in the s2-ZipA spectra.[25]

Detection of the interaction of FtsZ with ZipA attached to the lipid membrane.

In order to confirm the successful immobilization of the membranes onto the beads, fluorescence images were acquired using DiI C18 (**Figure 4A**), which selectively attaches to the lipidic membranes, and anti-ZipA+ anti-rabbit-488 (**Figure 4B**), which selectively recognises the s2-ZipA attached to the lipid membrane. Negative controls using antibodies and fluorescence dies as performed successfully. The SERS spectrum of *E. coli* polar lipids doped with DGS-NTA (**Figure 4C**) is dominated by the lipidic CH_2 scissoring and

twisting (1378 and 1322 cm^{-1}) and the alkyl skeletal vibrations (1125 and 1033 cm^{-1}).[26] Concerning the polar headgroups, the SERS bands corresponding to the C-N stretching of the O-C-C-N+ segment are observed at 1003 cm^{-1}, while 904 and 759 cm^{-1} are ascribed to the trans conformation of this fragment as described previously.[27]

The attachment of s2-ZipA to these microbeads coated with the lipid bilayer containing DGS-NTA-Ni produce minimum changes as compared with those detected in the previous experiment did not produce significant changes regarding the lipid bands in the SERS spectra (**Figures 4C**). Binding of FtsZ, either unpolymerized or polymerized, to s2-ZipA there produced a difference in the behavior depending on the association state of FtsZ. Thus, while there were no remarkable changes by binding of GDP-FtsZ, several significant changes were detected upon binding to GTP-FtsZ polymers (**Figure 5C**). New several bands appeared at 1724 cm^{-1} (Amide), 1580 (Phe, Tyr), 1366 and 1332 cm^{-1} (Trp, Val, Phe), 1115 cm^{-1} (Ala), 1178 cm^{-1} (Tyr, Phe), 909 cm^{-1} (Ala), 686 cm^{-1} and 665cm^{-1} [(21)].

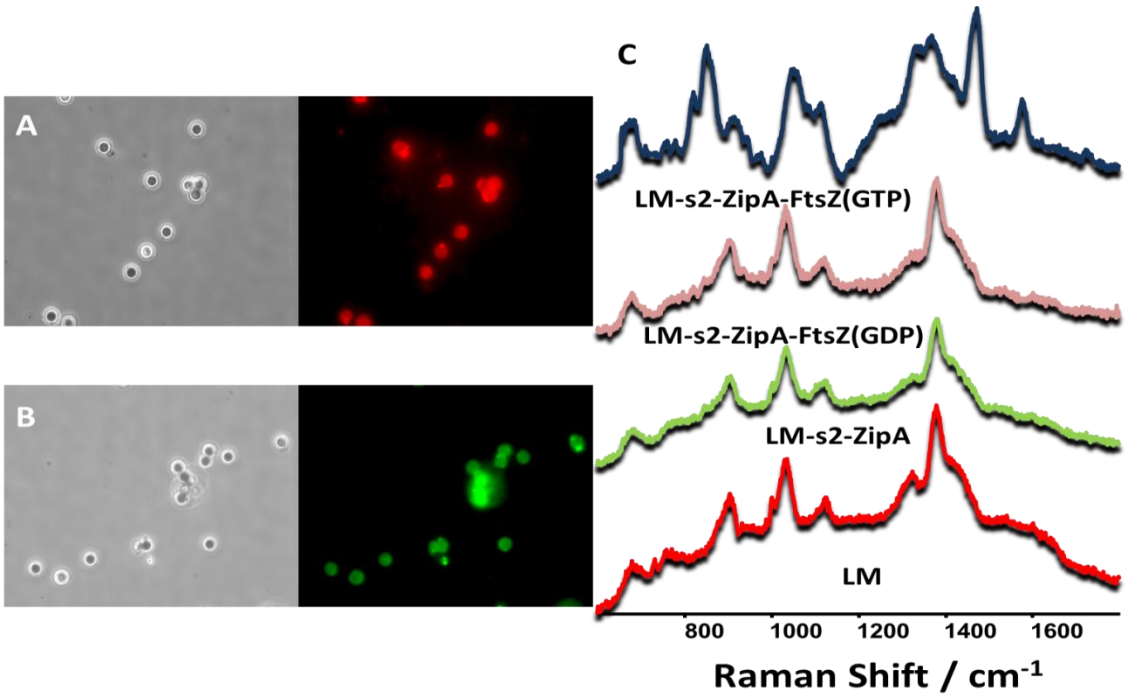

Figure 4. PS@Au@Ag@Lipid membrane (LM)-s2-ZipA incubated with (A, B) DiI C18 and Anti-ZipA+ Anti-rabbit-488. (C) SERS spectra of the PS@Au@Ag@Lipid membrane before and after the attachment of s2-ZipA, and the interaction of s2-ZipA with FtsZ, in the GDP and GTP forms.

SERS detection of assembled FtsZ polymers on the *E. coli* inner membrane.

In subsequent experiments, bacterial membranes were deposited onto the plasmonic beads. The inner membrane vesicles were isolated from wild-type *E. coli* (strain JM600) exponential phase culture.[28] The inner and outer membranes were separated by sucrose gradient centrifugation,[29] washed and diluted to reach 20 absorbance units at 280 nm, and stored frozen.[30] For the deposition, the membranes were added to the bead dispersion and incubated at 37 ^{o}C. In this case, entire ZipA is a natural component of the bacterial membrane. In order to confirm the successful immobilization of the membranes onto the beads, fluorescence images were acquired using DiI C18 (**Figure 5A**), which selectively attaches to the lipidic membranes, and anti-ZipA+ anti-rabbit-488 (**Figure 5B**), which selectively recognises the ZipA membrane protein.

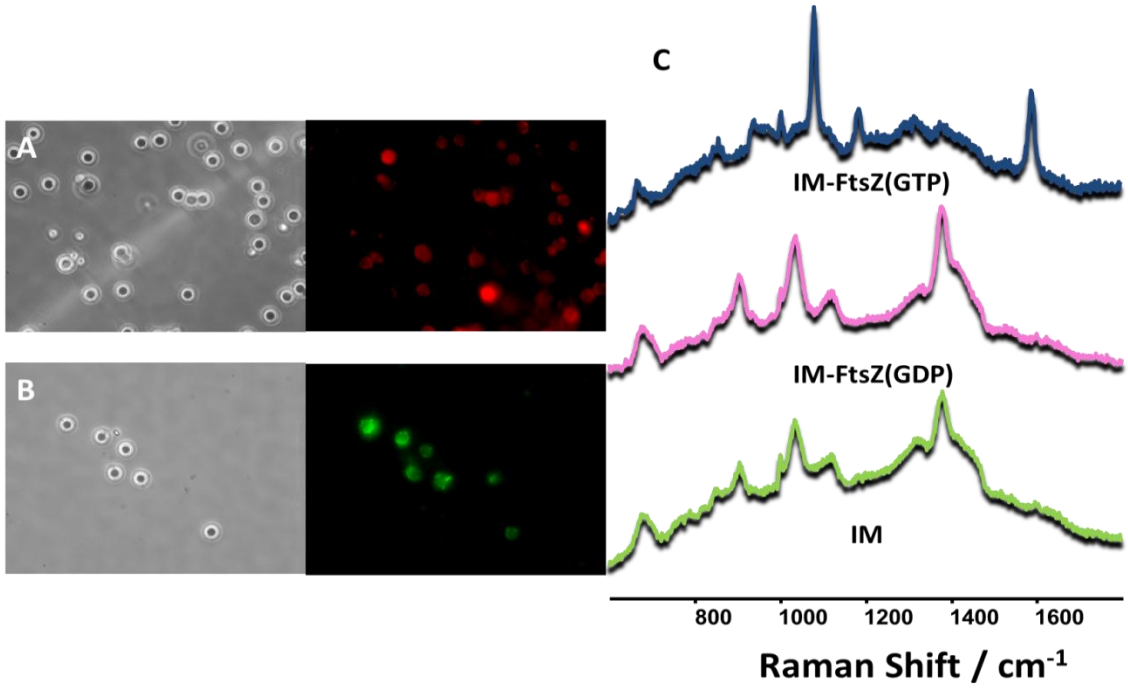

Figure 5. PS@Au@Ag@inner membrane (IM) incubated with (A, B) DiI C18; and, Anti-ZipA+ Anti-rabbit-488. Negative control experiments were carried out, thus evidencing the absence of nonspecific adsorption of the dyes and the successful immobilization of the membrane. (C) SERS spectra of the PS@Au@Ag@inner membrane before and after the interaction with FtsZ, in the presence and absence of GTP.

The PS@Au@Ag@inner membrane beads were characterized by SERS prior to the interaction with the FtsZ protein (**Figure 5C**). The SERS spectrum, as in lipid membrane case, is dominated by the lipidic CH_2 scissoring and twisting (1378 and 1322 cm^{-1}) and the alkyl skeletal vibrations (1125 and 1033 cm^{-1}).[26] Concerning the polar headgroups, the SERS bands corresponding to the C-N stretching of the O-C-C-N+ segment are observed at 1003 cm^{-1}, while 904 and 759 cm^{-1} are ascribed to the trans conformation of this fragment as described previously.[27] Notably, several aminoacids can be recognized as well, especially those of Phe (1000 cm^{-1}) and Tyr (1319 cm^{-1}), which is consistent with the high SERS cross-sections of their aromatic groups, as compared with the essentially alkylic nature of the membrane. As in the case of lipid membrane-coated beads, when the GDP-FtsZ protein is added minimum changes can be inferred from the spectrum as compared with those detected in the previous experiments without membranes. This is most likely due to the fact that the lipidic membrane increases the distance between ZipA and the plasmonic surface but also because the oligomeric FtsZ does not affect sufficiently the membrane elements. When GTP is added, FtsZ forms a polymer that directly interacts with different membrane elements. The SERS spectrum of this complex shows notable differences as compared to that of the membrane. Basically, the spectrum presents several new bands at 1589 cm^{-1} (Phe, Tyr), 1182 cm^{-1} (Tyr, Phe, C-C stretch) and 1080 cm^{-1} (C-C skeleton gauche structure). On the other hand, bands at 1380 cm^{-1} (CH_2 scissoring from lipid chains) and 906 cm^{-1} (C-C stretch and skeletal bend) decreases in intensity. The presence of these aminoacid bands, together with the shifts in those of the lipidic membrane, suggests that the polymeric FtsZ not only interacts with ZipA but also are interacting with other membrane elements. Further, these results are compatible with data from two-hybrid and other interaction assays indicating the existence of a complex network of interactions between *E.coli* cell division proteins.[31]

DISCUSSION

The result of the reconstitution of proto-ring elements provides enough evidences to confirm the role of membrane protein ZipA that is anchoring FtsZ filaments to the inner membrane. It was observed in SEM images that the growth of FtsZ polymers attached

from membrane through ZipA is forming three-dimensional network, even grow into fibers that link different microbeads.

In addition, we present the fabrication of a highly efficient SERS substrate, shaped as discrete microbeads instead of metal films or other conventional SERS supports, as the basis for the study and detection of the interaction between biological macromolecules. These nanostructured platforms, carrying a high dense collection of silver hotspots homogeneously distributed on the surface, present several advantages that make them especially suitable as portable sensors. Besides are very stable and observable under a conventional optical microscope. The high sensitivity of SERS, allowing to work with very small amounts of beads, and consequently lipids, membrane and proteins, decreasing in turn the effective cost and lowering the detection limits as compared with conventional colloidal suspensions [15, 17]. As seen in this work, they also provide the ability to detect specific macromolecular assemblies, thus overcoming the need to use specific antibodies or fluorescence dies.

The interaction between ZipA and FtsZ induces a modification in the structure of the C-terminal domain of ZipA,[3] that produces changes in the frequencies and intensities of the signals characterizing the spectra of the protein. Although by SERS those changes are easily detectable because they reflect modifications in chains and aromatic residues that are very sensitive to small changes in secondary and higher-order structures. Thus, while the spectra of mutant s2-ZipA (attached to either plain or lipid coated PS@Au@Ag beads) were modified in the presence of FtsZ polymers (GTP-FtsZ), the interaction with oligomeric FtsZ (GDP-FtsZ) was detected only in the absence of lipids, indicating the conformational changes produced in s2-ZipA by binding of FtsZ are different depending on the association state of the later and/or the environment of the sensor. The fact that the interaction with both species in the absence of lipids is actually detected rendering different vibrational spectra suggests a different structural conformation of s2-ZipA on the sensor surface in the presence of oligomers (GDP-FtsZ) and polymers (GTP-FtsZ). In the case of GDP-FtsZ, was demonstrated that the interaction does not significantly affect the interaction between GDP-FtsZ monomers [15]. On the other hand, in the case of GTP-FtsZ,

were reported clear evidences about the bundle formation of GTP-FtsZ polymers by interaction with ZipA [31]. Also, in the case of lipid coating, the bilayer might be dissipating the SERS signal, making an interaction undetectable.

Regarding s1-ZipA mutant, none of the interactions tested produced a significant change in the SERS spectra. The P/Q domain would provide, enough distance between the interaction domain in s1-ZipA and the silver sensor, meaning the structural changes induced in ZipA would have not been transmitted from that point to the sensor along the linker chain.

As in the case of lipid coated beads, the interaction between the beads coated with bacterial inner membrane and GDP-FtsZ oligomers is not detectable. In the case of the interaction with the polymer (GTP-FtsZ), however, FtsZ is interacting not only with ZipA but with other elements of the bacterial division machinery present in the membrane as part of a downstream complex network of interactions [2, 31].

The considerable changes observed in the SERS spectra might, therefore, reflect significant conformational changes arising from this cascade of events in the macromolecular complexes present in the inner membrane and distinguishing them clearly from the spectra of the lipid coated beads, lacking all membrane protein components but ZipA.

The work presented here is intended to improve the development of direct detection assays based in the generation of portable sensors combined with SERS spectroscopy for fast and ultrasensitive detection of relevant macromolecular assemblies, as protein-protein non-covalent interactions on the natural membrane environment. This system provides the benefits of the very high sensitivity of SERS spectroscopy to detect small conformational changes of macromolecules attached to a sensor surface at micro-molar concentrations by weak non-covalent interactions. It is here presented its application to the detection of the interactions between elements of the bacterial cell division machinery, enlightening how these nanostructured sensors are of special interest for the detection of potential antibiotic targets.

CONCLUSIONS

In summary, the vibrational changes in SERS spectra of ZipA when is attached to oligomeric or polymeric FtsZ forms reveal that FtsZ interacts with ZipA differently as a function of the polymeric state of the former. The vibrational SERS spectra of ZipA reveal important conformational differences in the hetero-association that are compatible with the observed behavior *in vitro* and *in vivo* regarding stabilization and bundle formation of FtsZ polymers by ZipA. In addition, considerable changes in the SERS spectra were detected due to a cascade of interactions initiated by polymeric FtsZ that produce significant conformational changes in the division machinery within the inner membrane environment. This system provides the benefits of the very high sensitivity of SERS spectroscopy to detect small conformational changes of macromolecules in micromolar concentrations and can be readily used, for example, for the ultrafast testing and evaluation of new antibiotics affecting the proteins modulating the bacterial division.

References

1 a) J. Drews, *Science* **2000**, *287*, 1960-1964; b) W. J. Galush, S. A. Shelby, M. J. Mulvihill, A. Tao, P. Yang, J. T. Groves, *Nano Lett.* **2009**, *9*, 2077-2082. c) Baciu CL, Becker J, Janshoff A, Sönnichsen C. *Nano Lett*. **2008** ;8(6):1724-8.

2 M. Vicente, A. I. Rico, R. Martínez-Arteaga, J. Mingorance, *J. Bacteriol.* **2006**, *188*, 19-27.

3 L. Mosyak, Y. Zhang, E. Glasfeld, S. Haney, M. Stahl, J. Seehra, W. S. Somers, *The Protein Data Bank (PDB ID: 1F46) EMBO J* **2000**, *19*, 3179-3191.

4 C. A. Hale, P. A. J. de Boer, *J. Bacteriol.* **1999**, *181*, 167-176.

5 C. A. Hale, P. A. J. de Boer, *Cell* **1997**, *88*, 175-185.

6 A. Martos, C. Alfonso, P. Lopez-Navajas, R. Ahijado-Guzmán, J. Mingorance, A. P. Minton, G. Rivas, *Biochem.* **2010**, *49*, 10780-10787.

7 M.-C. Daniel, D. Astruc, *Chemical Reviews* **2004**, *104*, 293-346.

8 G. Rivas, A. Lopez, J. Mingorance, A. P. Minton, M. J. Ferrándiz, M. Vicente, S. Zorrilla, J. M. Andreu, *J. Biol. Chem.* **2000**, *275*, 11740-11749.

9 H. P. Erickson, D. W. Taylor, K. A. Taylor, D. Bramhill, *Proc. Nat. Acad. Sci. USA* **1996**, *93*, 519-523.

10 a) J. M. González, M. Vélez, M. Jiménez, C. Alfonso, P. Schuck, J. Mingorance, M. Vicente, A. P. Minton, G. Rivas, *Proc. Nat. Acad. Sci. USA* **2005**, *102*, 1895-1900; b) A. Mukherjee, K. Dai, J. Lutkenhaus, *Proc. Nat. Acad. Sci. USA* **1993**, *90*, 1053-1057; c) D. E. Anderson, F. J. Gueiros-Filho, H. P. Erickson, *J. Bacteriol.* **2004**, *186*, 5775-5781; d) J. M. González, M. Jiménez, M. Vélez, J. Mingorance, J. M. Andreu, M. Vicente, G. Rivas, *J. Biol. Chem.* **2003**, *278*, 37664-37671.

11 a) K. A. Willets, R. P. Van Duyne, *Ann. Rev. Phys. Chem.* **2007**, *58*, 267-297; b) M. Moskovits, *J. Raman Spectrosc.* **2005**, *36*, 485-496.

12 K. Kneipp, Y. Wang, H. Kneipp, L. T. Perelman, I. Itzkan, R. Dasari, M. S. Feld, *Phys. Rev. Lett.* **1997**, *78*, 1667-1670.

13 R. A. Alvarez-Puebla, L. M. Liz-Marzan, *Small* **2010**, *6*, 604-610.

14 a) T. M. Cotton, J.-H. Kim, G. D. Chumanov, *J. Raman Spectrosc.* **1991**, *22*, 729-742; b) M. Mahmoudi, I. Lynch, M. R. Ejtehadi, M. P. Monopoli, F. B. Bombelli, S. Laurent, *Chem. Rev.* **2011**, *111*, 5610-5637; c) N. L. Rosi, C. A. Mirkin, *Chem. Rev.* **2005**, *105*, 1547-1562; d) M. Sanles-Sobrido, L. Rodriguez-Lorenzo, S. Lorenzo-Abalde, A. Gonzalez-Fernandez, M. A. Correa-Duarte, R. A. Alvarez-Puebla, L. M. Liz-Marzan, *Nanoscale* **2009**, *1*, 153-158; e) L. Fabris, M. Dante, G. Braun, S. J. Lee, N. O. Reich, M. Moskovits, T. Q. Nguyen, G. C. Bazan, *J. Am. Chem. Soc.* **2007**, *129*, 6086-6087; f) R. A. Alvarez-Puebla, A. Agarwal, P. Manna, B. P. Khanal, P. Aldeanueva-Potel, E. Carbo-Argibay, N. Pazos-Perez, L. Vigderman, E. R. Zubarev, N. A. Kotov, L. M. Liz-Marzan, *Proc. Nat. Acad. Sci. USA* **2011**, *108*, 8157-8161.

15 a) D. Tsoutsi, J. M. Montenegro, F. Dommershausen, U. Koert, L. M. Liz-Marzan, W. J. Perak, R. A. Alvarez-Puebla, *ACS Nano* **2011**, *5*, 7539-7546; b) M. Spuch-Calvar, L. Rodriguez-Lorenzo, M. P. Morales, R. A. Alvarez-Puebla, L. M. Liz-Marzan, *J. Phys. Chem. C* **2009**, *113*, 3373-3377; c) R. A. Alvarez-Puebla, L. M. Liz-Marzan, *Chem. Soc. Rev.* **2012**, *41*, 43-51.

16 S. Abalde-Cela, J. M. Hermida-Ramon, P. Contreras-Carballada, L. De Cola, A. Guerrero-Martinez, R. A. Alvarez-Puebla, L. M. Liz-Marzan, *ChemPhysChem* **2011**, *12*, 1529-1535.

17 B. Rodriguez-Gonzalez, A. Burrows, M. Watanabe, C. J. Kiely, L. M. Liz Marzan, *J. Mater. Chem.* **2005**, *15*, 1755-1759.

18 V. L. Schlegel, T. M. Cotton, *Anal. Chem.* **1991**, *63*, 241-247.

19 R. Alvarez-Puebla, L. M. Liz-Marzán, F. J. García De Abajo, *J. Phys. Chem. Lett.* **2010**, *1*, 2428-2434.

20 F. J. Moy, E. Glasfeld, L. Mosyak, R. Powers, *The Protein Data Bank (PDB ID: 1F7W) Biochemistry* **2000**, *39*, 9146-9156.

21 a) R. Tuma, *J. Raman Spectrosc.* **2005**, *36*, 307-319; b) G. J. Thomas, *Biopolymers* **2002**, *67*, 214-225; c) S. A. Overman, G. J. Thomas, *Biochemistry* **1999**, *38*, 4018-4027.

22 M. Moskovits, D. P. Dilella, K. J. Maynard, *Langmuir* **1988**, *4*, 67-76.

23 M. Moskovits, J. S. Suh, *J. Phys. Chem.* **1984**, *88*, 5526-5530.

24 T. Mohammadi, G. E. J. Ploeger, J. Verheul, A. D. Comvalius, A. Martos, C. Alfonso, J. van Marle, G. n. Rivas, T. den Blaauwen, *Biochemistry* **2009**, *48*, 11056-11066.

25 C. A. Hale, A. C. Rhee, P. A. J. de Boer, *J. Bacteriology* **2000**, *182*, 5153-5166.

26 F. Lhert, F. Capelle, D. Blaudez, C. Heywang, J. M. Turlet, *J. Phys. Chem. B* **2000**, *104*, 11704-11707.

27 R. J. H. Clark, R. E. Hester, *Advances in Infrared and Raman Spectroscopy*, Wiley, New York, **1984**.

28 S. Rueda, M. Vicente, J. Mingorance, *J. Bacteriology* **2003**, *185*, 3344-3351.

29 M. J. Osborn, J. E. Gander, E. Parisi, J. Carson, *J. Biol. Chem.* **1972**, *247*, 3962-3972.

30 M. Jiménez, A. Martos, M. Vicente, G. Rivas, *J. Biol. Chem.* **2011**, *286*, 11236-11241.

31 a) M. Vicente, A. I. Rico, R. Martínez-Arteaga, J. Mingorance, *J. Bacteriology* **2006**, *188*, 19-27; b) G. Butland, J. M. Peregrin-Alvarez, J. Li, W. Yang, X. Yang, V. Canadien, A. Starostine, D. Richards, B. Beattie, N. Krogan, M. Davey, J. Parkinson, J. Greenblatt, A. Emili, *Nature* **2005**, *433*, 531-537.

SUPLEMENTARY MATERIAL

EXPERIMENTAL SECTION

Materials:

Reagents, metallic salts, buffers, microsized polystyrene (PS) beads (3□m), guanosine 5´-diphosphate (GDP), guanosine 5´-triphosphate (GTP), benzenethiol (BT) and other analytical grade chemicals were acquired from Sigma-Aldrich or Merck; 1,2-dioleoyl-sn-glycero-3-[(N-(5-amino-1-carboxypentyl)iminodiacetic acid)succinyl] (DGS-NTA(Ni)) and E. coli polar lipid extract were purchased from Avanti Polar Lipids. All proteins from this work were extensively dialyzed against the working buffer, 50 mM Tris-HCl pH 7.5, 100 mM KCl, 5 mM $MgCl_2$.

Polystyrene micro-beads functionalization and coating:

Polystyrene microbeads of 3 μm (0.5 ml of 100 mg mL^{-1} suspension) were first wrapped with alternating polyelectrolyte monolayers using the layer-by-layer (LbL) electrostatic self-assembly protocol.[1] Four alternative layers of polystyrenesulfonate (PSS, Mw = 1000000), poly(diallyldimethylammoniumchloride) (PDDA , Mw = 100000 - 200000), PSS and, finally, poly(allylaminehydrochloride) (PAH, Mw = 56000) Polystyrene microbeads (0.5 ml of 100 mg mL^{-1} suspension) were added to a 25 ml of 2 mg mL^{-1} PSS aqueous solution supplemented with 0.5 M NaCl. After 30 min of sonication, and 2 hours of agitation the PS microbeads were extensively washed with Milli-Q water and centrifuged (5000 rpm, 15min). The same protocol (concentrations, elapsed times and washing protocol) were carry out to next layers of PDDA, PSS and PAH polyelectrolytes. Gold seeds of 15 nm were prepared by heating to the boil 50 ml of $HAuCl_4$ 0.5 mM and addition of 2.5 ml of sodium citrate solution 1% under mechanical stirring.

The adsorption of the gold seeds onto the functionalized PS beads was carried out by adding 12 mL of as prepared seeds 0.5 mM to a 4 mL of PS beads (5 mg mL^{-1}). After 15 min of sonication, the PS@Au beads were washed firstly 3 times by centrifugation (3000

rpm x 15 min) and 3 times by decantation with Milli-Q water. Silver was epitaxially grown on gold seeds as follows: 4 mL of PS@Au 5 mg mL^{-1} were mixed with a solution containing 33 mL of glycine 0.4 M at pH 9.5 and 2.4 mL of Ag_2SO_4 15 mM.[1] During sonication in cold water, 3.3 mL of ascorbic acid 0.1 M were added. After 1 hour in sonication bath, the solution was washed with Milli-Q water for 3 times by centrifugation (3000 rpm x 15min) and 3 times by decantation.

Protein purification:

Escherichia coli wild type FtsZ was expressed and purified by the calcium-induced precipitation method.[2] FtsZ was frozen and stored at -80^{o}C in 20 µL aliquots. In this study FtsZ was used in different bound states: GDP-FtsZ (non-polymerized or oligomeric protein) and GTP-FtsZ (polymerized protein).

Mutagenesis of the ZipA gene, overexpression and purification of both soluble mutants were constructed by elimination of certain regions within the N-terminal domain of native ZipA, the hydrophobic (transmembrane) N-terminal domain in the case of s1-ZipA (amino acids 1-25) and this one together with the P/Q domain in the case of s2-ZipA (amino acids 1-188).[3] The proteins preserves the hexahistidine-tag.

Preparation of lipid MLVs:

The required amount of *E. coli* polar lipids and DGS-NTA(Ni) in chloroform/methanol were mixed in a ratio 10:1, then dried under a Nitrogen stream and kept under vacuum for four hours to remove traces of organic compounds. The dried film was resuspended in working buffer by three cycles of 10 min vortexing with rest periods of 15 min in a 37^{o}C water bath, and finally was sonicated at 4^{o}C for 5 min.

Isolation of E. coli inner membranes:

The inner membrane vesicles were isolated from wild-type *E. coli* (strain JM600) exponential phase culture.[4] The inner and outer membrane were separated by sucrose

gradient centrifugation,[5] washed and diluted to reach 20 absorbance units at 280 nm, and stored frozen at −80 °C.[6]

Lipid-coated and Inner membrane-coated PS@Au@Ag beads: PS@Au@Ag beads were washed three times with working buffer by centrifugation (3000 rpm x 15min), mixed with the lipid or inner membrane solution, incubated with gentle shaking for 2 hours at 4^{o}C and sonicated (lipids for 5 min, membrane for 30 sec) in a water bath at 4^{o}C. These lipid coated PS@Au@Ag beads were washed three times (3000rpm x 15min), sonicated in a cold water bath (lipids for 1 min, membrane for 30 sec) and washed three more times.

ZipA immobilization on the plain or lipid coated PS@Au@Ag beads and FtsZ interaction with plain, lipid or membrane coated PS@Au@Ag beads: Plain or lipid coated PS@Au@Ag beads were washed three times by centrifugation (3000 rpm x 15min) with 50 mM Tris-HCl pH 7.5, 100 mM KCl, 5 mM $MgCl_2$. The recombinant mutant of ZipA was equilibrated against the same buffer solution. Different amounts of protein solution were mixed with the beads (3.3 mg mL^{-1}) to a final concentration of protein between 5 to 20 µM, the solution was stored in soft shaker at 4ºC for 1h and washed three times (3000 rpm x 15 min) at 4^{o}C. Finally we found 15 µM as optimal concentration of ZipA protein in order to obtain the better SERS signal. The hexahistidine-tag from ZipA is attached to Ni-NTA groups in the case of lipid coated beads and strongly attached to the nanostructured silver in the case of plain PS@Au@Ag beads.[7]

A dispersion of plain, lipid or membrane coated PS@Au@Ag-ZipA beads as described before was mixed with GDP-FtsZ protein and incubated in soft shaker at 4ºC for 30 min. GDP-FtsZ was previously equilibrated against the working buffer. The final concentrations of beads are 3.3 mg mL^{-1} and FtsZ 25 µM. In the case of GTP-FtsZ, an aliquot of the beads was mixed with GTP to a final concentration of 1 mM supplemented with enzymatic GTP-regenerating system as previously described,[8] and incubated at room temperature for 5 min. The GTP control of plain, lipid or membrane coated PS@Au@Ag-ZipA beads was done without FtsZ.

Characterization:

UV-Vis-NIR spectra were recorded using an Agilent 8453 diode array spectrophotometer. Scanning electron microscopy images were obtained with a JEOL JSM6700F microscope operating at an acceleration voltage between 2 and 20 kW and a secondary electron detector mode was used for characterization. Fluorescence images were taken with a Zeiss Axioplan Universal Microscope equipped with a Leica DFC 350 FX digital camera and EC Plan-Neofluar objective.

Surface-enhanced Raman scattering spectroscopy:

Raman and SERS experiments were conducted in a micro-Renishaw InVia Reflex system. The spectrograph uses high-resolution grating (1200 groves mm^{-1}) with additional band-pass filter optics, a confocal microscope, and a 2D-CCD camera. Excitation was carried out at 785 nm (diode). Measurements were made in a confocal microscope in backscattering geometry using a 100x objective with NA value of 0.9, providing a spatial resolution of 500 nm with accumulation times of 10 s. For SERS characterization of the PS@Au@Ag beads, 10 µL of a Benzenethiol (BT) solution (10^{-3} M) was added to 1 mL of the sample reaching a final concentration of 10^{-5} M in BT. 10 µL of the mixture were then cast and air-dried onto a clean glass slide. For SERS measurements 10 µL of the different samples of coated PS@Au@Ag beads were deposited on a clean glass slide and air-dried. Each sample was prepared at least twice at the same conditions and at least ten different beads were measured for each sample to ensure reproducibility.

References

1 a) K. A. Willets, R. P. Van Duyne, *Ann. Rev. Phys. Chem.* **2007**, *58*, 267-297; b) M. Moskovits, *J. Raman Spectrosc.* **2005**, *36*, 485-496.

2 K. Kneipp, Y. Wang, H. Kneipp, L. T. Perelman, I. Itzkan, R. Dasari, M. S. Feld, *Phys. Rev. Lett.* **1997**, *78*, 1667-1670.

3 R. A. Alvarez-Puebla, L. M. Liz-Marzan, *Small* **2010**, *6*, 604-610.

4 a) T. M. Cotton, J.-H. Kim, G. D. Chumanov, *J. Raman Spectrosc.* **1991**, *22*, 729-742; b) M. Mahmoudi, I. Lynch, M. R. Ejtehadi, M. P. Monopoli, F. B. Bombelli, S. Laurent, *Chem. Rev.* **2011**, *111*, 5610-5637; c) N. L. Rosi, C. A. Mirkin, *Chem. Rev.* **2005**, *105*, 1547-1562; d) M. Sanles-Sobrido, L. Rodriguez-Lorenzo, S. Lorenzo-Abalde, A. Gonzalez-Fernandez, M. A. Correa-Duarte, R. A. Alvarez-Puebla, L. M. Liz-Marzan, *Nanoscale* **2009**, *1*, 153-158; e) L. Fabris, M. Dante, G. Braun, S. J. Lee, N. O. Reich, M. Moskovits, T. Q. Nguyen, G. C. Bazan, *J. Am. Chem. Soc.* **2007**, *129*, 6086-6087; f) R. A. Alvarez-Puebla, A. Agarwal, P. Manna, B. P. Khanal, P. Aldeanueva-Potel, E. Carbo-Argibay, N. Pazos-Perez, L. Vigderman, E. R. Zubarev, N. A. Kotov, L. M. Liz-Marzan, *Proc. Nat. Acad. Sci. USA* **2011**, *108*, 8157-8161.

5 a) D. Tsoutsi, J. M. Montenegro, F. Dommershausen, U. Koert, L. M. Liz-Marzan, W. J. Perak, R. A. Alvarez-Puebla, *ACS Nano* **2011**, *5*, 7539-7546; b) M. Spuch-Calvar, L. Rodriguez-Lorenzo, M. P. Morales, R. A. Alvarez-Puebla, L. M. Liz-Marzan, *J. Phys. Chem. C* **2009**, *113*, 3373-3377; c) R. A. Alvarez-Puebla, L. M. Liz-Marzan, *Chem. Soc. Rev.* **2012**, *41*, 43-51.

6 S. Abalde-Cela, J. M. Hermida-Ramon, P. Contreras-Carballada, L. De Cola, A. Guerrero-Martinez, R. A. Alvarez-Puebla, L. M. Liz-Marzan, *ChemPhysChem* **2011**, *12*, 1529-1535.

7 B. Rodriguez-Gonzalez, A. Burrows, M. Watanabe, C. J. Kiely, L. M. Liz Marzan, *J. Mater. Chem.* **2005**, *15*, 1755-1759.

8 V. L. Schlegel, T. M. Cotton, *Anal. Chem.* **1991**, *63*, 241-247.

APENDIX 2

Reconstitution of proto-ring elements on microbeads

The reconstitution and assembly of several proto-ring elements on non-functionalized micron sized beads were characterized by fluorescence microscopy and scanning electron microscopy (SEM). In order to confirm the successful immobilization of the lipids, membrane and proteins onto the beads, fluorescence images were acquired using DiI-C18 (**Figure 1A**), which selectively attaches to the membranes, anti-ZipA+ anti-rabbit-488 (**Figure 1B**), which selectively recognises the membrane protein ZipA, and labelled FtsZ-Alexa Fluor 488 (**Figure 1C**). Figure 1 D and E show SEM images at different magnifications of membrane coated beads with FtsZ polymers.

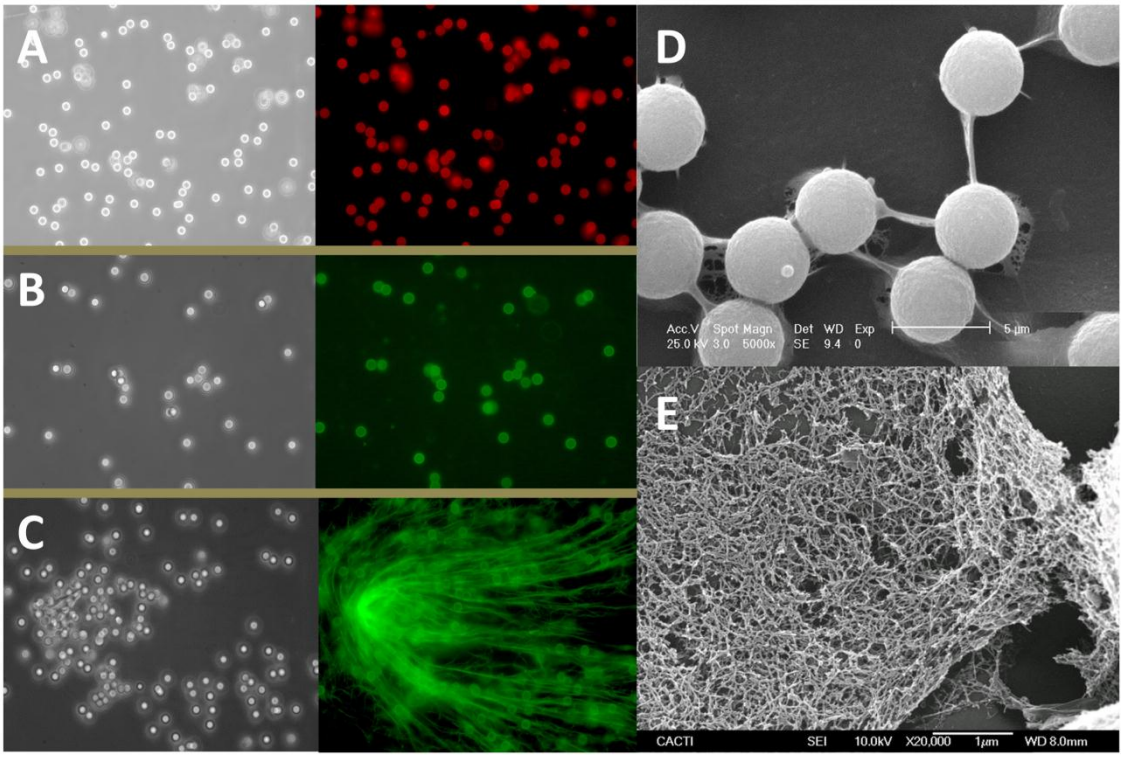

Figure 1. (A)Membrane coated microbeads were incubated with DiI-C18, (B) anti-ZipA+ anti-rabbit-488 and (C) a polymeric form of FtsZ-Alexa-Fluor 488 suplemented with Ficoll 70. Negative control experiments were carried out, thus evidencing the absence of nonspecific adsorption of the dyes and the successful immobilization of the membrane and ZipA. Figure 1 D and E show SEM images at different magnifications of membrane coated beads with FtsZ polymers.

This result provides enough evidences to confirm the role of membrane protein ZipA that is anchoring FtsZ filaments to the inner membrane. It was observed in SEM images that the growth of FtsZ polymers attached from membrane through ZipA is forming three-dimensional network, even grow into fibers that link different microbeads.

However, we test the case of the s1-ZipA mutant (described in experimental section) and the interaction cannot be detected by SERS, probably because of the long length of the P/Q domain (10-20 nm) separating the interaction region and enhancer silver sensor. The coating and characterization details were described in the experimental section (supplementary material) of Chapter 3, and SEM sample preparations is described below.

PREPARATION OF BILOGICAL SEM SAMPLES: Fix sample in a buffer containing 2.5% Gluteraldehyde for 3 hours in room temperature. Rinses in Milli-Q water 3 x 15 min. Before proceed to following steps. Rinses twice in room temperature with:

30% EtOH 10 min

50% EtOH 10 min

70% EtOH 10 min or overnight

85% EtOH 20 min

95% EtOH 20 min

100% EtOH 20 min

100% EtOH 20 min or overnight

Critical point drying or freeze drying.

Spattering with Au or Ag.

Observation under Scanning electron microscope.

APENDIX 3

Biochemistry 2010, 49, 10780–10787

CHARACTERIZATION OF SELF- AND HETERO-ASSOCIATIONS OF BACTERIAL CELL DIVISION PROTEINS FtsZ AND ZipA IN SOLUTION BY COMPOSITION GRADIENT – STATIC LIGHT SCATTERING (CG-SLS)

We have characterized the self-association of FtsZ in its GDP-bound state (GDP-FtsZ) and the hetero-association of FtsZ and a soluble recombinant ZipA (sZipA) lacking the N-terminal trans-membrane domain by means of composition gradient static light scattering (CG-SLS) and by measurement of sedimentation equilibrium. CG-SLS experiments at high ionic strength and in the presence of 5 mM Mg^{2+} show that, while FtsZ self-associates in a non-cooperative fashion, sZipA acts as a monomer. CG-SLS data obtained from mixtures of FtsZ (A) and sZipA (B) in the presence of Mg^{2+} are quantitatively described by an equilibrium model which takes into account significant scattering contributions from B, A_1, A_2, A_3, A_4, A_5, A_6, A_1B, A_2B, A_3B and A_4B. However, in the absence of Mg^{2+} (with EDTA) the data are best accounted for by an equilibrium model in which only B, A_1, A_2, A_3, A_1B and A_2B contribute significantly to scattering. The best-fit molecular weights of monomeric A and B are in good agreement with values calculated from amino-acid composition and with values obtained from sedimentation equilibrium. The latter technique also confirmed the interaction between sZipA and GDP-FtsZ. Moreover, the association model that best describes the CG-LS data is in qualitative agreement with the sedimentation data. From these results it follows that the binding of sZipA to GDP-FtsZ is of moderate affinity and does not affect significantly the interactions between FtsZ monomers. Under the working conditions used, only one sZipA binds to FtsZ oligomers of length 6 or less. The observed behavior would be compatible with FtsZ fibrils being anchored *in vivo* to the bacterial inner plasma membrane by substoichiometric binding of membrane-bound ZipA.

INTRODUCTION

The components of the bacterial cell division machinery assemble in a concerted manner to form a dynamic ring at mid-cell towards the end of the cell cycle. The ring is formed by at least fifteen division specific proteins, most of them integral membrane proteins. The first multi-protein complex formed is the bacterial proto-ring that initiates division. In *Escherichia coli* the proto-ring is a complex of three proteins (FtsZ, FtsA, and ZipA) assembling on the cytoplasmic membrane which are required for the incorporation of the remaining proteins at the mature ring [1][2]. The best characterized proto-ring protein is FtsZ, which shares structural, but not sequence, homology with eukaryotic tubulin, as well as its GTPase activity and its capacity to polymerize [3] [4]. In its GDP-bound state the FtsZ monomer self-associates in a non-cooperative manner to form oligomers, a reaction that is promoted by magnesium, low pH, and excluded volume effects in highly crowded media and that it is attenuated upon increasing the solution ionic strength [5-7]. GTP triggers FtsZ assembly *in vitro* to form polymers whose structural organization is highly polymorphic (single stranded protofilaments, circles, toroidal structures, bundles, etc) depending upon the solution composition and experimental conditions [5, 7, 8] [9, 10] [11-14] . The GTP-mediated assembly/disassembly cycle of FtsZ is thought to be essential for the formation of the dynamic septal ring during cell division [2, 3, 15] [4].

FtsZ is anchored to the cytoplasmic membrane through the interaction of its carboxy-terminal region with ZipA or FtsA. FtsA belongs to the actin family and contains a short amphipatic helix that seems to mediate its association to the membrane [16]. *E. coli* ZipA is a 36.4 kDa protein that contains an amino-terminal helix that is integrated into the membrane and connected to a cytoplasmic FtsZ-interacting domain via a flexible linker [17-20] . FtsA and ZipA are involved in the attachment of FtsZ to the membrane, but no localization of FtsZ occurs in the simultaneous absence of both. In fact, under normal conditions ZipA is required and essential for *E. coli* Z-ring formation [21]. ZipA stabilizes GTP-FtsZ polymers *in vitro* and *in vivo* that might be related with the effect of ZipA on the bundling of FtsZ polymers, in which the C-terminal domain seems to be involved [19, 22] . The interaction between FtsZ and ZipA has been studied by means of genetical and structural approaches [17-27] but the mechanism of

association between the two proteins is largely unknown. The only quantitative information on ZipA-FtsZ complex formation was reported by Mosyak and co-workers [26]. They used surface plasmon resonance to measure the binding of a 17-aa region from the C-terminal domain of FtsZ (in its GDP-bound state) to two soluble fragments of ZipA immobilized onto the sensor chip and found the interactions in the complexes were weak (apparent dissociation constants > 20 μM); these interactions did not change when the two protein fragments were in solution, as measured by isothermal titration calorimetry.

The aim of this work was the biophysical analysis of the association between ZipA and GDP-FtsZ in solution to measure the binding parameters of ZipA-FtsZ complex formation. This information is important to undertake the quantitative characterization of these multi-protein complexes at different levels of organization (like reconstituted and natural membrane systems). We first isolate and analyze the full length ZipA protein in the absence of detergent. We found that detergent-free ZipA existed mainly as an 16S oligomer, much larger than the expected s-value of the monomer (~ 3 S) and compatible with a 450-500 kDa globular oligomer (ZipA decamer). Upon incubation with GDP-FtsZ, the oligomers of ZipA formed large aggregates, observations also confirmed by electron and atomic force microscopy. These results hampered the use of full length ZipA for a quantitative study of binding to FtsZ in solution. However, from these preliminary studies we concluded that ZipA in solution retained the capacity of binding to FtsZ, with moderate affinity ($K > 10^5\ M^{-1}$). We also found, by means of electron microscopy and differential centrifugation assays, that full length ZipA in a low salt buffer (with 50 mM KCl, but not with 500 mM) promoted FtsZ polymer bundling formation at sub-stoichiometric concentration of ZipA, results that confirm previous studies done in lower pH buffers with 0.05 M KCl [19] . To overcome these technical difficulties associated with the tendency of ZipA to aggregate, we have generated a soluble fragment of the protein which do not contain the trans-membrane region (sZipA) and measured the binding of sZipA and GDP-FtsZ in solution by means of recently developed composition-gradient static light scattering methods in combination with sedimentation equilibrium measurements. The former technique is a new powerful tool to rapidly and accurately measure protein self- and hetero-associations in

solution [28-32]. In composition-gradient static light scattering (CG-SLS) experiments, light scattering data are acquired from a solution whose composition is being continuously varied with time in a controlled fashion. The resulting profiles of light scattering intensity as a function of solution composition are then modeled in the context of schemes postulating different combinations of self- and/or hetero-association equilibria, in order to determine the simplest scheme capable of accounting for the data to within experimental precision. This approach has allowed us to define the scheme of association between sZipA and FtsZ as well as the affinity and stoichiometry of the different species present in the solution. Finally, the potential implications of these results to understand the association of FtsZ with ZipA at the cytoplasmic membrane are discussed.

EXPERIMENTAL PROCEDURES

Materials: All the assays described in this paper were done at 25ºC with the proteins equilibrated in 50mM Tris-HCl, pH 7.4, 500mM KCl buffer, with either 5mM $MgCl_2$ (Tris-500KCl-Mg buffer) or 1mM EDTA (Tris-500KCl-EDTA buffer), in the presence of the nucleotide (GDP or GTP) specified in the text. Guanine nucleotides, GDP and GTP, were purchased from Sigma-Aldrich and Roche, respectively. Other analytical grade chemicals were from Merck or Sigma.

Proteins: *E. coli* FtsZ was purified by the Ca^{2+}-induced precipitation method described by Rivas *et al.* [7]. In this study we have mainly used FtsZ in the GDP-bound state (non-polymerized protein) and we will refer to it as GDP-FtsZ.

Mutagenesis of Gene *zipA*; over-expression and purification of sZipA: A soluble mutant of ZipA was constructed by eliminating the hydrophobic N-terminal domain (aa 1-25) of the full length protein. The deletion was obtained by inverse-PCR using plasmid pET-15ZIP as template DNA and the primers 5'-CATATGGCTGCCGCGCG -3' and 5'-ACCAGCCGTAAAGAACG -3'. The PCR product was purified, digested with *DpnI* and ligated with T4 DNA-ligase. The presence of the desired deletion and absence of other mutations was checked by DNA sequencing.

To overproduce sZipA, BL21/DE3 cells transformed with pET-15ZIP (*22*) were grown at 37ºC in LB supplemented with ampicillin (50 µg/ml) and chloramphenicol (50 µg/ml), to reach

an optical density of 0.4. Protein expression was induced with 1mM IPTG for 3 h. Cells were harvested, centrifuged at 10 000g (4 ºC, 15min.) and resuspended in 0.02 culture volume of buffer A (20mM Tris-HCl pH 8.0, 500mM NaCl, 5mM imidazole). After sonication, cell extracts were centrifuged at 200000 g (4ºC, 30 min) to pellet membranes. sZipA was recovered from the soluble fraction and loaded on a 5 ml Ni-NTA resin (Novagen) equilibrated in buffer A. The protein was eluted sequentially with 50, 100, 200 and 500mM imidazole in buffer A. Most of the sZipA protein eluted with 200 mM imidazole. The protein concentration was determined by Bradford assay. The protein yield was typically 4-6 mg sZipA per liter of cell culture. sZipA fractions were pooled and stored at -80ºC. The purity of sZipA was > 90% according to SDS-PAGE.

Static light-scattering: Composition-gradient static light scattering experiments were performed using the Calypso system (Wyatt Technology, Santa Barbara, CA) according to procedures developed by Minton and co-workers (*30-32*). In brief, a programmable three injector-syringe pump was used to introduce a solution of defined protein composition (that changes with time) into parallel flow cells for concurrent measurement of Rayleigh light scattering at multiple angles (using a DAWN-EOS multi-angle laser light scattering detector, Wyatt Technology, Santa Barbara, CA) and solute composition (using a Optilab rEX refractive index detector, Wyatt Technology, Santa Barbara, CA). A single composition gradient experiment yields several thousand values of scattering intensity as a function of scattering angle and solution composition. The specific refractive increments of FtsZ and sZipA were measured using an Optilab rEX differential refractometer (Wyatt Technology, Santa Barbara) and both found to be equal to 0.185 $\pm$ 0.002 cm^3/g at 25^{o}C.

Experiments with a single protein were performed as described by Attri and Minton (*31*). One of the pump channels (syringe + reservoir) was filled with a solution of either GDP-FtsZ or sZipA and a second filled with a buffer solution. Stepwise gradients of increasing or decreasing protein concentration were formed by increasing in incremental intervals the flow rate of one of the syringes and simultaneously decreasing by the same amount the flow rate of the other syringe. Experiments with mixtures of two proteins were performed as described by

Attri and Minton [30]. A solution of sZipA (solution B) at w/v concentration $w_{B,load}$ was loaded into one of the pump channels and a solution of GDP-FtsZ (solution A) at w/v concentration $w_{A,load}$ was loaded into the second pump channel. Initially the flow cells were filled with pure solution B, permitting determination of the scattering intensity at multiple angles and absorbance of sZipA at the loading concentration. Composition gradients were created by simultaneously increasing the flow rate of pump channel A and decreasing the flow rate of pump channel B, so that the fraction of solution B in the solution mixture gradually decreases from 1 to 0 while that of solution A gradually increases from 0 to 1. Absorbance data were processed to yield the concentration of either one protein (in a single protein experiment) or both proteins (in a two protein experiment), as described in [30, 31]. The scattering data were processed as previously described by Attri and Minton [30, 31] to yield the Rayleigh ratio *R* scaled to an optical constant

$$K_{opt} = \frac{4\pi \tilde{n}^2 (d\tilde{n}/dw)^2}{\lambda^4 N_A} \qquad [1]$$

where λ, N_A, and $\tilde{n}$ denote the wavelength of incident light (690 nm), Avogadro's number, and the refractive index of the solution respectively. $d\tilde{n}/dw$ is the specific refractive increment of both proteins, determined as described above, where w denotes the w/v concentration of protein. In the present study, all solute species were small relative to the wavelength of light. Therefore, the scaled Rayleigh ratio is independent of scattering angle, and depends only upon the solute composition:

$$\frac{R}{K_{opt}} = \sum_i M_i w_i = \sum_i c_i M_i^2 \qquad [2]$$

where M_i, w_i, and c_i respectively denote the molar mass, w/v concentration, and molar concentration of the *i*th solute species. The fractional contribution of a given species to the total scattering intensity is then given by

$$f_j = \frac{c_j M_j^2}{\sum_i c_i M_i^2} \qquad [3]$$

The composition dependence of R/K_{opt} is modeled in the context of equilibrium schemes described below that specify the molar masses of all significant scattering species, and the dependence of all c_i upon one or more postulated equilibrium association constants and the total concentrations of each or both proteins.

Models for equilibrium self- and hetero-association: Several equilibrium models were constructed to calculate the molar concentration of each macromolecular species present as a function of the total concentration of each macromolecular component and one or more equilibrium association constants. The results of these models were then combined with equation [2] to calculate the dependence of total scattering upon solution composition. Below we describe the simplest models found to describe the data obtained in the present study to within experimental uncertainty. In a solution containing only a single protein component (A), the subscript *i* denotes a property of the oligomeric species A_i. In a solution containing two protein components (A and B), the subscript *ij* denotes a property of the oligomeric species A_iB_j.

Model 1: *Isodesmic model for self-association of GDP-FtsZ (component A).* It is assumed that monomeric A may bind to another monomer or any oligomer of A with equal affinity.

$$K_{AA} = c_{i+1}/c_1 c_i \quad \text{for all } i \qquad [4]$$

$$c_{tot} = \frac{w_{tot}}{M_1} = \sum_{i=1}^{\infty} i c_i = \frac{1}{K_{AA}} \sum_{i=1}^{\infty} i \left(K_{AA} c_1\right)^i = \frac{1}{K_{AA}} \frac{q}{(1-q)^2} \qquad [5]$$

where $q \equiv K_{AA} c_1$. Given values of w_{tot}, M_1, and K_{AA}, eqn [5] may be solved for the values of q and c_1. It follows from eqn [2] that the normalized scattering is then given by

$$\frac{R}{K_{opt}} = \sum_{i=1}^{\infty} c_i \left(iM_1\right)^2 = \frac{M_1^2}{K_{AA}} \sum_{i=1}^{\infty} i^2 \left(K_{AA} c_1\right)^i = \frac{M_1^2}{K_{AA}} \times \frac{q+q^2}{(1-q)^3} \qquad [6]$$

Model 2: *Isodesmic self-association of GDP-FtsZ (component A), and hetero-association of each oligomeric species of A with one or two molecules of sZipA (component B).* It is assumed that one or two molecules of B may bind to a monomer or any oligomer of A with an affinity that is independent of the size of the oligomer. The second molecule of B binds to monomeric

or oligomeric A with an equilibrium constant for association that differs from the equilibrium constant for binding the first B by a factor α.

$$K_{AA} = \frac{c_{(i+1)0}}{c_{i0}c_{10}} \qquad \text{for all } i \qquad [7]$$

$$K_{AB} = \frac{c_{i1}}{c_{i0}c_{01}} \qquad \text{for all } i \qquad [8]$$

$$\alpha K_{AB} = \frac{c_{i2}}{c_{i1}c_{01}} \qquad \text{for all } i \qquad [9]$$

The conservation of mass equations may be written as

$$c_{A,tot} = \frac{w_{A,tot}}{M_{10}} = \left[1 + B^* + \alpha B^{*2}\right]\frac{1}{K_{AA}}\frac{A^*}{\left(1-A^*\right)^2} \qquad [10]$$

$$c_{B,tot} = \frac{w_{B,tot}}{M_{01}} = c_{01} + \left[B^* + 2\alpha B^{*2}\right]\frac{1}{K_{AA}}\frac{A^*}{1-A^*} \qquad [11]$$

where $A^* = K_{AA}c_{10}$ and $B^* = K_{AB}c_{01}$. Given values of $w_{A,tot}, w_{B,tot}, M_{10}, M_{01}, K_{AA}, K_{AB}$ and α, equations [10] and [11] may be solved numerically for the equilibrium values of c_{10} and c_{01}. Then equations [7-9] may be used to calculate the equilibrium values of all c_{ij}. The corresponding value of R/K_{opt} is calculated numerically by summing over all significantly populated species in the following special case of equation [2]

$$\frac{R}{K_{opt}} = c_{01}M_{01}^2 + \sum_{i=1}^{\infty}\sum_{j=0}^{2} c_{ij}\left(iM_{10} + jM_{01}\right)^2 \qquad [12]$$

When evaluating the infinite sum indicated above, terms in increasing *i* were successively added until convergence was established.

All data processing and modeling calculations were performed using user-written scripts and functions written in MATLAB (Mathworks, Natick MA) available from APM upon request.

Sedimentation equilibrium: Sedimentation equilibrium was done to determine the state of association of the individual components (sZipA and GDP-FtsZ) and to measure the association properties of sZipA-FtsZ complexes. The analytical ultracentrifugation analysis of sZipA, GDP-FtsZ and the sZipA-FtsZ mixtures was performed using several protein

concentrations (in the range of 0.3 to 1 g/L) equilibrated in either Tris-500KCl-Mg or Tris-500KCl-EDTA buffer containing 0.05 mM GDP. Sedimentation velocity runs were carried out at 42,000 rpm and 25°C in. Sedimentation profiles were registered every 5 minutes at the appropriate wavelength (230 or 275 nm). Short-column (70-80µl) experiments were carried our at 25ºC in an XL-A analytical ultracentrifuge (Beckman-Coulter Inc.) with UV-VIS optics detection system, using an An60Ti rotor and 12mm double-sector centrepieces. The equilibrium runs were done at two speeds (10,000 and 12,000 rpm) and the gradients were monitored at two different wavelengths (230 and 275 nm). Following the equilibrium scans, the solutions were centrifuged at high speed (40,000 rpm) to deplete the meniscus and obtain the corresponding baseline offsets. The measured equilibrium concentration (signal) gradients of sZipA and FtsZ alone were fit by the equation that characterizes the equilibrium gradient of an ideally sedimenting solute (*33*) to get the whole-cell buoyant signal average molecular weights of the individual proteins.

Analysis of sedimentation equilibrium data: For two components (A = FtsZ, and B = sZipA), the absorbance average molecular weight is given by [(34)]:

$$M_{absav} = \frac{\sum_{i,j} \left(iM_A\alpha_A + jM_B\alpha_B\right)c_{ij}\left(iM_A + jM_B\right)}{\sum_{i,j} \left(iM_A\alpha_A + jM_B\alpha_B\right)c_{ij}} \qquad [13]$$

where M_X is the molecular weight of monomeric X, α_X is the extinction coefficient of X at the wavelength of measurement, and c_{ij} is the molar concentration of A_iB_j. If the two components have the same density increment $(d\rho/dw_A) = (d\rho/dw_B) = (d\rho/dw)$, then the experimentally measured buoyant signal average molecular weight is just: $M^*_{abs,av} = M_{abs,av}\,(d\rho/dw)$. A MATLAB function using equations [7-11] and [13] was written to calculate the buoyant absorbance average molecular weight as a function of the total w/v concentrations of A and B.

It follows from eqns [2], [6] and [12] that any equilibrium model used to generate a calculated dependence of R/K_{opt} upon protein concentration may be also used to generate a calculated dependence of M_w upon protein concentration, which is the form of the sedimentation equilibrium results presented in this work. Therefore, with minor modifications,

the same association schemes described above to model the composition dependence data of light scattering can also be used to model the composition dependence data of sedimentation equilibrium experiments.

RESULTS AND DISCUSSION

sZipA: The normalized scattering intensity of sZipA in the absence and presence of Mg^{2+} is plotted as a function of protein concentration in **Figure 1**. Both sets of data are fit quantitatively by a model according to which sZipA behaves as a single species with M_w = 34,000 ± 1,000, in good agreement with the sequence molecular weight of the monomer (35,829). The best fit of this model to each data set is plotted together with the data. It follows that sZipA does not self-associate to a significant extent in either buffer over the measured range of concentrations. We confirmed that sZipA was a monomer in solution by analytical ultracentrifugation (**Figure 2**). The buoyant average molecular weight of sZipA, determined by sedimentation equilibrium, was 9,500 ± 1,000 (M_w = 36,000 – calculated using 0.736 cm^3/g as the partial specific volume of sZipA) corresponding to protein monomer. The sedimentation properties of sZipA did not change upon lowering KCl concentration to 0.05 M neither when EDTA was added to the buffer (not shown).

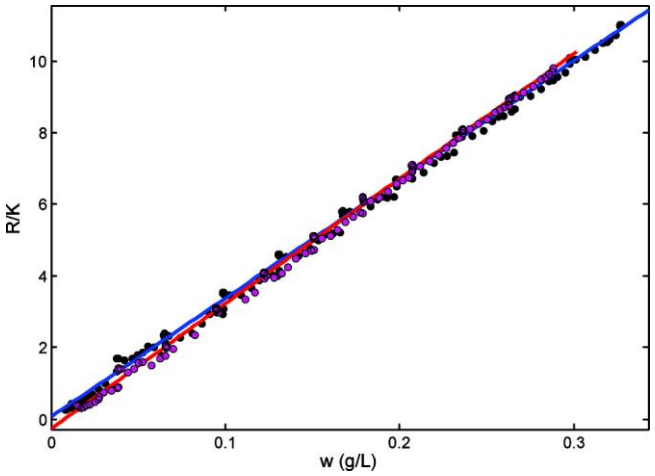

Figure 1. Normalized scattering intensity plotted as a function of sZipA concentration in the absence (black symbols) and presence (red symbols) of 5 mM Mg^{2+}. Blue line is the best fit of a single species model with M_w = 34,000 $\pm$ 1,000.

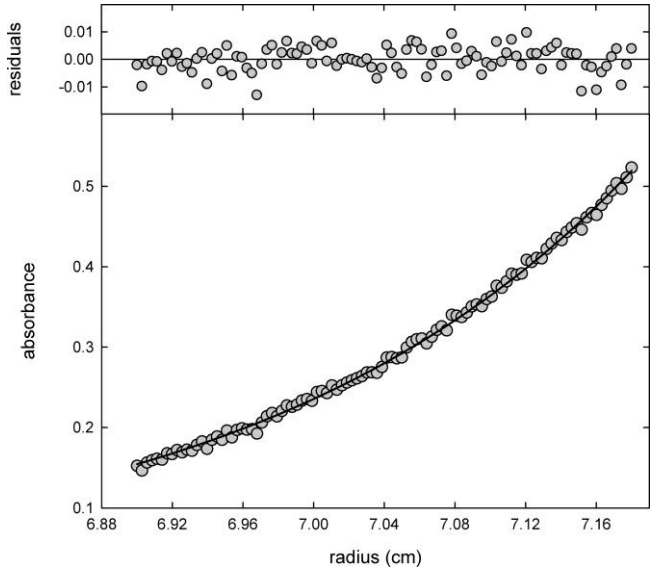

Figure 2. Analytical ultracentrifugation analysis of sZipA. Sedimentation equilibrium absorbance gradient of 14 µM sZipA at 12,000 rpm. The solid line is the best-fit distribution from the single-species with M_w = 36,000 ± 2,000, that corresponds to a protein monomer.

GDP-FtsZ: The concentration-dependent scattering of FtsZ in (high salt) Tris-500KCl buffer in the absence and presence of Mg^{2+} is plotted in **Figure 3**. Both sets of data are fit

quantitatively by the isodesmic self-association model described above. The best fit of this model to each data set, calculated using the parameter values given in the figure caption, is plotted together with the data. The fractional contribution of each significant species to the total scattering, calculated according to eqn [3], is plotted as a function of total protein concentration, and the corresponding mass fractional distributions are plotted in **Figures S1** and **S2**, respectively. In the presence of Mg^{2+} the scattering data are well accounted for by an equilibrium model which takes into account significant scattering contributions of several FtsZ species, from monomers to hexamers. In the presence of EDTA, FtsZ self-association is attenuated, as expected, and only monomers, dimers and trimers contributed to the scattering signal.

In parallel we carried out low-speed sedimentation equilibrium analysis with the same FtsZ preparations (loading concentrations ranging from 0.3 to 1.0 g/L, or 7.5 to 25μM) that yielded signal buoyant average molecular weights from 15,200 to 21,800 (M_w from 57,000 to 82,000 – calculated using 0.738 cm^3/g as the partial specific volume of FtsZ) (for the protein in 5 mM Mg^{2+}) and from 11,200 to 14,600 (M_w from 42,000 to 55,000) (EDTA). The dependence of the molecular weight of FtsZ with total protein concentration confirmed the results obtained in previous studies from our laboratory [5] and, more important, is in good quantitative agreement with the isodesmic model that accounts for the results obtained from composition gradient light scattering (**Figure 4**).

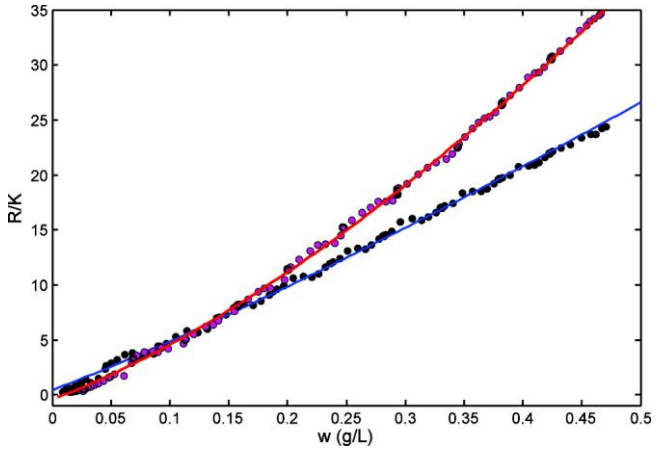

Figure 3. Normalized scattering intensity plotted as a function of GDP-FtsZ concentration in the absence (black symbols) and presence (red symbols) of 5 mM Mg2+. Plotted curves represent the best fits of model 1 with M1 = 40,000 (constrained) and log KAA = 4.3 (- Mg2+) or 4.8 (+ Mg2+).

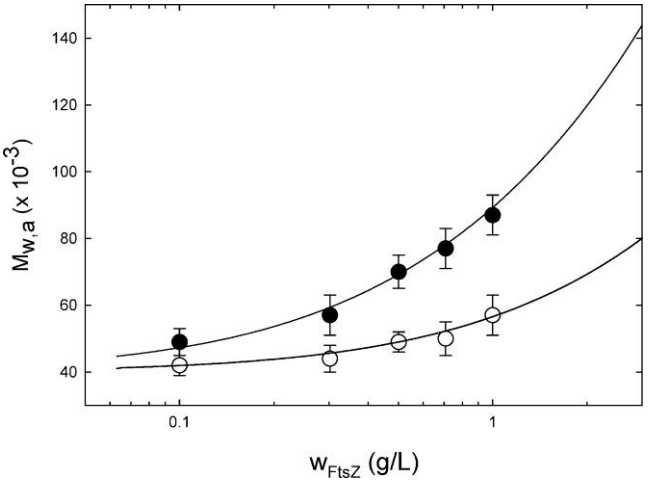

Figure 4. Dependence of signal-average molecular weight of GDP-FtsZ upon protein concentration in the absence (white circles) and presence (black circles) of 5 mM Mg2+ measured by sedimentation equilibrium. The plotted curves represents the best fit of model 1 with M1 = 40,000 (constrained) and log KAA = 4.2 (- Mg2+) or 4.7 (+ Mg2+).

sZipA + GDP-FtsZ: We then conducted composition-gradient light scattering to detect and quantify the association between GDP-FtsZ and sZipA. A 0.35 g/L solution of ZipA (B) was automatically mixed in various proportions with a 0.5 g/L solution of FtsZ (A), to produce a gradient of composition continuously varying from mole fraction 0 to mole fraction 1 of A. The

normalized scattering of these mixtures, in the absence and presence of Mg^{2+}, is plotted as functions of the fraction of solution A in the mixture in **Figure 5**.

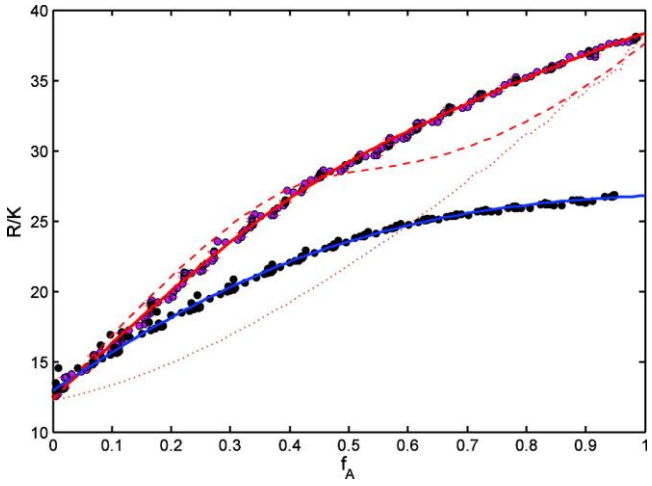

Figure 5. Normalized scattering intensity plotted as a function of fraction of solution A (0.5 g/L FtsZ) mixed with solution B (0.35 g/L sZipA) in the absence (black symbols) and presence (red symbols) of 5 mM Mg^{2+}. Plotted solid lines represent the best fits of model 2 with M_A = 40,000, M_B = 35,000, log K_{AA} = 4.18 ± 0.02 (EDTA) or 4.79 ± 0.02 (+ Mg^{2+}), log K_{AB} = 5.24 ± 0.07 (EDTA) or 5.78 ± 0.20 (+ Mg^{2+}), and α < 0.1 (EDTA) or < 0.03 (+ Mg^{2+}). The dashed and dotted lines represent the calculated dependence of scattering (+ Mg^{2+}) upon fA, assuming either binding of B only to monomeric A (no binding to oligomeric A) or no binding of B to A in any form, respectively.

Both sets of data are fit quantitatively by Model 2, and exclude the binding of more than one molecule of B to each monomer or oligomer of A. In this model it is assumed that GDP-FtsZ self-associates isodesmically (with equal stepwise equilibrium constants for addition of monomer to oligomer). This is the model that satisfactorily describes the self-association of GDP-FtsZ in the absence of sZipA (see below and reference (*32*)). In addition, it allows for the possibility of binding either one or two molecules of sZipA to each monomer or oligomer of GDP-FtsZ. The binding constant for the binding of the first molecule of sZipA is K_{AB}, and the binding constant for binding of the second molecule is $\alpha * K_{AB}$. The data indicate that the binding

of one molecule of sZipA to an oligomer of FtsZ reduces the affinity for binding of a second molecule of sZipA to the same oligomer by a factor greater than 10 ($\alpha < 0.03$). The best fit of this model to each data set, calculated using the parameter values given in the figure caption (see also Table 1), is plotted in Figure 5 together with the data. The best-fit values of K_{AA} obtained from the analysis of the mixtures of FtsZ and sZipA are in very good agreement with those previously obtained from the concentration dependence of the light scattering of GDP-FtsZ in the absence of sZipA under comparable conditions. This lends confidence in the robustness of our more general analysis of the two-component systems. The best-fit values of log K_{AA} and log K_{AB} are well defined by the data assuming that the concentrations and molecular weights of the two proteins have the assumed values. Even if the concentrations and molecular weights were a little uncertain, the best-fit values of log K_{AA} and log K_{AB} were still well-defined, however, with tolerances somewhat larger than those presented in the caption of Figure 5. To illustrate how sensitive the results are to variation in model parameters, the CG-LS profile of the mixture assuming either no binding of sZipA to FtsZ (dotted line) or binding of sZipA only to monomeric A (dashed line) are also plotted in Figure 5.

The fractional contribution of each species to total scattering in the absence of Mg^{2+}, calculated according to eqn [3], and the corresponding mass fractional distributions are plotted as a function of solution composition in **Figures S3** and **S4**, respectively. The fractional distribution plots in the presence of 5 mM Mg^{2+} are shown in **Figures S5** and **S6**. From these results we concluded that the scattering data obtained in the presence of Mg^{2+} are fit by an equilibrium model which takes into account significant scattering contributions not only of the species observable in the EDTA (B, A, A_2 A_3, AB and A_2B), but also A_4, A_5, A_6, A_3B and A_4B.

TABLE 1: Equilibrium association values for self- and hetero-associations of FtsZ and sZipA as determined by composition-gradient static light scattering (CG-SLS) and sedimentation equilibrium (SE)

Protein	$[Mg^{2+}]$	Log K_{AA}	Log K_{A-B}
FtsZ (A)	-	4.2 ± 0.1 (LS1)	
		4.3 (SE1	
FtsZ (A) + ZipA (B)	-	4.18 ± 0.02 (LS2)	5.24 ± 0.02 (LS2)
		3.8 (SE2)	5.1 (SE2)
FtsZ (A)	+	4.7 ± 0.1 (LS1)	
		4.8 (SE1)	
FtsZ (A) + ZipA (B)	+	4.79 ± 0.02 (LS2)	5.78 ± 0.02 (LS2)
		4.6 (SE2)	5.4 (SE2)

Table legend:

-: experiment conducted in the presence of 1 mM EDTA

+: experiment conducted in the presence of 5 mM $MgCl_2$

LS1: Best fit parameter values from the analysis of the CG-LS data using model 1 (eqns [4] – [6]), with $M_A = 40,000$

SE1: Best fit parameter values from the analysis of the sedimentation equilibrium data using model 1 (eqns [4] – [5] + [13]), with M_A = 40,000

We confirmed the interaction between sZipA and GDP-FtsZ by low-speed sedimentation equilibrium. **Figure 6** shows the equilibrium gradients of the mixture of sZipA (0.5 g/L; 14 µM) and FtsZ (0.5 g/L; 12.5 µM) obtained in Tris-500KCl buffer with either 5 mM Mg^{2+} (panel A) or 1 mM EDTA (panel B) together with the calculated best fit gradients assuming a single species model. The data are well described by species with single average buoyant M_w of 19,000 ± 800 (Mg^{2+}) and 15,700 ± 1,000 (EDTA) values that in both cases are significantly higher than the signal average buoyant M_w of the non-interacting mixtures (Mg^{2+}: 14,200 ± 1,000; EDTA: 10,500 ± 1,000), calculated from the buoyant M_w measured in parallel for isolated sZipA and FtsZ at the

same concentration, in the presence and in the absence of Mg^{2+}. These results demonstrated the presence of hetero-complexes in the two experimental conditions studied. The analysis of the dependence of the average molecular weight as a function of the sZipA and FtsZ concentrations in the mixtures, calculated using model 2 as described in the Materials and Methods section, are in qualitative agreement with the results obtained from composition-gradient light scattering (**Figure 7).** The model fits the data reasonably well, and both K_{AA} and K_{AB} appear to increase in the presence of Mg^{2+} (Table 1). However, the values are lower of log K_{AA} and log K_{AB}, with one exception (log K_{AB} in EDTA), are lower than the values obtained from the analysis of light scattering data.

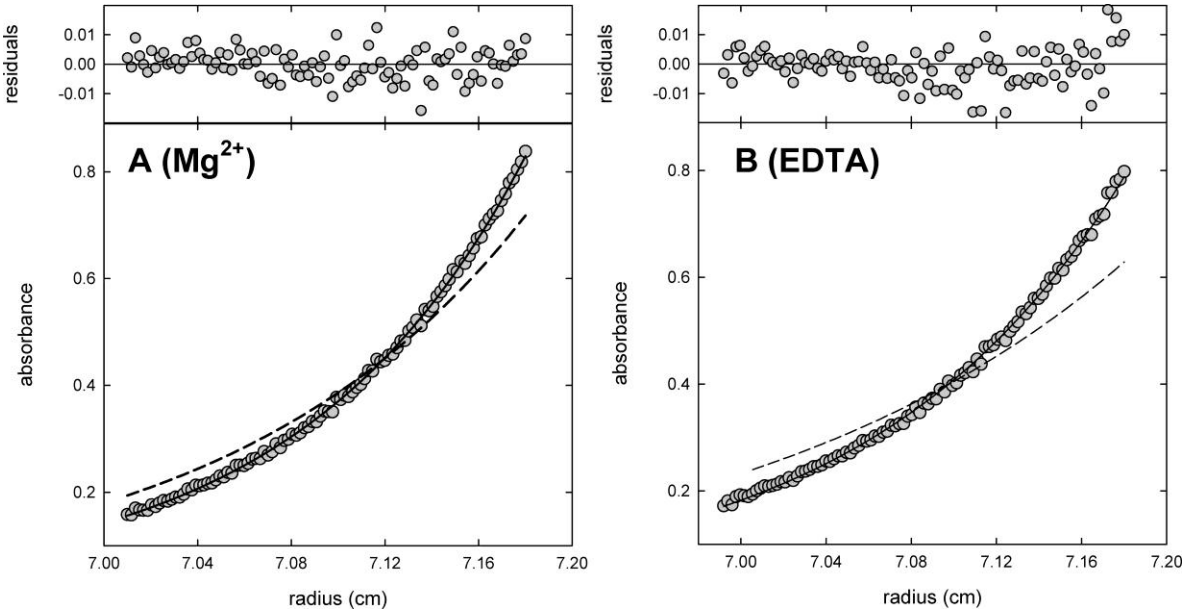

Figure 6. Sedimentation equilibrium analysis of sZipA binding to GDP-FtsZ. Sedimentation equilibrium absorbance profiles obtained at rotor speed 10,000 rpm and 20ºC for a sZipA-FtsZ mixture (0.5 g/L of each protein) equilibrated in Tris-500KCl buffer containing either 5mM $MgCl_2$ (panel A) or 1mM EDTA (panel B). Solid lines are the best-fit equilibrium gradient for an ideally sedimenting species with signal average buoyant M_w of 19,000 ± 800 (Mg^{2+}) and 15,700 ± 1,000 (EDTA). The dashed lines are the predicted gradient of the non-interacting mixture at the same protein concentration in the presence and in the absence of Mg^{2+}, respectively.

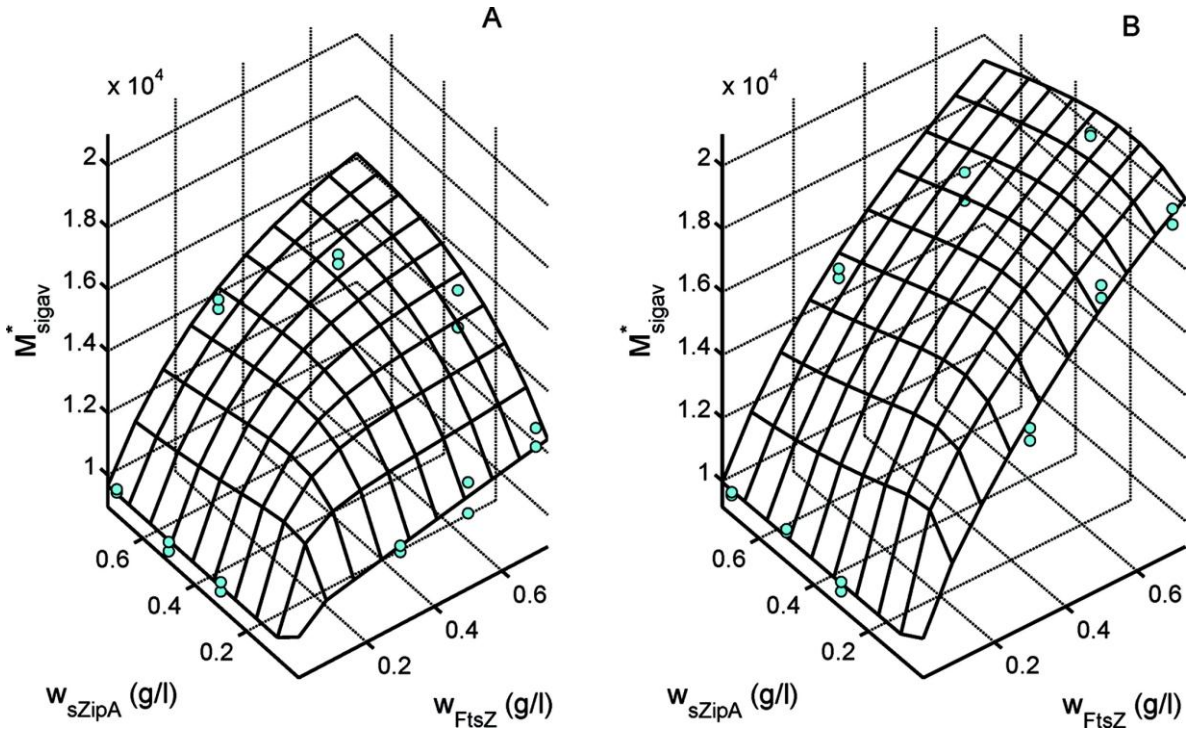

Figure 7. Analysis of the dependence of the signal average molecular weight of sZipA-FtsZ mixtures upon sZipA and FtsZ concentration as measured by sedimentation equilibrium. Panel A: 5 mM Mg^{2+}. Panel B: 1 mM EDTA. The grid lines represent the best fits of model 2 with M_A = 40,000, M_B = 35,000, log K_{AA} = 3.8 (- Mg^{2+}) or 4.6 (+ Mg^{2+}), and log K_{AB} = 5.1 (- Mg^{2+}) or 5.4 (+ Mg^{2+}).

CONCLUDING REMARKS

Our composition-gradient static light scattering study of ZipA-FtsZ mixtures of known composition has allowed us to determine that sZipA is monomeric, and that one molecule sZipA can bind to a GDP-FtsZ monomer or oligomer (up to hexamers in our buffer conditions) with moderate affinity (**Figure 7**). These results are compatible with results of parallel measurements of composition-dependent sedimentation equilibrium. Moreover they are in good agreement with earlier studies indicating that the C-terminal FtsZ-binding domain of ZipA binds with micromolar affinity to a C-terminal fragment of FtsZ [(26)]. The observed dependence of the values of K_{AA} and K_{AB} upon Mg^{2+} concentration is probably of greater biological relevance than the absolute values of these constants. Over the range of concentrations explored in our

experiments, the largest FtsZ oligomer present at significant abundance is the hexameric species. Our data do not permit us to determine whether additional sZipA molecules can bind to larger GDP-FtsZ oligomers but they establish that ZipA-FtsZ complex formation does not alter the self-association equilibrium between FtsZ molecules.

This work provides an additional example of the capability of the recently developed CG-SLS method to quantitatively characterize complex systems of self- and/or hetero-association equilibria in solutions containing one or two macromolecular components. Our conclusions are reinforced by parallel results obtained via measurements of sedimentation equilibrium. These results suggest a possible mechanism for anchoring of FtsZ fibers to the *E. coli* inner membrane via binding to membrane-localized ZipA.

SUPPLEMENTARY FIGURES

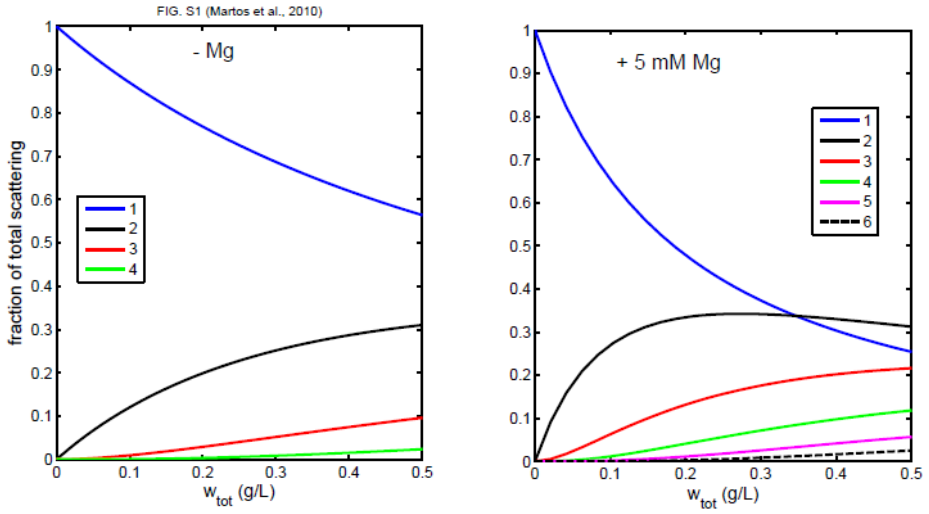

FIGURE S1. Fractional contribution of individual species to the total scattering intensity of GDP-FtsZ in the absence (panel A) and presence (panel B) of 5 mM Mg2+, calculated using model 1 with best-fit parameter values given in the caption to Fig 3.

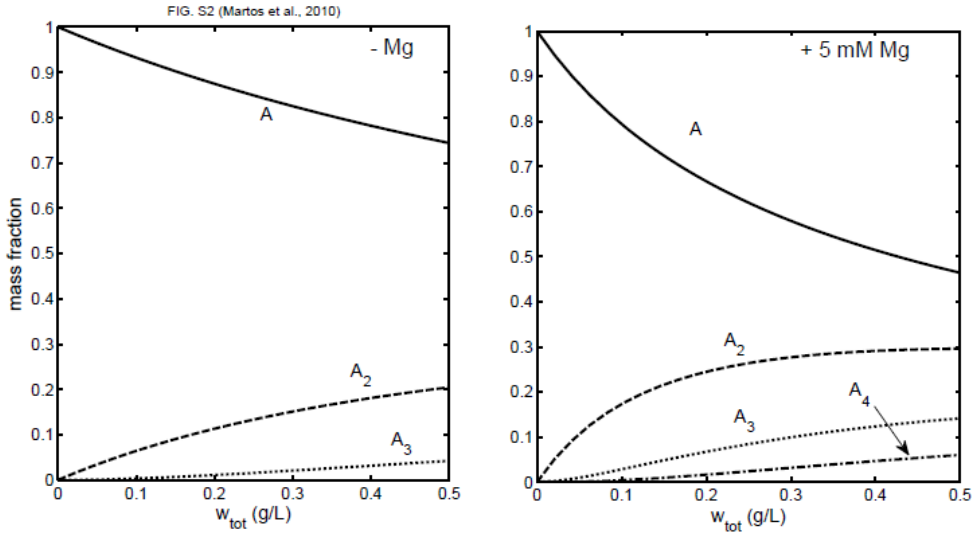

FIGURE S2. Weight fractional distribution of individual species plotted as a function of total concentration of GDP-FtsZ in the absence (left panel) and presence (right panel) of 5 mM Mg2+, calculated using model 1 with best-fit parameter values given in the caption to Fig 3.

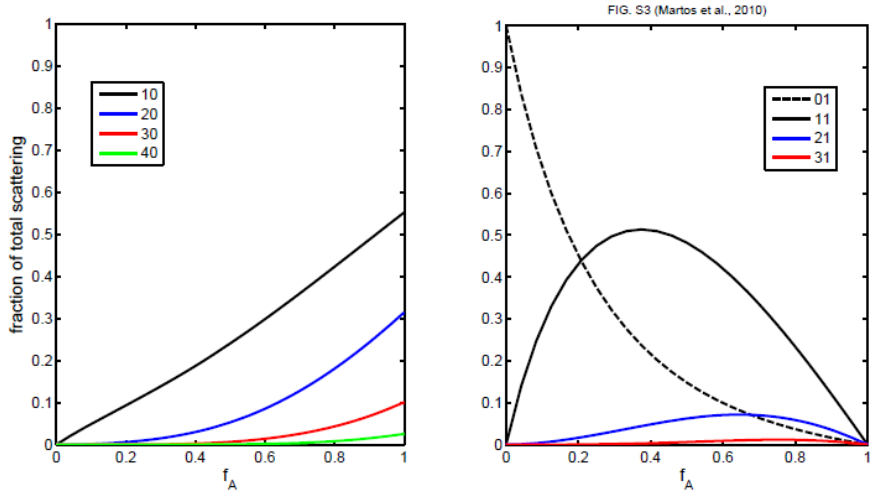

FIGURE S3. Fractional contribution of individual species to the total scattering intensity of GDP-FtsZ – sZipA mixtures in the absence of Mg2+, plotted as a function of solutio composition as described in the caption of Figure 4. Left and right hand panels show contributions of species lacking and containing B (sZipA) respectively, calculated using best-fit parameter values given in the caption to Fig. 5.

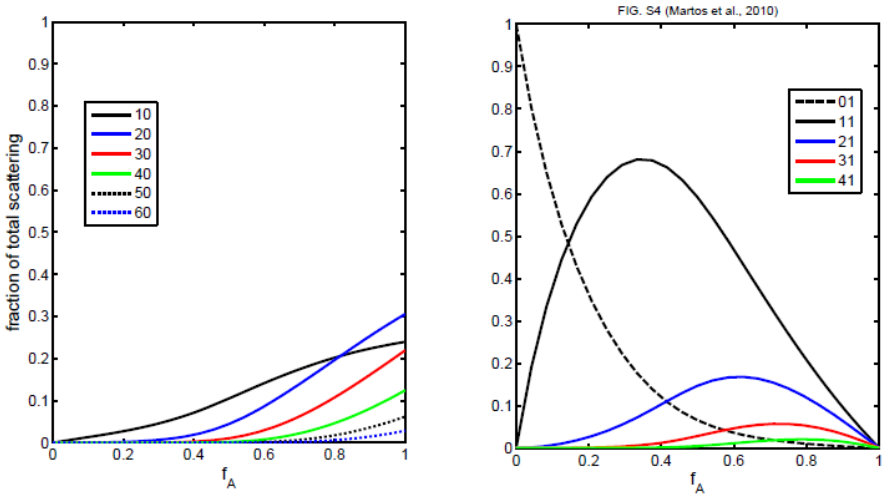

FIGURE S4. Weight fractional distributions of individual species in GDP-FtsZ – sZipA mixture without Mg2+, plotted as a function of solution composition as described in the caption of Figure 4. Left and right hand panels show contributions of species lacking and containing B (sZipA) respectively, calculated using best-fit parameter values given in the caption to Fig. 4.

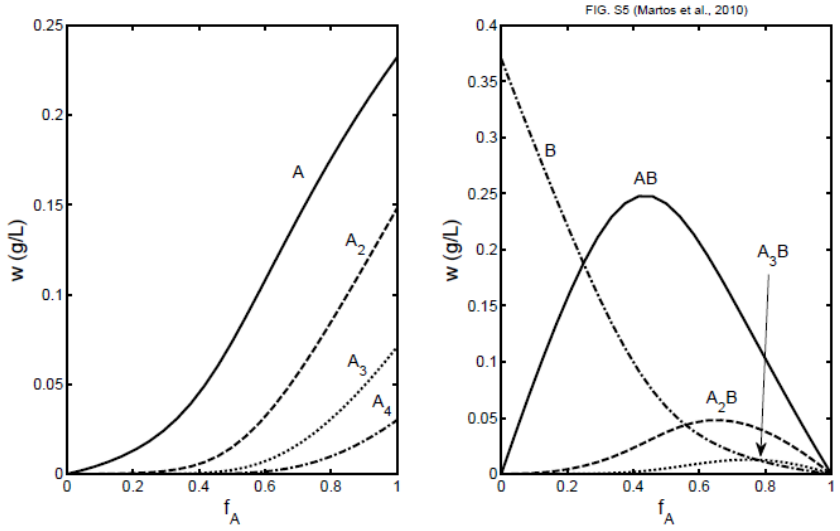

FIGURE S5. Fractional contribution of individual species to the total scattering intensity of GDP-FtsZ – sZipA mixtures in the presence of 5 mM Mg2+, plotted as a function of solution composition as described in the caption of Figure 3. Left and right hand panels show contributions of species lacking and containing B (sZipA) respectively, calculated using best-fit parameter values given in the caption to Fig. 4.

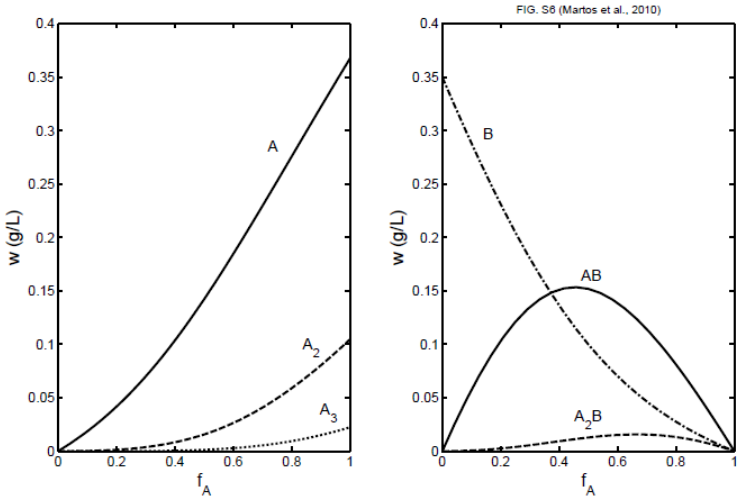

FIGURE S6. Weight fractional distributions of individual s 1 pecies in GDP-FtsZ – sZipA mixtures with 5 mM Mg2+, plotted as a function of solution composition as described in the caption of Figure 3. Left and right hand panels show contributions of species lacking and containing B (sZipA) respectively, calculated using best-fit parameter values given in the caption to Fig. 4.

References

1. Vicente, M., and Rico, A. I. (2006) The order of the ring: assembly of Escherichia coli cell division components, *Molecular microbiology 61*, 5-8.
2. Adams, D. W., and Errington, J. (2009) Bacterial cell division: assembly, maintenance and disassembly of the Z ring, *Nature reviews 7*, 642-653.
3. Mingorance, J., Rivas, G., Velez, M., Gomez-Puertas, P., and Vicente, M. (2010) Strong FtsZ is with the force: mechanisms to constrict bacteria, *Trends in microbiology 18*, 348-356.
4. Dajkovic, A., and Lutkenhaus, J. (2006) Z ring as executor of bacterial cell division, *J Mol Microbiol Biotechnol 11*, 140-151.
5. Gonzalez, J. M., Jimenez, M., Velez, M., Mingorance, J., Andreu, J. M., Vicente, M., and Rivas, G. (2003) Essential cell division protein FtsZ assembles into one monomer-thick ribbons under conditions resembling the crowded intracellular environment, *The Journal of biological chemistry 278*, 37664-37671.
6. Rivas, G., Fernandez, J. A., and Minton, A. P. (2001) Direct observation of the enhancement of noncooperative protein self-assembly by macromolecular crowding: indefinite linear self-association of bacterial cell division protein FtsZ, *Proceedings of the National Academy of Sciences of the United States of America 98*, 3150-3155.
7. Rivas, G., Lopez, A., Mingorance, J., Ferrandiz, M. J., Zorrilla, S., Minton, A. P., Vicente, M., and Andreu, J. M. (2000) Magnesium-induced linear self-association of the FtsZ bacterial cell division protein monomer. The primary steps for FtsZ assembly, *J Biol Chem 275*, 11740-11749.
8. Gonzalez, J. M., Velez, M., Jimenez, M., Alfonso, C., Schuck, P., Mingorance, J., Vicente, M., Minton, A. P., and Rivas, G. (2005) Cooperative behavior of Escherichia coli cell-division protein FtsZ assembly involves the preferential cyclization of long single-stranded fibrils, *Proc Natl Acad Sci U S A 102*, 1895-1900.
9. Huecas, S., and Andreu, J. M. (2003) Energetics of the cooperative assembly of cell division protein FtsZ and the nucleotide hydrolysis switch, *The Journal of biological chemistry 278*, 46146-46154.
10. Huecas, S., Llorca, O., Boskovic, J., Martin-Benito, J., Valpuesta, J. M., and Andreu, J. M. (2008) Energetics and geometry of FtsZ polymers: nucleated self-assembly of single protofilaments, *Biophysical journal 94*, 1796-1806.
11. Chen, Y., Bjornson, K., Redick, S. D., and Erickson, H. P. (2005) A rapid fluorescence assay for FtsZ assembly indicates cooperative assembly with a dimer nucleus, *Biophysical journal 88*, 505-514.
12. Chen, Y., and Erickson, H. P. (2008) In vitro assembly studies of FtsZ/tubulin-like proteins (TubZ) from Bacillus plasmids: evidence for a capping mechanism, *The Journal of biological chemistry 283*, 8102-8109.
13. Erickson, H. P., and Stoffler, D. (1996) Protofilaments and rings, two conformations of the tubulin family conserved from bacterial FtsZ to alpha/beta and gamma tubulin, *The Journal of cell biology 135*, 5-8.

14. Mingorance, J., Tadros, M., Vicente, M., Gonzalez, J. M., Rivas, G., and Velez, M. (2005) Visualization of single Escherichia coli FtsZ filament dynamics with atomic force microscopy, *J Biol Chem 280*, 20909-20914.
15. Margolin, W. (2005) FtsZ and the division of prokaryotic cells and organelles, *Nat Rev Mol Cell Biol 6*, 862-871.
16. Sanchez, M., Valencia, A., Ferrandiz, M. J., Sander, C., and Vicente, M. (1994) Correlation between the structure and biochemical activities of FtsA, an essential cell division protein of the actin family, *The EMBO journal 13*, 4919-4925.
17. Erickson, H. P. (2001) The FtsZ protofilament and attachment of ZipA--structural constraints on the FtsZ power stroke, *Current opinion in cell biology 13*, 55-60.
18. Hale, C. A., and de Boer, P. A. (1997) Direct binding of FtsZ to ZipA, an essential component of the septal ring structure that mediates cell division in E. coli, *Cell 88*, 175-185.
19. Hale, C. A., Rhee, A. C., and de Boer, P. A. (2000) ZipA-induced bundling of FtsZ polymers mediated by an interaction between C-terminal domains, *Journal of bacteriology 182*, 5153-5166.
20. Ohashi, T., Hale, C. A., de Boer, P. A., and Erickson, H. P. (2002) Structural evidence that the P/Q domain of ZipA is an unstructured, flexible tether between the membrane and the C-terminal FtsZ-binding domain, *Journal of bacteriology 184*, 4313-4315.
21. Hale, C. A., and de Boer, P. A. (1999) Recruitment of ZipA to the septal ring of Escherichia coli is dependent on FtsZ and independent of FtsA, *Journal of bacteriology 181*, 167-176.
22. RayChaudhuri, D. (1999) ZipA is a MAP-Tau homolog and is essential for structural integrity of the cytokinetic FtsZ ring during bacterial cell division, *The EMBO journal 18*, 2372-2383.
23. Hale, C. A., and de Boer, P. A. (2002) ZipA is required for recruitment of FtsK, FtsQ, FtsL, and FtsN to the septal ring in Escherichia coli, *Journal of bacteriology 184*, 2552-2556.
24. Haney, S. A., Glasfeld, E., Hale, C., Keeney, D., He, Z., and de Boer, P. (2001) Genetic analysis of the Escherichia coli FtsZ.ZipA interaction in the yeast two-hybrid system. Characterization of FtsZ residues essential for the interactions with ZipA and with FtsA, *J Biol Chem 276*, 11980-11987.
25. Moreira, I. S., Fernandes, P. A., and Ramos, M. J. (2006) Detailed microscopic study of the full zipA:FtsZ interface, *Proteins 63*, 811-821.
26. Mosyak, L., Zhang, Y., Glasfeld, E., Haney, S., Stahl, M., Seehra, J., and Somers, W. S. (2000) The bacterial cell-division protein ZipA and its interaction with an FtsZ fragment revealed by X-ray crystallography, *EMBO J 19*, 3179-3191.
27. Moy, F. J., Glasfeld, E., Mosyak, L., and Powers, R. (2000) Solution structure of ZipA, a crucial component of Escherichia coli cell division, *Biochemistry 39*, 9146-9156.
28. Attri, A. K., Fernandez, C., and Minton, A. P. (2010) pH-dependent self-association of zinc-free insulin characterized by concentration-gradient static light scattering, *Biophysical chemistry 148*, 28-33.

29. Attri, A. K., Fernandez, C., and Minton, A. P. (2010) Self-association of Zn-insulin at neutral pH: investigation by concentration gradient--static and dynamic light scattering, *Biophysical chemistry 148*, 23-27.
30. Attri, A. K., and Minton, A. P. (2005) Composition gradient static light scattering: a new technique for rapid detection and quantitative characterization of reversible macromolecular hetero-associations in solution, *Analytical biochemistry 346*, 132-138.
31. Attri, A. K., and Minton, A. P. (2005) New methods for measuring macromolecular interactions in solution via static light scattering: basic methodology and application to nonassociating and self-associating proteins, *Analytical biochemistry 337*, 103-110.
32. Kameyama, K., and Minton, A. P. (2006) Rapid quantitative characterization of protein interactions by composition gradient static light scattering, *Biophysical journal 90*, 2164-2169.
33. Cole, J. L., Lary, J. W., T, P. M., and Laue, T. M. (2008) Analytical ultracentrifugation: sedimentation velocity and sedimentation equilibrium, *Methods in cell biology 84*, 143-179.
34. Minton, A. P. (1997) Alternative strategies for the characterization of associations in multicomponent solutions via measurement of sedimentation equilibrium, *Progr. Colloid Polym. Sci. 107*, 11-19.

5.-DISCUSIÓN INTEGRADORA

FtsZ es la proteína mayoritaria de la maquinaria macromolecular que lleva a cabo el proceso esencial de la división bacteriana. Además, FtsZ, es la primera proteína que se localiza en el sitio de división. El primer complejo multiproteico en formarse es el proto-anillo, su ensamblaje tiene lugar en el citoplasma bacteriano, en el entorno de la membrana, a través de interacciones macromoleculares reversibles, que están moduladas en una buena parte, por diferentes cofactores [1, 2]. Por tanto, la caracterización biofísica de las interacciones implicadas en los primeros pasos de la formación del proto-anillo, y la dependencia con sus cofactores, es de esencial interés en los campos de la biología, medicina y la farmacología, ya que estas proteínas y sus interacciones suponen potenciales dianas en el desarrollo de nuevos agentes antibacterianos [3].

Pequeños microgradientes en variables físico-químicas como fuerza iónica, pH, agentes de aglomeración macromolecular, entre otras, son habituales entre los diferentes microentornos del citoplasma bacteriano. En algunos casos, sutiles diferencias en estas variables, son en gran medida, las responsables de modular las interacciones interproteicas, y por tanto, de regular el ensamblaje y actividad de maquinarias macromoleculares en sistemas biológicos. Los cationes Ca^{2+} y Mg^{2+}, juegan un papel muy importante como moduladores de los procesos funcionales biológicos. El Mg^{2+} es el catión más abundante en el citoplasma bacteriano después del K^{+}, y está implicado en numerosas funciones celulares, como activador de algunas enzimas, formando complejos, modificando sustratos y manteniendo estable la estructura de algunas proteínas y ácidos nucleicos entre otras [4].

FtsZ, posee motivos estructurales potencialmente implicados en la unión de cationes monovalentes y divalentes que podrían ser importantes en la regulación de la estructura y función de la proteína [5]. Otros cationes como K^{+} o Na^{+}, también están implicados en procesos de gran relevancia, por ejemplo, modulando la actividad GTPasa de FtsZ y por tanto la dinámica de los proto-filamentos [2]. Por estos motivos, se hace de esencial

importancia el estudio del efecto de estos cofactores sobre la oligomerización y el ensamblaje de la proteína. Estas propiedades, hacen que el ensamblaje de FtsZ sea un proceso tan dinámico y dificultan su estudio y caracterización, de manera que el uso de algunos métodos bioquímicos y biofísicos para la caracterización cuantitativa del proceso quedan restringidos. Para evitar en parte estas limitaciones, se utilizó en todos los ensayos en los que se promueve la polimerización con GTP, un sistema enzimático de regeneración del GTP [6]. Mediante el uso de este sistema de regeneración, se pudieron mantener estables los polímeros durante un tiempo de al menos 80 minutos, suficiente para llevar a cabo los experimentos que se describen en la caracterización del polímero de GTP-FtsZ (ver apéndice 1). El uso de este sistema de regeneración del GTP es muy importante, ya que simula la situación *in vivo*, donde los polímeros de FtsZ están bajo condiciones de una elevada y constante relación de GTP/GDP [7].

La polimerización de FtsZ en presencia de GTP o GMPCPP y su dependencia con la concentración de Mg^{2+} se analiza en el capitulo I. En trabajos anteriores, se observaba cierta dependencia entre la actividad GTPasa y la concentración de Mg^{2+} [8, 9]. Nuestros resultados, confirman los resultados previos y además, proporcionan un estudio minucioso de la dependencia del grado de polimerización, tanto con la concentración de Mg^{2+} a concentraciones submilimolares, como con la concentración de FtsZ. Mediante este estudio, podemos confirmar la formación de especies poliméricas de tamaño definido [10]. La distribución de tamaños de estas especies, se encuentra en un rango muy estrecho y definido, con lo que hemos podido determinar por primera vez la masa molecular promedio, y por tanto, el número promedio de subunidades de las que consta el proto-filamento de FtsZ, pieza clave en la maquinaria de división bacteriana. Los resultados obtenidos mediante varias técnicas, están en buen acuerdo y apuntan en la misma dirección en cuanto a la formación de polímeros de tamaño definido. Este hecho, por un lado, apoya resultados previos observados por criotomografía electrónica [11], que sugieren, que el anillo-Z no es una estructura continua, si no que está formada por agrupación de filamentos más cortos como se muestra en la figura 1 de la discusión.

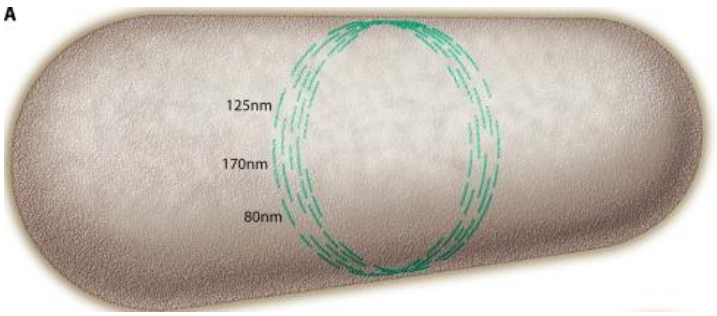

Figura 1. Modelo propuesto por Erickson *et al*, [12] basandose en resultados de criotomógrafía electronica , [11] de manera que el anillo de división estaría compuesto por multitud de proto-filamentos de longitud definida superponiendose.

El hecho de tener un tamaño definido en los proto-filamentos, también esta en buen acuerdo con el mecanismo propuesto anteriormente de polimerización, donde se postula una etapa de ciclación [10] (ver figura 5 de la introducción). Además, se ha podido observar, que la polimerización, no solamente es dependiente de la concentración de Mg^{2+}, si no que a concentraciones micromolares de Mg^{2+}, es también dependiente de la concentración de proteína.

La polimerización de FtsZ en presencia de GTP, puede describirse como una transición concertada, termodinámicamente similar a una transición de fase de segundo orden entre especies de bajo y elevado peso molecular. Sin embargo, en presencia de GMPCPP puede describirse más apropiadamente como una transición de primer orden, desde especies oligoméricas pequeñas hasta polímeros, a partir de un determinado valor de concentración crítica de proteína, característica de un proceso cooperativo [13].

Centrándonos en el estudio y la caracterización biofísica de FtsZ en su forma GDP, y la dependencia de la oligomerización a concentraciones submilimolares Mg^{2+} en todo el rango fisiológico (Apéndice 1), obtenemos una clara dependencia de la oligomerización, tanto con la concentración de Mg^{2+}, como con la concentración de proteína. Estudios previos realizados a media y baja fuerza iónica indicaban una asociación isodésmica para formar oligómeros lineales de longitud indefinida y dependiente de la fuerza iónica, concentraciones milimolares variables de Mg^{2+}, y agentes de aglomeración

macromolecular [14 - 16]. En este estudio incorporado en el Apéndice 1, nos centramos fundamentalmente en condiciones de alta fuerza iónica, donde la reacción dominante es la dimerización de FtsZ. La importancia de este estudio radica en que la especie dimérica es la unidad de actividad GTPasa. El análisis mediante las técnicas biofísicas empleadas, indica que las especies predominantes en disolución son monómeros y dímeros en equilibrio, aunque existe una pequeña proporción de especies de mayor orden. Además, ha sido posible aplicar un modelo de ajuste a los datos de dispersión de luz estática. A través de los resultados del ajuste, se han obtenido las constantes de equilibrio, además de los coeficientes de sedimentación y de difusión de las especies presentes en este equilibrio mediante otras técnicas.

Por otro lado, el rango de concentraciones del catión Mg^{2+} en las que suceden tanto la oligomerización como el ensamblaje de FtsZ se encuentran próximas y dentro del rango micromolar. De esta manera, la oligomerización y la polimerización de FtsZ deben estar correlacionadas, y en los dos casos, se encuentra una fuerte dependencia con la concentración de Mg^{2+}. En ambos casos, la concentración de Mg^{2+} en la que las reacciones de polimerización y oligomerización alcanzan el 50% se encuentra muy cercana al rango milimolar, entre 1 y 5 $x10^{-5}$ M, siendo la reacción de polimerización, aparentemente más sensible a cambios en la concentración del catión.

La caracterización de FtsZ en las formas GTP y GMPCPP y su dependencia con la fuerza iónica se aborda en el capitulo II. Algunos autores, habían estudiado el efecto del K^+ y otros cationes sobre la actividad GTPasa bajo diferentes condiciones de pH, observando, que el K^+ estimula la actividad GTPasa de FtsZ [2, 6, 8, 17, 18]. Nosotros, además, aportamos un estudio exhaustivo del ensamblaje de FtsZ, su dependencia con la composición salina y fuerza iónica del medio. Asimismo, observamos un comportamiento inverso entre la polimerización inducida en presencia de GTP y la polimerización por GMPCPP, un análogo lentamente hidrolizable de GTP. De esta manera, en el caso de GTP-FtsZ, el grado de polimerización decrece notablemente al disminuir la fuerza iónica del medio desde 500 mM a 100 mM. Por el contrario, en el caso de GMPCPP-FtsZ, el tamaño de los polímeros formados, aumenta drásticamente al disminuir la concentración iónica.

En el caso de GTP-FtsZ, la polimerización es un proceso muy dinámico. La actividad GTPasa está muy fuertemente ligada a la concentración de K^+ y otros cationes monovalentes [2, 6, 8, 18]. Según explica Erickson y colaboradores, [18, 19] la actividad GTPasa de FtsZ es óptima a baja fuerza iónica (100 mM), viéndose ligeramente atenuada al aumentar la fuerza iónica (500 mM). Este efecto, condiciona fuertemente la dinámica de hidrólisis e intercambio de nucleótido, por tanto, el tamaño observado de los polímeros en ambas condiciones de salinidad. De esta manera, el grado de polimerización de la proteína en presencia de GTP, se encuentra aparentemente dominado por el efecto de la fuerza iónica sobre la actividad GTPasa. A 100 mM de K^+ los polímeros formados son más dinámicos, por tanto, su tamaño promedio, será más pequeño que los formados a 500 mM.

En el caso de GMPCPP-FtsZ la actividad GTPasa está en gran parte inhibida, de manera que a 37^{o}C la proteína cuenta solamente con el 4% de su actividad [20], por tanto, la dinámica de los polímeros formados está también fuertemente inhibida. Posiblemente, al igual que sucede en el caso de GTP-FtsZ, a baja fuerza iónica (100 mM) la actividad GTPasa sea algo mayor que en el caso de alta fuerza iónica (500 mM), por tanto, los polímeros de GMPCPP-FtsZ a baja sal serán también de menor tamaño. A parte de este efecto, debe haber otro tipo de interacciones que están atenuadas por el incremento de la fuerza iónica y por tanto, aparentemente, con cierta componente electrostática entre las diferentes cadenas de polímero proteico. De manera que al ir aumentando la fuerza iónica, estas posibles interacciones atractivas polímero-polímero se ven cada vez más apantalladas, por tanto, el tamaño de las especies formadas disminuye al aumentar la fuerza iónica. Este efecto es comparable al que sufre la tubulina eucariota, que tiene una actividad GTPasa unas 100 veces menor que FtsZ [21], y similar al caso de GDP-FtsZ [14], lo cual nos sugiere, que los estados poco activos o dinámicos de FtsZ ven favorecido su ensamblaje a baja fuerza iónica de una manera aparentemente dirigida por efectos electrostáticos.

Mediante experimentos de microscopía electrónica de transmisión, (ver material suplementario del capítulo 2) pudimos corroborar esta tendencia. De esta manera, a baja

fuerza iónica (100 mM), mientras los polímeros de GMPCPP se asocian formando redes de polímeros de varios filamentos de espesor, los polímeros de GTP son sencillos y aparentemente más cortos que en el caso de alta fuerza iónica.

Por otro lado, mediante la utilización del anión Acetato en vez de Cloruro, hemos podido observar algunas leves diferencias en las especies poliméricas formadas en presencia de Mg^{2+}, pero la tendencia del grado de polimerización con la fuerza iónica, va en el mismo camino que usando Cloruro. Sin embargo, utilizando Acetato en ausencia de Mg^{2+} y presencia de EDTA, hemos podido observar mediante velocidad de sedimentación y dispersión de luz, la precipitación de parte de la proteína, en condiciones, en las que usando el anión Cloruro teníamos mayoritariamente monómero. Por tanto, la presencia conjunta de Acetato y EDTA produce una agregación importante de la proteína, dato a tener en cuenta, ya que en algunos trabajos previos de Erickson y colaboradores, [18] utilizaban esta combinación en alguno de sus tampones.

Con objeto de obtener información sobre los primeros pasos del mecanismo por el cuál tiene lugar la división bacteriana, el estudio de la interacción entre las proteínas FtsZ y ZipA en un sistema reconstituido de membrana, constituye un tema de estudio esencial. La reconstitución funcional de los elementos del proto-anillo en sistemas biomiméticos de membrana, es una de las bases del estudio de la funcionalidad y especificidad de interacciones en biología sintética aplicada a sistemas mínimos, así como una herramienta para la detección y cuantificación de interacciones. En el apéndice 2 del capitulo III, hemos reconstituido la membrana bacteriana, tanto la formada por fosfolípidos comerciales, como la formada por membrana natural interna aislada directamente de la bacteria, en la superficie de microesferas monodispersas. Mediante el desarrollo de este sistema, hemos podido reconstituir y detectar con muy elevada sensibilidad las interacciones entre ZipA y FtsZ en diferentes estados de asociación, en un entorno biomimético de membrana. Los resultados de la reconstitución (apéndice 2), junto con el estudio en disolución (apéndice 3), proporcionan argumentos suficientes para confirmar el papel de ZipA como anclaje de FtsZ a la membrana. ZipA, como hemos visto, es capaz de unir a la membrana tanto las formas oligoméricas (GDP-FtsZ) como poliméricas (GTP-FtsZ). En este caso, se ha

observado cómo los polímeros de FtsZ crecen anclados a la membrana formando redes tridimensionales, incluso crecen formando haces de filamentos que unen diferentes microesferas (ver apéndice 2). Si cada subunidad de FtsZ del polímero, se uniera a la membrana, no se formarían redes tridimensionales, y los polímeros formados, no se separarían de la superficie de las esferas. Este hecho apoya los resultados obtenidos previamente por dispersión de luz estática en gradiente de concentración y equilibrio de sedimentación [15], que indican una unión subestequiométrica entre oligómeros de diferente tamaño de FtsZ (desde monómero hasta hexámero) y una sola unidad de ZipA (ver apéndice 3).

El desarrollo de sistemas de detección directa proteína-proteína en medios biomiméticos de membrana es de elevada complejidad, ya que, normalmente, implica la necesidad del marcaje con sondas fluorescentes o la inmunodetección con anticuerpos. La fabricación de sustratos con elevada densidad de "SERS hot spots", (ve sección de métodos), en la superfie de microesferas es una de las piezas clave en el desarrollo de sistemas de detección ultrasensible. Este tipo de sistemas supone un gran avance en el desarrollo de sistemas miniaturizados de detección de interacciones y diagnóstico portátil y rápido. Mediante la utilización de estos sensores plasmónicos, en el capítulo III, hemos podido detectar los cambios conformacionales producidos en ZipA por interacción con GDP-FtsZ y GTP-FtsZ. Mediante este ensayo, hemos podido determinar que estos cambios conformacionales confirman, por un lado, la existencia de la interacción, además de revelar, que la unión de FtsZ afecta estructuralmente a ZipA de manera diferente dependientemente del estado de asociación de FtsZ. Además, hemos detectado la interacción entre polímeros de FtsZ con ZipA en la propia membrana formada por fosfolípidos de *E. coli*. Asimismo, hemos podido detectar la interacción de polímeros de FtsZ con el resto de componentes de la maquinaria de división, además de ZipA, en la propia membrana interna bacteriana, a través de cambios estructurales revelados por los espectros vibracionales de SERS.

Este sistema de detección nos proporciona una gran sensibilidad para detectar cambios conformacionales de la espectroscopía SERS, además, la ventaja de la miniaturización del

sistema de detección, nos permite utilizar mínimas cantidades de muestra. Por otro lado, el ensayo desarrollado, permitirá evaluar la acción de nuevos potenciales agentes antibióticos en el ensamblaje de la maquinaria de división bacteriana o en la interacción FtsZ-ZipA.

Referencias

1. Vicente M, Rico AI, Martínez-Arteaga R, Mingorance J. Septum enlightenment: assembly of bacterial division proteins. J Bacteriol. 2006;188(1):19-27. Review

2. Tadros M, González JM, Rivas G, Vicente M, Mingorance J. Activation of the Escherichia coli cell division protein FtsZ by a low-affinity interaction with monovalent cations. FEBS Lett. 2006 Sep 4;580(20):4941-6.

3. Awasthi D, Kumar K, Ojima I. Therapeutic potential of FtsZ inhibition: a patent perspective. Expert Opin Ther Pat. 2011 May;21(5):657-79.

4. Romani A, Scarpa A. Regulation of cell magnesium. Arch Biochem Biophys. 1992 Oct;298(1):1-12. Review

5. Yu XC, Margolin W. Ca2+-mediated GTP-dependent dynamic assembly of bacterial cell division protein FtsZ into asters and polymer networks in vitro. EMBO J. 1997 Sep 1;16(17):5455-63.

6. González JM, Jiménez M, Vélez M, Mingorance J, Andreu JM, Vicente M, Rivas G. Essential cell division protein FtsZ assembles into one monomer-thick ribbons under conditions resembling the crowded intracellular environment. J Biol Chem. 2003 Sep 26;278(39):37664-71.

7. Small E, Addinall SG. Dynamic FtsZ polymerization is sensitive to the GTP to GDP ratio and can be maintained at steady state using a GTP-regeneration system. Microbiology. 2003 Aug;149(Pt 8):2235-42.

8. Mingorance J, Rueda S, Gómez-Puertas P, Valencia A, Vicente M. Escherichia coli FtsZ polymers contain mostly GTP and have a high nucleotide turnover. Mol Microbiol. 2001 Jul;41(1):83-91.

9. Mukherjee A, Lutkenhaus J. Analysis of FtsZ assembly by light scattering and determination of the role of divalent metal cations. J Bacteriol. 1999 Feb;181(3):823-32.

10. González JM, Vélez M, Jiménez M, Alfonso C, Schuck P, Mingorance J, Vicente M, Minton AP, Rivas G. Cooperative behavior of Escherichia coli cell-division protein FtsZ assembly involves the preferential cyclization of long single-stranded fibrils. Proc Natl Acad Sci U S A. 2005 Feb 8;102(6):1895-900

11. Li Z, Trimble MJ, Brun YV, Jensen GJ. The structure of FtsZ filaments in vivo suggests a force-generating role in cell division. EMBO J. 2007 Nov 14;26(22):4694-708. Epub 2007 Oct 18.

12. Erickson HP, Anderson DE, Osawa M. FtsZ in bacterial cytokinesis: cytoskeleton and force generator all in one. Microbiol Mol Biol Rev. 2010 Dec;74(4):504-28.

13. Hall D, Minton AP. Effects of inert volume-excluding macromolecules on protein fiber formation. I. Equilibrium models. Biophys Chem. 2002 Jul 10;98(1-2):93-104.

14. Rivas G, López A, Mingorance J, Ferrándiz MJ, Zorrilla S, Minton AP, Vicente M, Andreu JM. Magnesium-induced linear self-association of the FtsZ bacterial cell division protein monomer. The primary steps for FtsZ assembly. J Biol Chem. 2000 Apr 21;275(16):11740-9.

15. Martos A, Alfonso C, López-Navajas P, Ahijado-Guzmán R, Mingorance J, Minton AP, Rivas G. Characterization of self-association and heteroassociation of bacterial cell division proteins FtsZ and ZipA in solution by composition gradient-static light scattering. Biochemistry, 2010. 49(51): p.10780–10787.

16. Rivas G, Fernández JA, Minton AP. Direct observation of the enhancement of noncooperative protein self-assembly by macromolecular crowding: indefinite

linear self-association of bacterial cell division protein FtsZ. Proc Natl Acad Sci U S A. 2001 13;98(6):3150-5.

17. Lu C, Erickson HP. Purification and assembly of FtsZ. Methods Enzymol. 1998;298:305-13.

18. Chen Y, Erickson HP. FtsZ filament dynamics at steady state: subunit exchange with and without nucleotide hydrolysis. Biochemistry. 2009 Jul 21;48(28):6664-73.

19. Lu C, Stricker J, Erickson HP. FtsZ from Escherichia coli, Azotobacter vinelandii, and Thermotoga maritima-quantitation, GTP hydrolysis, and assembly. Cell Motil Cytoskeleton. 1998;40(1):71-86.

20. Salvarelli E, Krupka M, Rivas G, Vicente M, Mingorance J. Independence between GTPase active sites in the Escherichia coli cell division protein FtsZ. FEBS Lett. 2011 Dec 15;585(24):3880-3.

21. Olmsted JB, Borisy GG. Characterization of microtubule assembly in porcine brain extracts by viscometry. Biochemistry. 1973 Oct 9;12(21):4282-9.

6.-APORTACIONES FUNDAMENTALES

CAPÍTULO I: CARACTERIZACIÓN BIOFÍSICA DE FtsZ EN PRESENCIA DE GTP O UN ANÁLOGO DE GTP: El ensamblaje de FtsZ activado por Mg^{2+} promueve la formación concertada de especies poliméricas definidas.

En este capítulo hemos podido confirmar la formación de especies de tamaño definido, obtener su masa molecular, además de proporcionar un estudio exhaustivo de la dependencia del grado de polimerización, tanto con la concentración de Mg^{2+}, como con la concentración de FtsZ. Las técnicas empleadas en este estudio son: Dispersión de luz estática en gradiente de concentración, velocidad de sedimentación, dispersión de luz dinámica y espectroscopía de correlación de fluorescencia. Las aportaciones más relevantes de este trabajo son:

- Hemos podido determinar por primera vez la masa molecular promedio y por tanto el número promedio de subunidades de las que consta el proto-filamento de FtsZ.
- La polimerización es dependiente de la concentración de Mg^{2+}, y en concentraciones micromolares de Mg^{2+}, es dependiente de la concentración de proteína.
- Parámetros termodinámicos e hidrodinámicos del ensamblaje de FtsZ en presencia de GTP y GMPCPP, un análogo lentamente hidrolizable de GTP.

APÉNDICE 1: CARACTERIZACIÓN BIOFÍSICA DE FtsZ EN PRESENCIA DE GDP. Efecto del Mg^{2+} como regulador del equilibrio de oligomerización.

En este apartado hemos caracterizado el equilibrio de oligomerización de FtsZ en su forma GDP. Además, hemos hecho un estudio minucioso de la dependencia de este equilibrio con la concentración de Mg^{2+} y de proteína. Las técnicas empleadas en este estudio son: Dispersión de luz estática en gradiente de concentración, velocidad de sedimentación y dispersión de luz dinámica. Este trabajo aporta:

- Parámetros termodinámicos e hidrodinámicos de la homoasociacion de FtsZ en su forma GDP. El análisis de los resultados indica que las especies predominantes en disolución son monómeros y dímeros en equilibrio.

CAPÍTULO II: EFECTO DE LA COMPOSICIÓN IÓNICA DEL TAMPÓN EN EL ENSAMBLAJE DE FtsZ EN PRESENCIA DE GTP O UN ANÁLOGO DE GTP.

En este capítulo hemos podido determinar la dependencia del grado de polimerización con la concentración de K^{+}. Además, hemos proporcionado un estudio exhaustivo de la dependencia del grado de polimerización, tanto con la composición salina del tampón, como con la concentración de FtsZ. Las técnicas empleadas en este estudio son: Dispersión de luz estática en gradiente de concentración, velocidad de sedimentación, dispersión de luz dinámica y espectroscopía de correlación de fluorescencia. Las aportaciones más relevantes de este trabajo son:

- El grado de polimerización de GTP-FtsZ decrece notablemente al disminuir la fuerza iónica del medio desde 500 mM a 100 mM.
- En el caso de GMPCPP-FtsZ, el grado de polimerización aumenta progresivamente al disminuir la concentración iónica.

- La utilización conjunta, por parte de algunos laboratorios, de disoluciones tampón con Acetato y EDTA, lleva consigo la agregación de buena parte de la proteína.
- Hemos establecido una clara y evidente dependencia del grado de polimerización con la composición iónica de la disolución tampón. Este estudio es clave en cuanto al entendimiento de las discrepancias encontradas a lo largo de la literatura sobre el ensamblaje de FtsZ en diferentes composiciones iónicas.

CAPÍTULO III: RECONSTITUCIÓN, AUTO-ENSAMBLAJE Y ESTUDIO MEDIANTE ESPECTROSCOPÍA SERS DE LA INTERACCIÓN DE FtsZ Y OTROS ELEMENTOS DE LA MEMBRANA BACTERIANA EN MICROESFERAS FUNCIONALIZADAS

En el capitulo III hemos recubierto microesferas con una alta densidad de nanosensores plasmónicos con propiedades ópticas avanzadas que nos sirven, tanto para la reconstitución, como soporte para espectroscopía SERS. Mediante el desarrollo de este sistema hemos podido reconstituir y detectar con muy elevada sensibilidad las interacciones entre ZipA y FtsZ en diferentes estados de oligo- o polimerización, además de reconstituir los elementos del divisoma en un entorno biomimético de membrana. Las aportaciones más relevantes de este trabajo son:

- Hemos funcionalizado la superficie de microesferas con nanosensores plasmónicos de oro y plata con alta actividad en espectroscopía SERS. La puesta a punto de estos sensores plamónicos es una pieza clave en el desarrollo de sistemas miniaturizados de diagnóstico rápido así como de sistemas de *screening* de alto rendimiento para la búsqueda de actividad de nuevo fármacos.
- Hemos estudiado los cambios conformacionales que sufre la proteína ZipA a través de la interacción con las diferentes formas de FtsZ reconstituidas en la superficie de sensores plasmónicos.
- Hemos detectado con gran sensibilidad la interacción del polímero de FtsZ con componentes del divisoma en la propia membrana interna bacteriana, tanto natural como sintética. Con este sistema podríamos detectar la interacción de

nuevos potenciales fármacos antibióticos que afectaran a la maquinaria de división o a alguno de sus componentes.

APÉNDICE 2: RECONSTITUCIÓN DE LOS ELEMENTOS DEL PROTO-ANILLO EN MICROESFERAS

En el apéndice 2 hemos reconstituido la membrana bacteriana, tanto la formada por fosfolípidos comerciales, como la membrana natural interna, en la superficie de microesferas monodispersas.

- Hemos puesto a punto un método mediante el que podemos depositar y recubrir homogéneamente con membrana bacteriana la superficie de microesferas monodispersas. Además hemos podido reconstituir la interacción FtsZ-ZipA en estos sistemas modelo de membrana.

APÉNDICE 3: CARACTERIZACIÓN DE LA HETEROASOCIACIÓN ENTRE ZipA Y LAS FORMAS GDP DE FtsZ MEDIANTE DISPERSIÓN DE LUZ ESTÁTICA EN GRADIENTE DE CONCENTRACIÓN

En el Apéndice 3, hemos caracterizado cuantitativamente las interacciones entre FtsZ (GDP) y la forma soluble de ZipA (carente del dominio transmembrana) mediante dispersión de luz estática en gradiente de concentración (CG-SLS) y ultracentrifugación analítica.

- Se han obtenido las constantes de asociación de la heteroasociacion de FtsZ en su forma GDP con la proteína ZipA. El análisis de los resultados indica que la naturaleza de la interacción es subestequiométrica, de manera que un sólo monómero de ZipA es capaz de unirse a oligómeros de FtsZ independientemente de su tamaño.

7.-CONCLUSIONES

I. El número promedio de subunidades de las que consta el proto-filamento de FtsZ en la forma GTP es 100 ± 15 protómeros y en la forma GMPCPP es 160 ± 20 monómeros.

II. El grado de polimerización de GTP-FtsZ decrece notablemente al disminuir la fuerza iónica del medio desde 500 mM a 100 mM. En el caso de GMPCPP-FtsZ, el grado de polimerización aumenta progresivamente al disminuir la concentración iónica.

III. Mediante la utilización de tampones que combinan Acetato y EDTA, parte de la proteína sufre un proceso de agregación. Este tipo de tampones, como se ha indicado anteriormente, es de uso habitual por algunos grupos de investigación relevantes.

IV. La oligomerización de FtsZ en presencia de GDP es un proceso controlado por la unión de Mg^{2+} y por la concentración de proteína. El análisis mediante técnicas biofísicas indica que las especies predominantes en disolución son monómeros y dímeros en equilibrio, aunque existe una pequeña proporción de especies mayores.

V. El ensamblaje de FtsZ, al igual que la oligomerización, es dependiente de la concentración de Mg^{2+} y en concentraciones micromolares de Mg^{2+} es dependiente de la concentración de proteína.

VI. El método de recubrimiento puesto a punto permite la obtención de microesferas recubiertas homogéneamente con membrana bacteriana y permite la reconstitución de la interacción ZipA-FtsZ en un medio biomimético.

VII. Los cambios conformacionales que sufre la proteína ZipA mediante la interacción con FtsZ dependen del estado de asociación de la última. Estos cambios

estructurales se estudiaron mediante espectroscopía SERS a través de la reconstitución de los complejos FtsZ-ZipA en la superficie de sensores plasmónicos.

VIII. Ha sido posible la detección con gran sensibilidad de la interacción del polímero de FtsZ con los componentes del divisoma en la propia membrana interna bacteriana mediante espectroscopía SERS. Mediante la utilización de este sistema, podríamos detectar la interacción de nuevos fármacos antibióticos que afectaran a la maquinaria de división o a alguno de sus componentes.

8.-PUBLICACIONES DURANTE LA TESIS

1.- Characterization of self-association and heteroassociation of bacterial cell division proteins FtsZ and ZipA in solution by composition gradient-static light scattering. Martos A, Alfonso C, López-Navajas P, **Ahijado-Guzmán R**, Mingorance J, Minton AP, Rivas G. Biochemistry. 2010 Dec 28; 49(51):10780-7.

2.- Mg^{2+}-linked self-assembly involves the concerted formation of a narrow distribution of oligomeric species. Begoña Monterroso, **Rubén Ahijado-Guzmán**, Belén Reija, Carlos Alfonso, Silvia Zorrilla, Allen P. Minton, and Germán Rivas. Biochemistry In press.

3.- Control by KCl of the strength of FtsZ self-assembly is nucleotide dependent. **Rubén Ahijado-Guzmán**, Carlos Alfonso, Belén Reija, Jesús Mingorance, Silvia Zorrilla, Germán Rivas, and Begoña Monterroso. Submitted to PlosONE.

4.- SERS-based detection of the interactions between the essential division FtsZ protein and bacterial membrane elements. **Rubén Ahijado-Guzmán**, Germán Rivas, Ramón A. Álvarez-Puebla, Luis M. Liz-Marzán. Submitted to SMALL.

5.- BIOPHISICAL CHARACTERIZATION OF FtsZ IN ITS GDP-BOUND STATE (GDP-FtsZ). Regulation by Mg^{2+} concentration of the protein association state. **Rubén Ahijado-Guzmán**, Pilar López-Navajas, Peter Schuck, Begoña Monterroso, Carlos Alfonso and Germán Rivas. Manuscript in preparation.